

**A Multi-Scale Hybrid Nanoparticle Platform with Controlled
Cellular Interaction and Targeting Kinetics**

BY

SUHAIR SUNOQROT

B.S., University of Jordan, 2007

Submitted as partial fulfillment of the requirements
for the degree of Doctor of Philosophy in Biopharmaceutical Sciences
in the Graduate College of the
University of Illinois at Chicago, 2013

Chicago, IL

Defense Committee:

Seungpyo Hong, Chair and Advisor
Hayat Onyuksel
Michael Cho, Bioengineering
Steven Swanson, Medicinal Chemistry and Pharmacognosy
Ying Liu, Chemical Engineering

TABLE OF CONTENTS

ACKNOWLEDGEMENTS	v
LIST OF TABLES	vi
LIST OF FIGURES	vii
LIST OF ABBREVIATIONS	xxi
CHAPTERS	
1. INTRODUCTION	
1.1 Background	1
1.2 References	6
2. KINETICALLY CONTROLLED CELLULAR INTERACTIONS OF POLYMER- POLYMER AND POLYMER-LIPOSOME NANOHYBRID SYSTEMS	
2.1 Introduction	10
2.2 Experimental Section	13
2.3 Results and Discussion	21
2.4 Conclusion	33
2.5 References	34
3. TEMPORAL CONTROL OVER CELLULAR TARGETING THROUGH HYBRIDIZATION OF FOLATE-TARGETED DENDRIMERS AND PEG-PLA NANOPARTICLES	
3.1 Introduction	40
3.2 Experimental Section	42
3.3 Results and Discussion	48

3.4	Conclusion	63
3.5	References	64
4.	IN VITRO EVALUATION OF DENDRIMER-POLYMER HYBRID NANOPARTICLES ON THEIR CONTROLLED CELLULAR TARGETING KINETICS	
4.1	Introduction	71
4.2	Experimental Section	74
4.3	Results and Discussion	81
4.4	Conclusion	98
4.5	References	100
5.	PROLONGED BLOOD CIRCULATION TIME AND ENHANCED TUMOR RETENTION OF FOLATE-TARGETED DENDRIMER-POLYMER NANOHYBRID SYSTEMS	
5.1	Introduction	105
5.2	Experimental Section	108
5.3	Results and Discussion	116
5.4	Conclusion	128
5.5	References	129
6.	CONCLUSIONS AND OUTLOOK	134
	BIBLIOGRAPHY	140
	APPENDICES	170
	VITA	175

ACKNOWLEDGEMENTS

First and foremost, I would like to extend my deepest gratitude to my advisor, Dr. Seungpyo Hong. His mentorship and continuous support throughout the years have been instrumental in getting to where I am today as a scientist. I would also like to thank my committee members, Drs. Michael Cho, Ying Liu, Hayat Onyuksel, and Steven Swanson for their invaluable feedback and helpful suggestions.

I would also like to acknowledge all my current and previous lab members, not just for their scientific contribution to my work, but also for their unconditional support throughout the years, which has truly made the lab feel like a second home. Drs. Jin Woo Bae, Su-Eon Jin, and Ja Hye Myung, thank you for being such great scientists and role models. Yang Yang, Ryan Pearson, Kevin Shyu, Hao-jui Hsu, Eri Iwasaki, and Jason Bugno, thank you guys for all your help and encouragement during this journey.

I also thank Drs. Beck, Onyuksel, Gemeinhart, and Tonetti, and their lab members, especially Martina Vaskova, Dr. Tonya Kuzmis, and Huiping Zhao, for sharing their labs' resources and equipment, which have been essential for my research. I would also like to acknowledge Dan Lantvit for his assistance with the biodistribution studies. I would be amiss if I didn't also thank Connie Bouye and Celina Tejada, the heart and soul of the Department of Biopharmaceutical Sciences, for their continuous dedication and support to me as well as fellow graduate students.

Last but not least, my heartiest gratitude goes out to my parents, Ziad Sinokrot and Najah Jweihan, my brothers Abdulhamid, Tariq, and Ahmad, and my sister Nour. Thank you all for believing in me and being my biggest fans!

LIST OF TABLES

TABLE	PAGE
Table 2.1. Characterization of PEI-RITC and PEI-RITC-encapsulated nanohybrids	23
Table 3.1. Characterization of the G4 PAMAM dendrimers and nanohybrids	53
Table 4.1. Characterization of the G4 PAMAM dendrimers and nanohybrids	86
Table 5.1. Characterization of G4 and G5 PAMAM dendrimers and nanohybrids	117

LIST OF FIGURES

FIGURE	PAGE
Figure 1.1. Scale comparison of different nanocarriers relative to cells and nature components.	2
Figure 1.2. Overview of the multi-scale nanohybrid formation. Actively targeted dendrimer conjugates (5-10 nm in diameter) are encapsulated within protective outer layers of biodegradable polymers (hybrid NPs), or lipids (hybrid liposomes) with controlled sizes for passive targeting.	4
Figure 2.1. Schematic diagram of preparation of the three PEI-based nanohybrid systems (<i>partially contributed by Jin Woo Bae</i>).	12
Figure 2.2. UV/Vis spectra of RITC standards and PEI-RITC.	21
Figure 2.3. ¹ H NMR spectrum of PEG-PLGA. The large peak at 3.7 ppm (b) corresponds to the methylene groups of mPEG, and the sharp peak at 3.4 ppm (a) is assigned for the methoxy end group of mPEG. The methyl groups in D- and L-lactide repeat units are observed at 1.6 ppm (g), and the multiplets at 4.8 and 5.2 ppm (f) correspond to the glycolic acid CH and the lactic acid CH, respectively. The ratio of PEG to PLGA was calculated based on the integration values of the characteristic values (see arrows), The measured ratio ranged from 1.3:1 to 2.3:1 (<i>acquired by Ryan M. Pearson</i>).	22
Figure 2.4. Scanning Electron Microscopy (SEM) images of (A) PEI-RITC-encapsulated PEG-PLGA NPs and (B) PLGA NPs, scale bar = 100 nm. (C) A	24

Transmission Electron Microscopy (TEM) image of PEI-RITC-encapsulated liposomes, scale bar = 100 nm (*partially acquired by Ryan M. Pearson*).

Figure 2.5. Release profiles of PEI-RITC from the three nanohybrids in PBS 25
buffer with pH 7.4 and acetate buffer with pH 4.0 at 37 °C. Little to no burst
release was observed across all nanohybrids, with a sustained release profile
up to 23 days. The overall release behavior was faster in pH 4.0 compared to
pH 7.4 between the same type of nanohybrid formulation. The inset represents
the zoomed-in release profiles for the first 2 days.

Figure 2.6. Cytotoxicity of PEI-RITC and the three nanohybrids after 27
incubation with MCF-7 cells for (A) 1 h, (B) 4 h, (C) 24 h, and (D) 48 h. PEI-
RITC exhibits cytotoxicity in a concentration and incubation time dependent
manner whereas all nanohybrids show a marked decrease in cytotoxicity
kinetics. After 48 h of treatment, all nanohybrids become comparatively toxic to
PEI-RITC. *denotes statistical significance ($p < 0.05$) between PEI-RITC and
the three nanohybrids, based on a 1-way ANOVA followed by Tukey's post hoc
test.

Figure 2.7. CLSM images of MCF-7 cells following treatment with PEI-RITC 29
and the three nanohybrids (PEI-RITC-encapsulated liposomes, PEG-PLGA
NPs, and PLGA NPs) all at a concentration of 0.5 $\mu\text{g}/\text{mL}$ based on PEI-RITC
for 1 h, 4 h, 24 h, and 48 h (red: PEI-RITC, blue: cell nuclei stained by DAPI,
green: cellular membrane stained by WGA-AF 488; scale bar: 20 μm).

Figure 2.8. Mean fluorescence following treatment of MCF-7 cells with PEI- 30

RITC and the three nanohybrids at a concentration of 0.5 $\mu\text{g/mL}$ based on PEI-RITC up to 48 h. Kinetic control over PEI-RITC internalization is further confirmed as unencapsulated PEI-RITC shows the fastest uptake, as indicated by having the highest fluorescence count compared to the three nanohybrid formulations. Cell binding and uptake of the nanohybrids occur in the order of liposomes, PEG-PLGA NPs, and PLGA NPs, which is consistent with the confocal data shown in Figure 2.7.

Figure 3.1. Schematic representation of (A) stepwise functionalization of G4 PAMAM dendrimers, and (B) preparation of nanohybrids (*partially contributed by Kevin Shyu*). 49

Figure 3.2. ^1H NMR spectra of (A) G4 PAMAM dendrimer, (B) G4-RHO-NH₂, and (C) G4-RHO-FA-OH. The ^1H NMR spectrum of G4 PAMAM dendrimers (A) shows 6 characteristic peaks at 2.46, 2.65, 2.84, 3.01, 3.32, and 3.43 ppm. After conjugation with RHO, new peaks between 6.50 and 8.50 ppm corresponding to the aromatic protons of RHO were observed (B). Based on the relative integration values at 8.04 ppm and the dendrimer peaks, it was calculated that each dendrimer has approximately 3.9 RHO molecules. For G4-RHO-FA-OH (C), an increase in the integration values at 6.68 and 7.76 ppm, compared to G4-RHO, indicated the successful FA conjugation. Based upon the difference in the relative integration values of the characteristic RHO and FA peaks, it was calculated that approximately 4.3 FA molecules were attached to a dendrimer molecule (*acquired by Ryan M. Pearson*). 51

Figure 3.3. ^1H NMR spectra of (A) PEG(5K)-PLA(30K), and (B) PEG(5K)- 52

PLA(45K). The ^1H NMR spectra of PEG-PLA shows two characteristic peaks of PLA at 5.15 and 1.55 ppm (c and d), corresponding to the protons of methine and methylene groups, respectively. As for mPEG, two characteristic peaks corresponding to the methoxy group (a) and the ethylene glycol repeating units (b) were observed at 3.62 and 3.35 ppm, respectively. The MWs of PEG-PLA were estimated using the relative integration ratios of peak b and c, based on the the integral value for the methoxy group of mPEG which was set to 3.

Figure 3.4. Scanning electron microscopy (SEM) images of the nanohybrids prepared in this study showing controlled particle sizes around 100 nm in diameter. Scale bar: 100 nm. 53

Figure 3.5. CLSM images of KB FR⁺ cells after incubation with G4-RHO-FA-OH and its corresponding NP45 nanohybrids at a concentration of 63 nM (based on the dendrimer conjugates) for 1 h (upper row) and 4 h (lower row) (red: dendrimer conjugates, blue: cell nuclei stained by DAPI, scale bar: 20 μm). The receptor targeting of the dendrimer-FA conjugates is confirmed by significant binding of the unencapsulated conjugates to the cell surface within 1 h (1st column), which was blocked by pre-incubating the cells with 1 mM of free FA (2nd column). Temporal control over targeting is demonstrated using G4-RHO-FA-OH-encapsulated nanohybrids that do not interact with cells until 4 h (3rd column), and the interaction was also blocked by free FA (4th column). 55

Figure 3.6. Mean fluorescence intensities measured by FACS after the treatment of FR⁺ KB cells with G4-RHO-FA-OH and its NP45 nanohybrid 56

formulation under the same conditions described in Figure 3.5. *denotes statistical significance ($p < 0.05$) between G4-RHO-FA-OH and the control conjugate groups, and # denotes statistical significance ($p < 0.05$) between G4-RHO-FA-OH/NP45 and the control nanohybrids, based on a 1-way ANOVA followed by Tukey's post hoc test. G4-RHO-NH₂ shows the interactions with the cells after 4 h due to non-specific electrostatic interactions.

Figure 3.7. CLSM images of KB FR⁻ cells after incubation with G4-RHO-FA-OH and its corresponding NP45 nanohybrids at a concentration of 63 nM (based on the dendrimer conjugates) for 1 h (upper row) and 4 h (lower row) (red: dendrimer conjugates, blue: cell nuclei stained by DAPI, scale bar: 20 μ m). 57

Figure 3.8. Release tests of G4-RHO-FA-OH nanohybrids conducted in (A) PBS buffer and (B) RPMI 1640 medium with 10% FBS for the first 48 h of incubation, and (C) PBS buffer up to 21 days. Nanohybrids with the smallest PLA MW (NP23) show the fastest release in both release media, followed by NP30, and lastly NP45. The release rates of all three nanohybrids in RPMI 1640 are much faster than those in PBS. 59

Figure 3.9. CLSM images of KB FR⁺ cells following incubation with G4-RHO-FA-OH and three types of nanohybrids prepared using PEG-PLA with different PLA MW: NP23, NP30, and NP45, at a concentration of 63 nM based on dendrimer conjugates for 1 h (top row), 4 h (middle row), and 8 h (bottom row) (red: dendrimer conjugates, blue: cell nuclei stained by DAPI, scale bar: 20 μ m). Temporal control over targeting is further demonstrated using G4-RHO- 61

FA-OH-encapsulated nanohybrids with different PLA MW. Nanohybrids with the smallest PLA (NP23) (2nd column) show the fastest receptor binding that is comparable to unencapsulated G4-RHO-FA-OH (1st column). NP30 (3rd column) and NP45 (4th column) nanohybrids do not show interaction with the cells until after 4 h incubation. After 8 h incubation, all nanohybrids are either bound to the surface or internalized into the cells.

Figure 3.10. Mean fluorescence intensities measured by FACS (n = 2) after the treatment of KB FR⁺ cells with G4-RHO-FA-OH and three types of nanohybrids with different PLA MW: NP23, NP30, and NP45, under the same conditions used for Figure 6. Temporal control over FR targeting is observed using the nanohybrids with different PLA MW. The nanohybrids with the smallest PLA (NP23) showed the highest fluorescence count that is comparable to unencapsulated G4-RHO-FA-OH over the time course of the experiment. The NP30 and NP45 nanohybrids start to show a significant increase in fluorescence after 4 h incubation. After 8 h incubation, all nanohybrids exhibit similar fluorescence intensities. Even though the release profiles in buffer and serum-containing medium are markedly different, no significant difference in the cellular interaction kinetics is observed between NP30 and NP45 nanohybrids. *denotes statistical significance (p < 0.05) between G4-RHO-FA-OH and the nanohybrids based on a 1-way ANOVA followed by Tukey's post hoc test. 62

Figure 4.1. Overview of nanohybrid preparation. (A) Sequential preparation of the targeted dendrimer conjugates, (B) Encapsulation of the dendrimer 82

conjugates into PEG-PLA copolymers to produce the nanohybrids.

Figure 4.2. ^1H NMR spectra of (A) G4 PAMAM dendrimer, (B) G4-RHO-NH₂, and (C) G4-RHO-FA-NH₂. The ^1H NMR spectrum of G4 PAMAM dendrimers (A) shows 6 characteristic peaks at 2.46, 2.65, 2.84, 3.01, 3.32, and 3.43 ppm. After conjugation with RHO, new peaks between 6.50 and 8.50 ppm corresponding to the aromatic protons of RHO were observed (B). Based on the relative integration values at 8.04 ppm and the dendrimer peaks, it was calculated that each dendrimer has approximately 3.9 RHO molecules. For G4-RHO-FA-NH₂ (C), an increase in the integration values at 6.68 and 7.76 ppm, compared to G4-RHO, indicated successful FA conjugation. Based upon the difference in the relative integration values of the characteristic RHO and FA peaks, it was calculated that approximately 4.3 FA molecules were attached to the dendrimer. 83

Figure 4.3. UV/Vis spectra of MTX, MTX-dendrimer conjugates, and the control dendrimers in ddH₂O. Based on the absorbance of the conjugates at 373 nm, G4-RHO-FA-OH-MTX and G4-RHO-OH-MTX each contain 4.7 and 5.6 MTX molecules per dendrimer, respectively. 84

Figure 4.4. ^1H NMR spectra of (A) PEG-PLA, (B) Boc-NH-PEG-PLA, (C) deprotected H₂N-PEG-PLA, and (D) FITC-PEG-PLA. The ^1H NMR spectrum of PEG-PLA shows two characteristic peaks of PLA at 5.15 and 1.55 ppm (b and c), corresponding to the protons of the methine and methylene groups, respectively. As for mPEG, the characteristic peak corresponding to the ethylene glycol repeating units (b) was observed at 3.62 ppm. The MWs of 85

PEG-PLA were estimated using the relative integration ratios of peaks b and c, based on the integral value for peak a of mPEG. This was calculated to be 44,900 g/mol for PEG-PLA and 48,800 g/mol for Boc-NH-PEG-PLA. Deprotection of Boc-NH-PEG-PLA was confirmed by the disappearance of peak d (0.85 ppm) corresponding to the Boc group. Conjugation of FITC to H₂N-PEG-PLA was confirmed by the appearance of peak e at 6.45 ppm corresponding to the aromatic protons of FITC, and it was calculated that 0.8 FITC molecules were attached to the polymer based on the relative integration ratio of peaks a and e.

Figure 4.5. SEM images of the nanohybrids prepared in this study showing controlled particle sizes around 100 nm in diameter (scale bar: 100 nm). 87

Figure 4.6. CLSM images of KB FR⁺ cells upon incubation with G4-RHO-FA-OH (left column), G4-RHO-FA-OH-encapsulated nanohybrids (middle column), and empty FITC-NPs (right column) up to 48 h. Red: RHO-labeled dendrimers, green: FITC-labeled NPs, blue: cell nuclei stained by DAPI, scale bar: 20 μm. 88

Figure 4.7. Ortho view of Z-stack images of KB FR⁺ cells upon incubation with G4-RHO-FA-OH (left column), G4-RHO-FA-OH-encapsulated nanohybrids (middle column), and empty FITC-NPs (right column) at 4 and 24 h. Red: RHO-labeled dendrimers, green: FITC-labeled NPs, blue: cell nuclei stained by DAPI, scale bar: 10 μm. The targeted dendrimers show specific interaction with KB FR⁺ throughout the incubation period. The targeted nanohybrids start to selectively interact with the cells after 4 h as the overlapping red and green fluorescence signals are observed. At longer incubation hours (24 h and 89

Figure 25), the red signals become predominant, indicating that the released dendrimers selectively interact with the KB FR⁺ cells. The empty NPs start to interact with the cells after 24 h likely due to non-specific interactions.

Figure 4.8. CLSM images of (L to R): KB FR⁻ cells incubated with G4-RHO-FA-OH, KB FR⁻ cells incubated with G4-RHO-FA-OH/FITC-NPs, KB FR⁺ cells incubated with G4-RHO-OH, and KB FR⁺ cells incubated with G4-RHO-OH/FITC-NPs up to 48 h. G4-RHO-FA-OH and its corresponding nanohybrids show limited interactions with KB FR⁻ cells. Nontargeted dendrimer conjugates (G4-RHO-OH) and their corresponding nanohybrids show a significantly lower degree of interactions with KB FR⁺ cells compared to the FA-targeted systems (Figure 25). Red: RHO-labeled dendrimers, green: FITC-labeled NPs, blue: DAPI, scale bar: 20 μ m. 90

Figure 4.9. Release kinetics of G4-RHO-FA-OH/FITC-NP in cell-conditioned basal FA-deficient RPMI 1640 media. Faster release kinetics were obtained compared to the release profile in PBS (red dotted line, adapted from Figure 17), with ~90% of the dendrimer conjugates released after 48 h of incubation. 92

Figure 4.10. Effect of endocytic inhibitors on cellular interactions of the nanohybrids observed using CLSM. KB FR⁺ cells were incubated with G4-RHO-FA-OH, nanohybrids (G4-RHO-FA-OH/FITC-NP), and empty FITC-NPs for 4 h and 24 h. Red: RHO-labeled dendrimers, green: FITC-labeled NPs, blue: cell nuclei stained by DAPI, scale bar: 20 μ m. Cellular uptake of the targeted dendrimers is fully inhibited at 4 h by filipin and filipin/M β CD, but not affected by M β CD alone. The uptake of the targeted nanohybrids is inhibited 94

by M β CD and filipin/M β CD at 4 h, exhibiting polymeric NP-like behavior. However, at 24 h, only filipin/M β CD blocks the interaction of the nanohybrids, and yet limited effect of M β CD is observed, indicating the selective cellular interactions by the released dendrimers (red fluorescence). As expected, non-specific uptake of the empty FITC-NPs at 24 h is inhibited by M β CD and filipin/M β CD.

Figure 4.11. (A) CLSM images of KB FR⁺ MCTS upon incubation with G4-RHO-FA-OH, G4-RHO-FA-OH/FITC-NP, and empty FITC-NPs up to 48 h. Red: RHO-labeled dendrimers, green: FITC-labeled NPs. Images shown were taken at a depth of 80 μ m into each spheroid, scale bar: 100 μ m. Only the free dendrimers and those released from the nanohybrids are able to penetrate deep into the spheroids. Empty FITC-NPs and intact nanohybrids accumulate at the periphery of the spheroids even after 48 h. 96

Figure 4.12. Cell proliferation kinetics of KB FR⁺ (n = 4) after treatment with MTX-conjugated dendrimers and nanohybrids at a concentration equivalent to 1 μ M MTX over 72 h. The MTS assay was performed after additional 72 h to allow the cells to proliferate. Free MTX and the MTX-conjugated FA-targeted dendrimers start to exhibit cytotoxicity after 24 h, as indicated by the reduction in cell proliferation (<80%) relative to untreated controls. G4-RHO-FA-OH-MTX-encapsulated nanohybrids show a similar effect on cell growth at the 72 h time point but with a time delay of 48 h due to the controlled release of the dendrimer conjugates. * and ** denote significant difference in cell proliferation relative to the non-targeted dendrimer conjugates (G4-RHO-OH-MTX) and 97

nanohybrids (G4-RHO-OH-MTX/NP), respectively. Statistical analysis was performed using OriginPro 8.5 using 1-way ANOVA followed by Tukey's post hoc test at $p < 0.05$.

Figure 5.1. Overview of the sequential passive and active targeting enabled by the nanohybrid system. The PEGylated larger NP allows the nanohybrids to be long circulating and passively accumulate at the tumor site through the EPR effect. Once there, actively-targeted dendrimers are gradually released and able to penetrate deep within the tumor tissue, ultimately resulting in enhanced targeting efficacy (*partially contributed by Kevin Shyu*). 108

Figure 5.2. ^1H NMR spectra of (A) G4 PAMAM dendrimer, (B) partially acetylated G4, (C) RITC conjugated, fully hydroxylated G4-RITC-OH, and (D) fully hydroxylated, RITC and FA conjugated G4-RITC-FA-OH. The ^1H NMR spectrum of G4 PAMAM dendrimers (A) has 6 characteristic peaks corresponding to the protons of the internal methylene groups and those adjacent to the surface amino groups at 2.46, 2.65, 2.84, 3.01, 3.32, and 3.43 ppm. After partial acetylation, a new peak appeared at 1.95 ppm corresponding to the acetamide protons. The dendrimer was 30% acetylated based on the integration ratio between peak g and peaks a-f (B). RITC conjugation resulted in new peaks corresponding to the aromatic protons between 6.75 – 7.65 ppm (C). FA conjugation also resulted in peaks around 6.55 – 7.85 which overlapped with the RITC peaks (D). 118

Figure 5.3. ^1H NMR spectra of (A) G5 PAMAM dendrimer, (B) partially acetylated G5, (C) RITC conjugated, fully hydroxylated G5-RITC-OH, and (D) 119

fully hydroxylated, RITC and FA conjugated G5-RITC-FA-OH. The ^1H NMR spectrum of G5 PAMAM dendrimers (A) has 6 characteristic peaks corresponding to the protons of the internal methylene groups and those adjacent to the surface amino groups at 2.46, 2.65, 2.84, 3.01, 3.32, and 3.43 ppm. After partial acetylation, a new peak appeared at 1.95 ppm corresponding to the acetamide protons. The dendrimer was 50% acetylated based on the integration ratio between peak g and peaks a-f (B). RITC conjugation resulted in new peaks corresponding to the aromatic protons between 6.75 – 7.65 ppm (C). FA conjugation also resulted in peaks around 6.55 – 7.85 which overlapped with the RITC peaks (D).

Figure 5.4. UV/Vis spectra of G4 and G5 PAMAM dendrimer conjugates prepared in this study compared to RITC and FA. The number of RITC and FA molecules attached to each dendrimer was calculated based on the absorbance of the conjugates at 556 nm and 275 nm, respectively. UV/Vis spectra revealed that the conjugates prepared in this study contained approximately 3.4 RITC and 5.8 FA molecules per G4 dendrimer, and 2.8 RITC and 5.9 FA molecules per G5 dendrimer. 120

Figure 5.5. ^1H NMR spectra of (A) PEG-PLA, (B) Boc-NH-PEG-PLA, (C) deprotected H_2N -PEG-PLA, and (D) RITC-PEG-PLA. The ^1H NMR spectrum of PEG-PLA shows two characteristic peaks of PLA at 5.15 and 1.55 ppm (b and c). As for mPEG, the characteristic peak corresponding to the ethylene glycol repeating units (b) was observed at 3.62 ppm. The MWs of PEG-PLA were estimated using the relative integration ratios of peaks b and c, based on 121

the integral value for peak a of mPEG. This was calculated to be 44,900 g/mol for PEG-PLA and 48,800 g/mol for Boc-NH-PEG-PLA. Deprotection of Boc-NH-PEG-PLA was confirmed by the disappearance of peak d (0.85 ppm) corresponding to the Boc group. Conjugation of RITC to H₂N-PEG-PLA was confirmed by the appearance of peak e at 6.45 ppm corresponding to the aromatic protons of RITC, and it was calculated that 0.9 RITC molecules were attached to the polymer based on the relative integration ratio of peaks a and e.

Figure 5.6. CLSM images of KB FR⁺ MCTS upon incubation with G4-RITC-FA-OH (top row), G5-RITC-FA-OH (second row), G4-RITC-OH (third row), and G5-RITC-OH (fourth row) up to 24 h. Red: RITC-labeled dendrimers. Images shown were taken at a depth of 80 μm into each spheroid, scale bar: 100 μm. Only the FA-targeted dendrimers are able to penetrate deep into the spheroids. G4-RITC-FA-OH conjugates display similar penetration ability to G5-RITC-FA-OH, which validates their use as FA-targeted vectors in the nanohybrid system. The nontargeted conjugates, G4-RITC-OH and G5-RITC-OH, exhibit a significantly lower penetration ability compared to FA-targeted conjugates. 122

Figure 5.7. Biodistribution profile of (A) nontargeted G4 dendrimers (G4-RITC-OH), (B) nontargeted nanohybrids, and (C) empty RITC-NPs, following a single IV injection. Nontargeted dendrimer conjugates are quickly cleared from the blood (<10% ID remaining) after 24 h, and appear mostly in the kidneys. In contrast, an equivalent dose of dendrimers encapsulated within the nanohybrids display a biodistribution profile closer to RITC-NPs. The nanohybrids and RITC-NPs persisted longer in the blood, with 18-23% ID 124

found after 24 h, and they were both mostly eliminated by the liver and spleen.

Figure 5.8. Biodistribution profile of (A) FA-targeted G4 dendrimers (G4-RITC-FA-OH), (B) FA-targeted nanohybrids, and (C) empty RITC-NPs, in BALB/c mice carrying human KB FR⁺ xenografts, following a single IV injection. FA-targeted dendrimers (A) are cleared from the blood faster than nontargeted conjugates (Figure 37(A)), with <5% ID remaining after 24 h, due to significant liver uptake (~15% ID). Only ~5% ID could be found in the tumor tissue after 1 h, and ~3% ID after 24 h. FA-targeted nanohybrids (B) not only persisted longer in the blood (14% ID remaining after 24 h), but also a higher % ID was found in the tumor tissue (12%) compared to the free conjugates. A similar biodistribution pattern was observed for RITC-NPs, including in tumor tissue (C).

LIST OF ABBREVIATIONS

CLSM	Confocal laser scanning microscopy
DAPI	4',6-diamidino-2-phenylindole
DCM	dichloromethane
ddH ₂ O	deionized distilled water
DI H ₂ O	Deionized water
DMF	dimethylformamide
DMSO	Dimethylsulfoxide
DOPG	1,2-dioleoyl- <i>sn</i> -glycero-3-phospho-(1'- <i>rac</i> -glycerol) sodium salt
DSPC	1,2-distearoyl- <i>sn</i> -glycero-3-phosphocholine
DSPE-PEG2000	1,2-distearoyl- <i>sn</i> -glycero-3-phosphoethanolamine-N-mPEG-2000
EDC	1-ethyl-3-(3-dimethylaminopropyl)carbodiimide)
EDTA	Ethylenediaminetetraacetic acid
EPR	Enhanced permeability and retention
FA	Folic acid
FACS	Fluorescence-activated cell sorting
FITC	Fluorescein isothiocyanate
FR	Folic acid receptor
GPC	Gel permeation chromatography
IP	Intraperitoneal
IV	Intravenous
KB FR ⁻	Folate receptor-downregulated KB cells

KB FR ⁺	Folate receptor-overexpressing KB cells
MCTS	Multicellular tumor spheroids
MTX	Methotrexate
MW	Molecular weight
MWCO	Molecular weight cutoff
M β CD	Methyl-beta-cyclodextrin
NHS	<i>N</i> -hydroxysuccinimide
NHS-RHO	<i>N</i> -hydroxysuccinimide-rhodamine
NMR	Nuclear magnetic resonance
NP	Nanoparticle
p-NPC	p-nitrophenyl chloroformate
PAMAM	Polyamidoamine
PBS	Phosphate buffered saline
PEG	Polyethyleneglycol
PEI	Polyethylenimine
PLA	Poly lactide
PLGA	Poly lactide-co-glycolide
PVA	poly(vinyl alcohol)
RES	Reticuloendothelial system
RITC	Rhodamine B isothiocyanate
RT	Room temperature
SEM	Scanning electron microscopy
TEA	triethylamine

TEM	Transmission electron microscopy
TFA	Trifluoroacetic acid
WGA-AF488	Wheat germ agglutinin-Alexafluor® 488 conjugate

CHAPTER 1

INTRODUCTION

1.1 BACKGROUND

Cancer is one of the most devastating diseases, with estimated 1,660,290 new cases diagnosed and 580,350 deaths in 2013 alone [1]. In addition to the detrimental effects on normal tissue and organ function, the side effects of existing chemotherapeutic agents can often be as devastating as the disease itself. This is due to nonspecific uptake of small drug molecules by the tumor cells and normal cells alike. The small size of drug molecules also causes their rapid elimination from the systemic circulation by renal and other clearance mechanisms [2].

In order to reduce the systemic side effects of common chemotherapeutic agents, selective delivery of those agents to the target tissues is highly desirable. Fortunately, recent advances in nanotechnology have enabled targeted delivery of therapeutic agents to cancer cells by two main mechanisms; active and passive targeting. Active targeting involves decorating the drug carrier with ligands that are specific to receptors overexpressed or uniquely expressed by the cancer cells. Passive targeting relies on using size-controlled nanocarriers, typically 50-200 nm in size, to passively accumulate at the tumor site due to the enhanced permeability and retention (EPR) effect, a characteristic of tumor biology [3-6].

As illustrated in Figure 1.1, nanocarriers come in different sizes, shapes, and attributes. For example, multifunctional polymer-drug conjugates can markedly improve

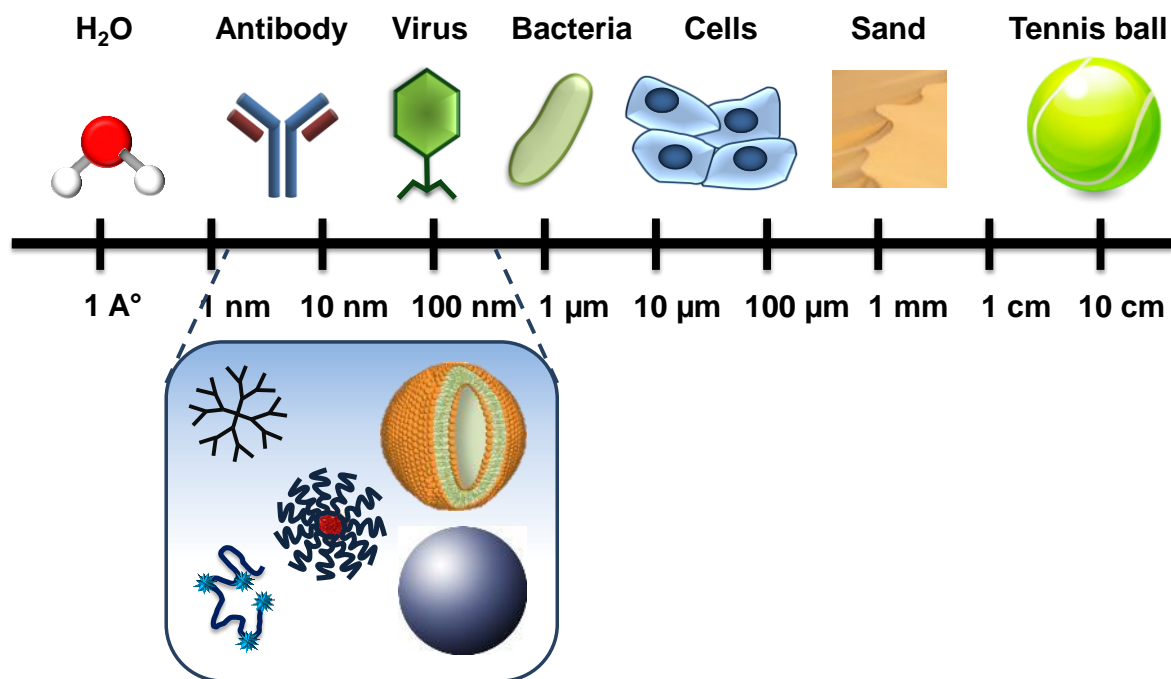


Figure 1.1 Scale comparison of different nanocarriers relative to cells and nature components (adapted from refs [7, 8]).

the solubility of hydrophobic drug molecules, while favorably altering their biodistribution [6, 9, 10]. The multifunctionality of such macromolecules also allows for surface decoration with targeting ligands for active targeting, and in certain cases, with polymers larger than 40,000 Da, passive targeting is also possible [9].

Dendrimers are nanometer-sized, hyperbranched, highly monodisperse, multifunctional macromolecules that have been widely explored for a variety of biomedical applications [11, 12]. Polyamidoamine (PAMAM) dendrimers are among the most widely investigated family of dendrimers for targeted drug delivery. The primary amine groups on their surface enable functionalization with targeting ligands as well as drug molecules and imaging agents, resulting in multifunctional nanodevices that have shown promising preclinical targeted drug delivery potential [13-18]. Due to their

molecular flexibility and deformability, conjugation of multiple targeting moieties to the outer surface of the dendrimers has been shown to enhance their targeting efficacy due to the strong multivalent binding effect [19, 20]. However, some of the disadvantages of using dendrimers for targeted drug delivery include their small size (5-10 nm) that limits passive targeting and results in rapid renal clearance [15, 21]. Additionally, conjugation of targeting ligands such as folic acid (FA) has led to significant uptake by the reticuloendothelial system (RES) including the liver [15].

Nanocarriers such as polymeric nanoparticles (NPs), liposomes, and micelles, have also been widely explored for targeted drug delivery [4, 22-24]. Their larger size compared to dendrimers can enable passive targeting to tumor tissues. Additionally, coating their surface with a stealth layer of hydrophilic polymers such as polyethylene glycol (PEG) has been shown to prolong their blood circulation time and delay their uptake by the liver and other organs of the RES [22]. However, these nanocarriers are typically more rigid in structure compared to dendrimers, which leads to limited tissue diffusivity and inefficient distribution of drug molecules within the tumor mass [25, 26]. This problem can be partially overcome by attaching targeting ligands to their surface, but the rigidity of these NPs prevents the full utilization of the multivalent binding effect. Additionally, the prolonged circulation time conferred by the stealth PEG layer can be compromised by the addition of targeting ligands to the surface [27].

Effective tumor targeting is largely dependent upon the size of the nanocarrier [2, 25, 26, 28]. Therefore, a multi-scale nanocarrier is needed for more efficient tumor targeting. We hypothesized that by creating a hybrid nanocarrier, or nanohybrid, of targeted dendrimer conjugates and polymeric NPs or liposomes, we can address the

limitations of each individual nanocarrier, thus enhancing their targeting efficacy. An overview of nanohybrid formation is illustrated in Figure 1.2. Functionalized dendrimer conjugates with targeting and imaging agents are prepared and then hybridized by encapsulation into larger polymeric NPs or liposomes, resulting in a multi-scale nanohybrid platform. The design rationale of the nanohybrid system is to take advantage of the controlled size of the polymeric NPs and liposomes to utilize passive targeting. By using PEGylated copolymers or lipids, the NPs will also have longer circulation times than free dendrimers, and thus protect against their premature elimination. At the same time, the smaller and more flexible dendrimers are more efficient at achieving active targeting following their release from the NPs at a controlled rate, ultimately resulting in more efficient tumor targeting.

To achieve this goal, we first conducted a proof-of-concept study where we

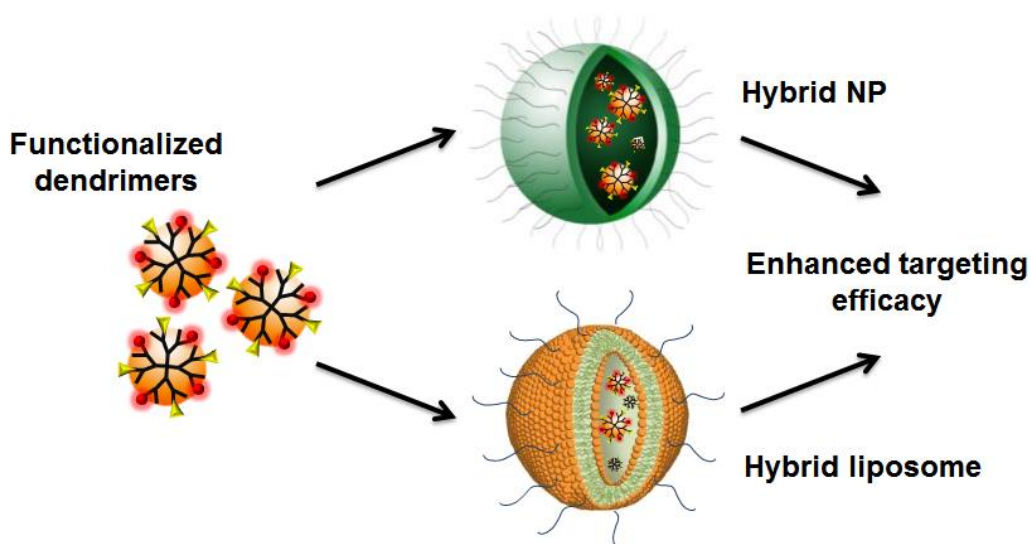


Figure 1.2. Overview of the multi-scale nanohybrid formation. Actively targeted dendrimer conjugates (5-10 nm in diameter) are encapsulated within protective outer layers of biodegradable polymers (hybrid NPs), or lipids (hybrid liposomes) with controlled sizes for passive targeting.

tested the feasibility of encapsulating functionalized polymers within different protective outer layers such as polymeric NPs and liposomes, and how that affects their cellular interactions [29]. Then, we wanted to investigate the ability of the nanohybrid platform to control the targeting kinetics of actively-targeted dendrimer conjugates forming the core of the nanohybrids [30]. This was followed by more in depth understanding of the cellular interactions of the targeted nanohybrids by a series of in vitro experiments to guide future in vivo studies [31]. Finally, biodistribution studies were conducted in both healthy and tumor-bearing mice to compare the blood circulation time, tumor targeting efficacy, and clearance pattern of the nanohybrids compared to free dendrimers and empty NPs. The results of this work serve as a promising starting point for future studies, where a chemotherapeutic drug will be incorporated into the nanohybrid system, which is expected to enhance the targeting efficacy through a combination of sequential passive and active targeting.

1.2 REFERENCES

1. *Defining Cancer*. National Cancer Institute, 2013. URL: <http://www.cancer.gov/cancertopics/cancerlibrary/what-is-cancer>
2. Popovic, Z., et al., *A Nanoparticle size series for in vivo fluorescence imaging*. *Angew. Chem. Int. Ed.*, 2010. **49**(46): p. 8649-8652.
3. Peer, D., et al., *Nanocarriers as an emerging platform for cancer therapy*. *Nat. Nanotechnol.*, 2007. **2**(12): p. 751-760.
4. Matsumura, Y. and H. Maeda, *A New concept for macromolecular therapeutics in cancer chemotherapy - Mechanism of tumorotropic accumulation of proteins and the antitumor agent SMANCS*. *Cancer Res.*, 1986. **46**(12): p. 6387-6392.
5. Maeda, H., *Tumor-selective delivery of macromolecular drugs via the EPR effect: Background and future prospects*. *Bioconjugate Chem.*, 2010. **21**(5): p. 797-802.
6. Duncan, R., *Polymer conjugates as anticancer nanomedicines*. *Nat. Rev. Cancer*, 2006. **6**(9): p. 688-701.
7. Gonzalez, L., et al., *Nanotechnology in Corneal Neovascularization Therapy-A Review*. *J. Ocul. Pharmacol. Th.*, 2013. **29**(2): p. 124-134.
8. Jin, S.-E., J.W. Bae, and S. Hong, *Multiscale observation of biological interactions of nanocarriers: From nano to macro*. *Microsc. Res. Techniq.*, 2010. **73**(9): p. 813-823.
9. Nori, A. and J. Kopecek, *Intracellular targeting of polymer-bound drugs for cancer chemotherapy*. *Adv. Drug Deliver. Rev.*, 2005. **57**(4): p. 609-636.

10. Duncan, R., *The dawning era of polymer therapeutics*. Nat. Rev. Drug Discov., 2003. **2**(5): p. 347-360.
11. Esfand, R. and D.A. Tomalia, *Poly(amidoamine) (PAMAM) dendrimers: from biomimicry to drug delivery and biomedical applications*. Drug Discov. Today, 2001. **6**(8): p. 427-436.
12. Lee, C.C., et al., *Designing dendrimers for biological applications*. Nat. Biotechnol., 2005. **23**(12): p. 1517-1526.
13. Quintana, A., et al., *Design and function of a dendrimer-based therapeutic nanodevice targeted to tumor cells through the folate receptor*. Pharm. Res., 2002. **19**(9): p. 1310-1316.
14. Baker, J.R., et al., *The Synthesis and testing of anti-cancer therapeutic nanodevices*. Biomed. Microdevices, 2001. **3**(1): p. 61-69.
15. Kukowska-Latallo, J.F., et al., *Nanoparticle targeting of anticancer drug improves therapeutic response in animal model of human epithelial cancer*. Cancer Res., 2005. **65**(12): p. 5317-5324.
16. Majoros, I.J., et al., *Poly(amidoamine) dendrimer-based multifunctional engineered nanodevice for cancer therapy*. J. Med. Chem., 2005. **48**(19): p. 5892-5899.
17. Patri, A.K., J.F. Kukowska-Latallo, and J.R. Baker, *Targeted drug delivery with dendrimers: Comparison of the release kinetics of covalently conjugated drug and non-covalent drug inclusion complex*. Adv. Drug Deliver. Rev., 2005. **57**(15): p. 2203-2214.

18. Majoros, I.J., et al., *PAMAM dendrimer-based multifunctional conjugate for cancer therapy: Synthesis, characterization, and functionality*. *Biomacromolecules*, 2006. **7**(2): p. 572-579.
19. Hong, S., et al., *The binding avidity of a nanoparticle-based multivalent targeted drug delivery platform*. *Chem. Biol.*, **2007**. **14**(1): p. 107-115.
20. Mecke, A., et al., *Deformability of poly(amidoamine) dendrimers*. *Eur. Phys. J. E*, 2004. **14**(1): p. 7-16.
21. Singh, P., et al., *Folate and folate-PEG-PAMAM dendrimers: Synthesis, characterization, and targeted anticancer drug delivery potential in tumor bearing mice*. *Bioconjugate Chem.*, 2008. **19**(11): p. 2239-2252.
22. Gref, R., et al., *Biodegradable long-circulating polymeric nanospheres*. *Science*, 1994. **263**(5153): p. 1600-1603.
23. Torchilin, V.P., *Recent advances with liposomes as pharmaceutical carriers*. *Nat. Rev. Drug Discov.*, 2005. **4**(2): p. 145-160.
24. Kataoka, K., A. Harada, and Y. Nagasaki, *Block copolymer micelles for drug delivery: design, characterization and biological significance*. *Adv. Drug Deliver. Rev.*, 2001. **47**(1): p. 113-131.
25. Wong, C., et al., *Multistage nanoparticle delivery system for deep penetration into tumor tissue*. *P. Natl. Acad. Sci. USA*, 2011. **108**(6): p. 2426-2431.
26. Yuan, F., et al., *Microvascular permeability and interstitial penetration of sterically stabilized (stealth) liposomes in a human tumor xenograft*. *Cancer Res.*, 1994. **54**(13): p. 3352-3356.

27. McNeeley, K.M., A. Annapragada, and R.V. Bellamkonda, *Decreased circulation time offsets increased efficacy of PEGylated nanocarriers targeting folate receptors of glioma*. *Nanotechnology*, 2007. **18**(38).
28. Tang, L., et al., *Synthesis and biological response of size-specific, monodisperse drug-silica nanoconjugates*. *ACS Nano*, 2012. **6**(5): p. 3954-3966.
29. Sunoqrot, S., et al., *Kinetically controlled cellular interactions of polymer-polymer and polymer-liposome nanohybrid systems*. *Bioconjugate Chem.*, 2011. **22**(3): p. 466-474.
30. Sunoqrot, S., et al., *Temporal control over cellular targeting through hybridization of folate-targeted dendrimers and PEG-PLA nanoparticles*. *Biomacromolecules*, 2012. **13**: p. 1223-1230.
31. Sunoqrot, S., et al., *In vitro evaluation of dendrimer-polymer hybrid nanoparticles on their controlled cellular targeting kinetics*. *Mol. Pharm.*, 2013. **ASAP Article**. DOI: 10.1021/mp300560n.

CHAPTER 2

KINETICALLY CONTROLLED CELLULAR INTERACTIONS OF POLYMER-POLYMER AND POLYMER-LIPOSOME NANOHYBRID SYSTEMS*

2.1 INTRODUCTION

Multifunctional macromolecules have demonstrated great potential as drug delivery vectors [1, 2]. In particular, polycationic polymers have been widely explored for many biomedical applications, including gene delivery [3]. One of the most commonly used cationic polymers is polyethylenimine (PEI) that has been mainly used as a nonviral gene delivery vector, as it is capable of protecting DNA from lysosomal degradation and promoting endosomal escape [4-7]. Another characteristic of PEI and other polycations, such as poly(lysine) and poly(amidoamine) (PAMAM) dendrimers, is that they spontaneously interact with biological membranes [8, 9]. Although the mechanism is not yet completely understood, this facilitates their cellular internalization without the need for ligands for receptor-mediated endocytosis or other internalization routes. However, toxicity issues related to the strong cationic surface charge have hindered clinical translation of the polycations in drug delivery, largely due to the lack of kinetic control over non-specific electrostatic interactions with blood components and rapid clearance by the reticuloendothelial system (RES) [10]. Therefore, a better understanding on the cellular interaction kinetics of polycation-based drug delivery

*Reproduced with permission from Sunoqrot, S.; Bae, J. W.; Jin, S. E.; Pearson, R. M.; Liu, Y.; Hong, S. *Bioconjugate Chem.* **2011**, *22*, (3), 466-474. Copyright 2011 American Chemical Society.

systems is required, which would eventually lead to fine control over their toxicity as well as cellular internalization.

Since most of the currently available anti-cancer treatment agents frequently accompany severe side effects through high toxicity to normal cells and tissues, it is highly desirable to home the drug delivery system to the tissue of interest. The passive targeting strategy using nanotechnology has proven to be efficient in reducing the toxic side effects, thereby increasing the therapeutic index of anti-cancer agents [11-13]. Passive targeting utilizes the enhanced permeability and retention (EPR) effect that is defined by leaky vasculature and poor lymphatic drainage around tumors, resulting in the accumulation of the nanoscale delivery system at the tumor site. In order to take advantage of the EPR effect, a nanoscale delivery system needs to be in the range of 50-200 nm, which can be achieved using well-established manufacturing techniques [14, 15].

As the first step in achieving kinetic control over the toxicity and cellular interactions of polycations, we have designed novel hybrid nanomaterials that combine functionalized PEI with relatively bio-inert, biodegradable polymer-based nanoparticles (NPs) and PEGylated liposomes. The design rationale of our nanohybrid systems is for a temporal control over interactions with cells, i.e. achieving passive targeting first by controlling the size of the nanohybrid materials and subsequent control over the kinetics of cellular interactions upon the release of PEI. The objectives of this study were to: i) encapsulate functionalized PEI into polymeric NPs or liposomes at a controlled size range of ~100 nm and ii) control the cellular uptake and cytotoxicity of PEI, depending upon the physical properties (such as biodegradability and structural stability) of the

encapsulating materials as the protective outer layers. We have prepared three types of the nanohybrid systems that encapsulate PEI-rhodamine (PEI-RITC) conjugates, as outlined in Figure 2.1. For the nanohybrid polymeric NPs, PEI was encapsulated into either polylactide-co-glycolide (PLGA) or polyethylene glycol-b-polylactide-co-glycolide (PEG-PLGA) using the double emulsion method. These systems were compared to PEGylated liposomes of mixed phospholipid composition, where PEI was encapsulated using the film rehydration method followed by extrusion.

Here we report three nanohybrid systems where a multifunctional polymer such as PEI is successfully encapsulated into either polymeric NPs or liposomes. Although similar hybrid systems that incorporate PEI into liposomes or biodegradable NPs have

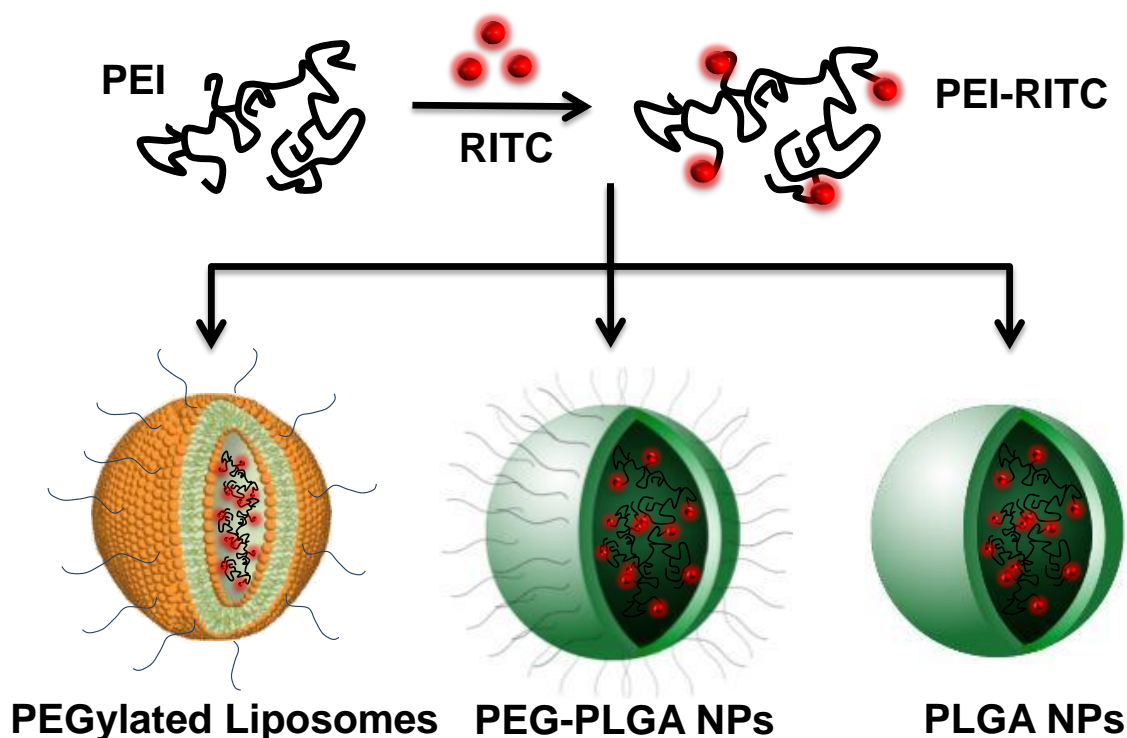


Figure 2.1. Schematic diagram of preparation of the three PEI-based nanohybrid systems (partially contributed by Jin Woo Bae).

been reported in the literature [16-18], no attempt has been made to compare them for the purpose of understanding the kinetics of their interactions with cells. By comparing the release profiles, cytotoxicity, and cellular uptake of the three PEI-based nanohybrids, we demonstrate that fine control over release and cellular uptake kinetics of the nanohybrids can be achieved depending on the type of the outer layers. Our results provide an important guideline in designing a drug delivery platform with tunable cellular interactions and cytotoxicity kinetics.

2.2 EXPERIMENTAL SECTION

2.2.1 Materials

Branched PEI (M_n 10,000), PLGA (50:50, M_w 40,000-75,000), poly(vinyl alcohol) (PVA, 87-89% hydrolyzed, M_w 13,000-23,000), rhodamine B isothiocyanate (RITC, mixed isomers), dichloromethane (DCM), pyridine, p-nitrophenyl chloroformate (p-NPC), triethylamine (TEA), diethyl ether, and cholesterol were all obtained from Sigma-Aldrich (St. Louis, MO). Amine-terminated methoxy PEG (mPEG-NH₂) (M_w 5,000) was obtained from Nektar (Huntsville, AL). 1,2-distearoyl-*sn*-glycero-3-phosphoethanolamine-N-mPEG-2000 (DSPE-PEG 2000), 1,2-distearoyl-*sn*-glycero-3-phosphocholine (DSPC), and 1,2-dioleoyl-*sn*-glycero-3-phospho-(1'-*rac*-glycerol) sodium salt (DOPG) were purchased from Avanti Polar Lipids Inc. (Alabaster, AL). All other chemicals used in this study were purchased from Sigma-Aldrich unless specified otherwise.

2.2.2 Preparation and characterization of PEI-RITC conjugates

PEI was fluorescently labeled by conjugation with RITC using a similar method as described earlier [9]. RITC (5.4 mg, 1.0×10^{-5} mol) dissolved in 1 mL deionized distilled water (ddH₂O) was added to PEI (20.0 mg, 2.0×10^{-6} mol) dissolved in 4 mL ddH₂O. The pH of the mixture was adjusted to 9.0 using 1.0 N hydrochloric acid (HCl), followed by vigorous mixing at room temperature (RT) for 24 h. Unreacted RITC was removed using membrane dialysis (Spectra/Por dialysis membrane, MWCO 3,500, Spectrum Laboratories Inc., Rancho Dominguez, CA) in 4 L of phosphate buffered saline (PBS) for 2 days, changing the buffer every 12 h, followed by dialysis in ddH₂O for 2 days, changing the water every 12 h. The purified PEI-RITC conjugates were lyophilized over 2 days using a Labconco FreeZone 4.5 system (Kansas City, MO) and stored at -20 °C.

2.2.3 UV/Vis Spectroscopy

A series of RITC solutions in ddH₂O (6.3, 12.5, 25.0, 37.5, and 50.0 µg/mL) were prepared and used as standards to calculate the RITC content of the conjugates in subsequent measurements. PEI-RITC conjugates were dissolved in ddH₂O at a concentration of 100 µg/mL. UV spectra were recorded against ddH₂O using a DU800 UV/Vis Spectrophotometer (Beckman Coulter, CA). A standard curve of RITC absorbance versus concentration was constructed, and the concentration of RITC in the PEI-RITC solution was calculated based on Beer's Law. The number of RITC molecules per PEI chain was determined based on the amount of RITC in the PEI-RITC solution.

2.2.4 Synthesis and characterization of PEG-PLGA copolymer

PEG-PLGA block copolymer used in this study was synthesized from mPEG-NH₂ and PLGA using a similar method as described earlier [19]. Five hundred milligrams of

PLGA (1.3×10^{-5} mol) were dissolved in 8 mL of DCM, to which 5.1 μ L (6.3×10^{-5} mol) of pyridine were added. p-NPC (12.6 mg, 6.3×10^{-5} mol) was dissolved in 1 mL of DCM, and then added dropwise to the PLGA and pyridine solution under vigorous stirring, and the reaction was carried out at RT for 24 h. The reaction product (p-NP-PLGA) was then precipitated using ice-cold diethyl ether and vacuum filtered. Next, p-NP-PLGA (400 mg, 1.0×10^{-5} mol) was dissolved in 8 mL of DCM. mPEG-NH₂ (93.8 mg, 1.9×10^{-5} mol) was dissolved in 3 mL of DCM, to which 7 μ L (5.0×10^{-5} mol) of TEA were added. The mPEG-NH₂ and TEA solution was then added dropwise to the p-NP-PLGA solution under vigorous stirring, and the reaction was carried out at RT for 24 h. The final product (PEG-PLGA) was precipitated using ice-cold diethyl ether and vacuum filtered. PEG-PLGA was characterized using ¹H NMR in CDCl₃ using a 400 MHz Bruker DPX-400 spectrometer (Bruker BioSpin Corp., Billerica, MA).

2.2.5 Encapsulation of PEI-RITC conjugates into polymeric NPs

PLGA and PEG-PLGA NPs were prepared using a double emulsion method as described previously [20, 21]. Briefly, 20 mg of either PLGA or PEG-PLGA were dissolved in 1 mL of DCM. PEI-RITC was dissolved in ddH₂O at a concentration of 1 mg/mL, and 100 μ L of the solution were added to either PLGA or PEG-PLGA solution in DCM. The mixture was sonicated for 1 min using a Misonix XL Ultrasonic Processor (100% duty cycle, 475 W, 1/8" tip, QSonica, LLC, Newtown, CT). Two milliliters of 3% PVA solution in ddH₂O was then added to the mixture, followed by sonication for 1 min at 100% duty cycle. The double emulsion was then poured into 20 mL of 0.3% PVA in ddH₂O, and vigorously stirred at RT for 24 h to evaporate DCM. The resulting aqueous solution was transferred to Nalgene high-speed centrifuge tubes (Fisher Scientific,

Pittsburg, PA). PVA and unencapsulated PEI-RITC were removed by ultracentrifugation at 20,000 rpm for 30 min using a Beckman Avanti J25 Centrifuge (Beckman Coulter, Brea, CA). After washing the NPs five times with ddH₂O, the pellet was resuspended in ddH₂O, lyophilized over 2 days, and stored at -20 °C.

2.2.6 Characterization of the PEI-RITC-encapsulated polymeric NPs

Particle size (diameter, nm) and surface charge (zeta potential, mV) of the NP-based nanohybrids were obtained from three repeat measurements by quasi-elastic laser light scattering using a Nicomp 380 Zeta Potential/Particle Sizer (Particle Sizing Systems, Santa Barbara, CA). The nanohybrid particles were suspended in ddH₂O at a concentration of 100 µg/mL, filtered through a 0.45 µm syringe filter, and briefly vortexed prior to each measurement. Loading was defined as the PEI-RITC content of the NP-based nanohybrids. Five milligrams of NP-based nanohybrids were completely dissolved in 1 mL of 0.5 M NaOH, followed by filtration through a 0.45 µm syringe filter. The fluorescence intensity from the filtrates containing PEI-RITC was then measured using a SpectraMAX GeminiXS microplate spectrofluorometer (Molecular Devices, Sunnyvale, CA). The amount of PEI-RITC released was determined from a standard curve of PEI-RITC fluorescence versus concentration in 0.5 M NaOH. Loading was expressed as µg PEI-RITC/mg PLGA or PEG-PLGA. Loading efficiency was defined as the ratio of the actual loading obtained to the theoretical loading (amount of PEI-RITC added divided by the mass of PLGA or PEG-PLGA used in each formulation).

2.2.7 Scanning Electron Microscopy (SEM)

The surface morphology of PLGA and PEG-PLGA NPs was examined using a JEOL-JSM 6320F field emission microscope (JEOL USA, Peabody, MA). Freeze dried

NP samples were placed onto a carbon adhesive strip mounted on an aluminum stub. Samples were sputter-coated with Pt/Pd at a coating thickness of 6 nm (Polaron E5100 sputter coater system, Polaron, UK) and then visualized at an accelerating voltage of 5.0 kV and 8.0 mm working distance.

2.2.8 Encapsulation of PEI-RITC conjugates into liposomes

Unilamellar liposomes were prepared using a film hydration method followed by extrusion as described previously [16]. Briefly, DOPG (5.0 mg, 6.3×10^{-6} mol), DSPC (4.9 mg, 6.2×10^{-6} mol), Cholesterol (2.4 mg, 6.2×10^{-6} mol), and DSPE-PEG 2000 (1.8 mg, 6.3×10^{-7} mol) were dissolved in 5 mL of DCM in a round-bottom flask. The flask was connected to a rotary evaporator (Rotavapor R11, Buchi, Switzerland) at 50 °C for 1 h to evaporate DCM until completely dried. The dried lipid film was hydrated in 1 mL of 0.1 mg/mL PEI-RITC solution in ddH₂O, followed by vortexing for 15 min to form multilamellar liposomes. Multilamellar liposomes were sonicated in a bath sonicator for 30 min, and then extruded 20 times through a polycarbonate membrane of 100 nm pore size using a Lipofast Pneumatic extruder (Avestin Inc., Ottawa, Canada). The resulting unilamellar liposome suspension was centrifuged at 20,000 rpm for 1 h to remove residual PEI-RITC. The pellet was resuspended in 1 mL of 5% sucrose, lyophilized over 2 days, and stored at -20 °C.

2.2.9 Characterization of the PEI-RITC-encapsulated liposomes

Particle size (diameter, nm) and surface charge (zeta potential, mV) were measured using the same method described for polymeric NPs. Loading was determined by dissolving 10 mg of lyophilized liposomes in 1 mL of 0.1% Triton X-100, followed by filtration through a 0.45 µm syringe filter and measuring the fluorescence of

the filtrate. The amount of PEI-RITC released was determined from a standard curve of PEI-RITC fluorescence versus concentration in 0.1% Triton X-100. Loading was expressed as μg PEI-RITC/mg lipids. Loading efficiency was calculated from the ratio of the actual measured loading to the theoretical loading (amount of PEI-RITC added divided by the mass of lipids and sucrose used in the formulation).

2.2.10 Transmission Electron Microscopy (TEM)

Size and shape of liposomal nanohybrids was examined using TEM. Liposomes were dissolved in ddH₂O at a concentration of 1 mg/mL. One drop of the solution was then placed on a 300-mesh copper grid and left to dry overnight, followed by negative staining with 2% phosphotungstic acid (PTA). TEM images were acquired using a JEOL JEM 1220 (JEOL USA) at an accelerating voltage of 80 kV.

2.2.11 Release kinetics study of PEI-RITC-encapsulated nanohybrids

Five milligrams of each nanohybrid in microcentrifuge tubes were dispersed in 1 mL PBS (pH 7.4) or acetate buffer (pH 4.0) in triplicates, and the solutions were placed in a shaking water bath (37 °C, 100 rpm). At designated time points (30 min, 1 h, 2, 4, 6, 8, 10, 12 and 24 h; every 2 days thereafter), solutions were centrifuged at 20,000 rpm for 5 min and the supernatants were collected. The nanohybrid systems were then redispersed in fresh PBS or acetate buffer and placed back in the water bath. The fluorescence of the supernatants was measured and the cumulative amount of PEI-RITC released over time was determined from a standard curve of PEI-RITC fluorescence versus concentration in either PBS or acetate buffer.

2.2.12 Cytotoxicity of PEI-RITC-encapsulated nanohybrids

MCF-7 cell line was obtained from ATCC (Manassas, VA) and grown continuously as a monolayer in GIBCO Dulbecco's modified Eagle medium (DMEM, Invitrogen Corporation, Carlsbad, CA) in a humidified incubator at 37 °C and 5% CO₂. DMEM was supplemented with penicillin (100 units/mL), streptomycin (100 mg/mL), and 10% heat-inactivated fetal bovine serum (FBS) (Invitrogen Corporation, Carlsbad, CA) before use. For the assay, MCF-7 cells were seeded in 96-well plates at a density of 2×10^4 cells/well and grown in DMEM for 24 h. Cells (n = 4) were then treated with PEI-RITC or nanohybrid systems (PEI-RITC encapsulated liposomes, PEG-PLGA NPs, and PLGA NPs) at 4 PEI-RITC concentrations (1, 5, 10, and 30 µg/mL) for 1, 4, 24, and 48 h. After each incubation time, cells were washed and incubated for an additional 24 h in a normal culture condition. Cell viability was assessed using a CellTiter 96 AQueous One Solution (MTS) Assay (Promega, Madison, WI) according to the manufacturer's protocol. The UV absorbance was measured at 490 nm using a Labsystems Multiskan Plus microplate reader (Labsystems, Finland). Mean cell viabilities were determined relative to a negative control (untreated cells). Statistical analysis was performed using OriginPro 8.1 (OriginLab, Northampton, MA). Mean cell viabilities were compared using 1-way ANOVA followed by Tukey's post hoc test at $p < 0.05$.

2.2.13 Cellular uptake of PEI-RITC-encapsulated nanohybrids: Confocal microscopy observation

MCF-7 cells were seeded in 4-well chamber slides (Millicell EZ Slide, Millipore, Billerica, MA) at a density of 2.0×10^5 cells/well and incubated in DMEM for 24 h. PEI-RITC (0.5 µg), liposomes (67 µg), PEG-PLGA NPs (242 µg), and PLGA NPs (106 µg) were each dispersed in 1 mL of DMEM to make the concentration of PEI-RITC constant

at 0.5 µg/mL throughout all nanohybrids. Cells were treated with the three nanohybrids and unencapsulated PEI-RITC for 1, 4, 24, and 48 h. Following the treatment, cells were washed with PBS three times, and then 50 µL of Wheat Germ Agglutinin Alexa Fluor® 488 conjugate (WGA-AF488, 5 µg/mL, Invitrogen Corporation, Carlsbad, CA) was added to each dish and incubated for 10 min at RT to stain the cell membrane. Cells were washed again with PBS, followed by fixation in 500 µL of 4% paraformaldehyde for 10 min at RT. After washing excess paraformaldehyde, cells were mounted with antiphotobleaching mounting media with DAPI (Vector Laboratory Inc., Burlingame, CA), and covered with glass cover slips. Cellular uptake was visualized using a Zeiss LSM 510 confocal laser scanning microscope (CLSM, Carl Zeiss, Germany). The 488 nm line of a 30 mW tunable argon laser was used for excitation of AF488, a 1 mW HeNe at 543 nm for RITC, and a 25 mW diode UV 405 nm laser for DAPI. Emission was filtered at 505-530 nm, 565-595 nm, and 420 nm for AF488, RITC, and DAPI, respectively.

2.2.14 Cellular uptake of PEI-RITC-encapsulated nanohybrids: Flow cytometry measurements

MCF-7 cells were seeded in 12-well plates at a density of 1×10^6 cells/well and incubated in DMEM for 24 h. Cells were then treated with unencapsulated PEI-RITC and the three nanohybrids under that same condition described in the cellular uptake experiment. After each incubation period, cells were washed with PBS and then suspended with trypsin/EDTA. Cell suspensions were centrifuged at 3500 rpm for 5 min, resuspended in 500 µL of 1% paraformaldehyde, and transferred to flow cytometry sample tubes. Fluorescence signal intensities from the samples were measured using a

MoFlo cell sorter (BD, Franklin Lakes, NJ) and data analysis was performed using Summit v4.3 software (Dako Colorado, Fort Collins, CO).

2.3 RESULTS AND DISCUSSION

2.3.1 Preparation and characterization of PEI-RITC conjugates and PEG-PLGA copolymer

The UV/Vis measurements revealed the number of RITC molecules attached to a PEI chain. By constructing a calibration curve of UV absorbance of RITC against various concentrations at 555 nm (λ_{\max}), the RITC concentration in a solution of the PEI-RITC conjugate was calculated from the absorbance at 555 nm. The molar ratio of PEI and RITC was then calculated by converting the concentration values to number of moles. The results indicate the presence of 6.2 RITC molecules per PEI chain (Figure 2.2). Particle size and zeta potential of the conjugates were measured to be 11.2 nm and 32.1 mV, respectively (Table 2.1). In addition, the chemical structure of PEG-PLGA is confirmed by ^1H NMR as shown in Figure 2.3. On basis of the relative

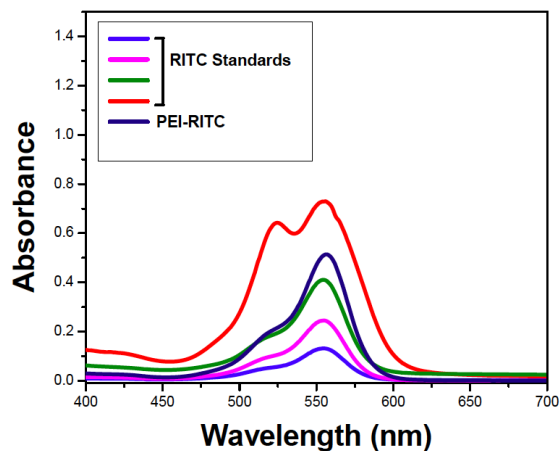


Figure 2.2. UV/Vis spectra of RITC standards and PEI-RITC.

integration values of the characteristic peaks of each polymer (see arrows), the ratio of the PEG block to the PLGA block was measured to be 1.3:1-2.4:1.

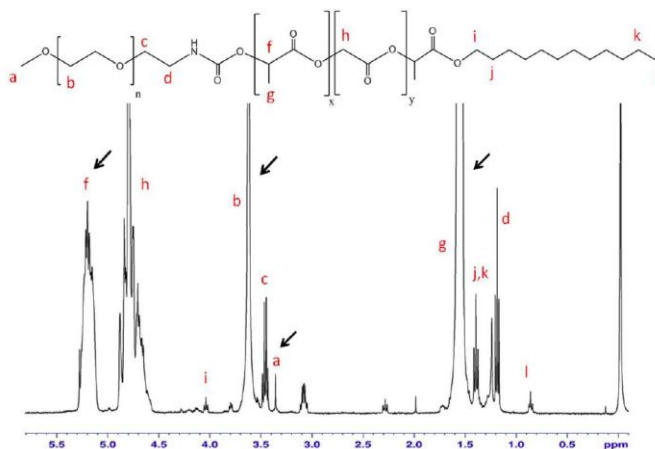


Figure 2.3. ^1H NMR spectrum of PEG-PLGA. The large peak at 3.7 ppm (b) corresponds to the methylene groups of mPEG, and the sharp peak at 3.4 ppm (a) is assigned for the methoxy end group of mPEG. The methyl groups in D- and L-lactide repeat units are observed at 1.6 ppm (g), and the multiplets at 4.8 and 5.2 ppm (f) correspond to the glycolic acid CH and the lactic acid CH, respectively. The ratio of PEG to PLGA was calculated based on the integration values of the characteristic values (see arrows). The measured ratio ranged from 1.3:1 to 2.3:1 (*acquired by Ryan M. Pearson*).

2.3.2 Preparation and characterization of PEI-RITC-encapsulated nanohybrids

It is highly desirable for a potential tumor-targeted delivery system to possess a size range of less than 200 nm in order to be able to passively accumulate into the tumor tissue. The size of the liposome-based system was controlled by extrusion using a membrane filter with pore size of 100 nm according to a slightly modified method from a previous report [16]. For encapsulation into the polymeric NPs, the double emulsion method was chosen as it enables encapsulation of hydrophilic materials into a variety of polymers or copolymers with a controlled particle size [20, 22].

As shown in Table 2.1 and Figure 2.4, the encapsulation methods employed herein have proven successful in controlling the size, as particle sizes for all three nanohybrids were in the range of 100-150 nm. Both methods also showed relatively good loading efficiencies (45-94%) that correlate well with the reported values [22]. The zeta potential results suggest that the net surface charges on the NP- and liposome-based nanohybrids are all negative. This is expected since the carboxylic acid groups in PLGA and PEG-PLGA copolymers are deprotonated in neutral pH, and the phospholipid 1,2-dioleoyl-*sn*-glycero-3-phospho-(1'-*rac*-glycerol) (DOPG) is anionic [23]. The negative zeta potential values indicate that the encapsulation process in all formulations masked the positive charge on PEI-RITC. The controlled size, along with protection of positive charge from surface exposure, confirmed that we have prepared the nanohybrid systems as designed (Figure 2.1).

Table 2.1. Characterization of PEI-RITC and PEI-RITC-encapsulated nanohybrids

Formulation	Particle Size (nm)	Zeta Potential (mV)	Loading ($\mu\text{g}/\text{mg}$)	Loading Efficiency (%)
PEI-RITC	11.2 ± 5.3	32.1 ± 2.1	--	--
Liposomes	154.2 ± 13.6	-40.2 ± 5.7	4.7	94.4
PEG-PLGA NPs	130.2 ± 9.4	-16.5 ± 7.0	7.5	75.1
PLGA NPs	117.4 ± 18.2	-23.6 ± 13.8	2.2	44.6

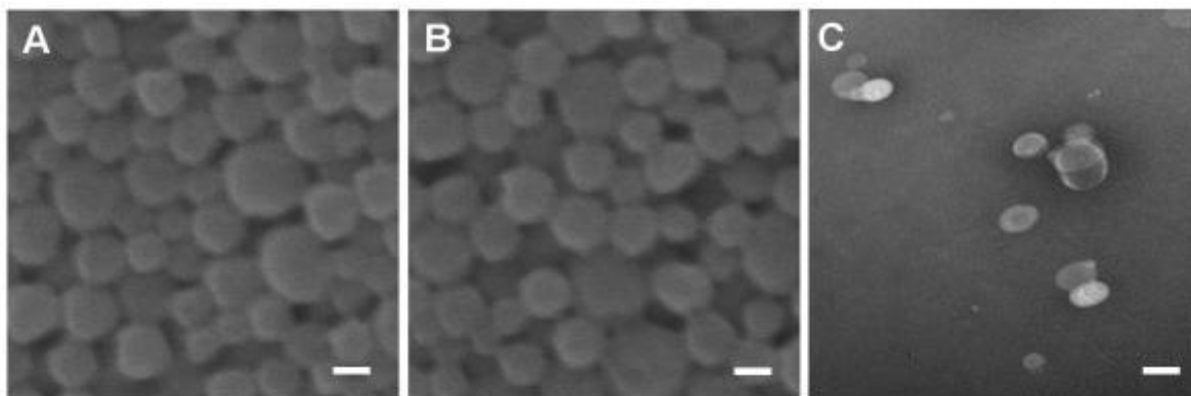


Figure 2.4. Scanning Electron Microscopy (SEM) images of (A) PEI-RITC-encapsulated PEG-PLGA NPs and (B) PLGA NPs, scale bar = 100 nm. (C) A Transmission Electron Microscopy (TEM) image of PEI-RITC-encapsulated liposomes, scale bar = 100 nm (*partially acquired by Ryan M. Pearson*).

2.3.3 Controlled release of PEI-RITC-encapsulated nanohybrids

Given that our hypothesis of the nanohybrid design is to temporally control cytotoxicity and cellular interactions through controlled release of the PEI conjugates, we first investigated the release kinetics of PEI-RITC from the three nanohybrid systems. The controlled release of PEI-RITC from the nanohybrids was studied by monitoring release profiles in buffers at pH 7.4 and 4.0, as shown in Figure 2.5.

Polymeric NP-based nanohybrids showed slow, sustained release profiles that are typical of degradable polymers, without significant initial burst release. More than one mechanism contributing to drug release from polymeric NPs have been reported, for example, dissolution, surface desorption, diffusion through polymer pores or water-swollen polymer, and surface/bulk erosion of polymer matrix [24-26]. Although no significant burst release effect was observed, the PEI-RITC release rate from PEG-PLGA and PLGA NPs was faster within the first 24 h, which can be attributed to

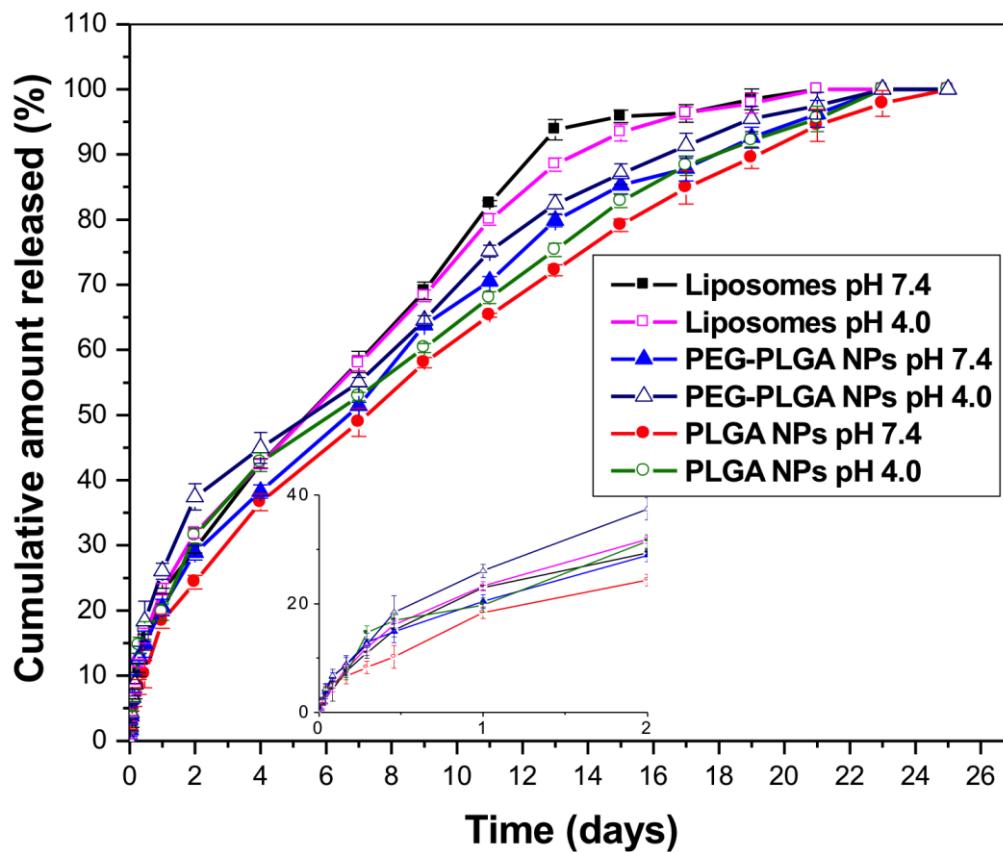


Figure 2.5. Release profiles of PEI-RITC from the three nanohybrids in PBS buffer with pH 7.4 and acetate buffer with pH 4.0 at 37 °C. Little to no burst release was observed across all nanohybrids, with a sustained release profile up to 23 days. The overall release behavior was faster in pH 4.0 compared to pH 7.4 between the same type of nanohybrid formulation. The inset represents the zoomed-in release profiles for the first 2 days.

desorption of PEI-RITC that was located near the surface of the particles. Afterwards, the primary mechanism likely becomes diffusion through small channels formed from bulk degradation of the copolymers. PEG-PLGA NPs displayed a higher release rate compared to PLGA NPs, attributable to the hydrophilic nature of the PEG block, which facilitates water penetration and subsequent hydrolysis of the polymer [27, 28]. As for the liposomes, release was faster within the first few hours, likely due to PEI-RITC

adsorbed on or encapsulated near the liposome surface, followed by a sustained release behavior [29]. In addition, PEI-RITC release occurred faster in acidic pH than in pH 7.4 when comparing the same type of nanohybrid system, which is expected since strongly acidic or basic environments can accelerate polymer degradation [30].

2.3.4 Kinetically controlled cytotoxicity of PEI-RITC-encapsulated nanohybrids

Although various mechanisms have been proposed, it is generally accepted that cellular internalization and cytotoxicity of cationic polymers are closely related to each other [31-35]. One of the proposed mechanisms of toxicity of cationic polymers was described by Hong et al. as being a consequence of nanoscale hole formation in the cell membranes [8, 9, 36, 37]. The nanoscale pores increased membrane permeability as observed by leakage of cytosolic enzymes and diffusion of small molecular probes into and out of cells. In this study, we investigated the cytotoxic concentration range of PEI-RITC and the three nanohybrids at extended incubation hours. Figure 2.6 shows the concentration effect of PEI-RITC and the nanohybrids on the viability of MCF-7 cells as a function of time. At earlier time points (1 and 4 h, Figure 2.6(A) and Figure 2.6(B), respectively), the nanohybrids were significantly less toxic to MCF-7 cells than unencapsulated PEI-RITC, even at high PEI-RITC concentrations of 10-30 $\mu\text{g}/\text{mL}$. Note that it was previously shown that PEI at a concentration of $>12 \mu\text{g}/\text{mL}$ causes significant cell death after 4 h exposure to the cells [36]. This temporal difference in inducing cytotoxicity can indirectly reflect the differences in rates of PEI-RITC release and internalization from those nanohybrids as compared to unencapsulated PEI-RITC. Within the first few hours of incubation, most of the PEI-RITC in the nanohybrids is still entrapped within either polymeric NPs or liposomes, which shield it from direct contact

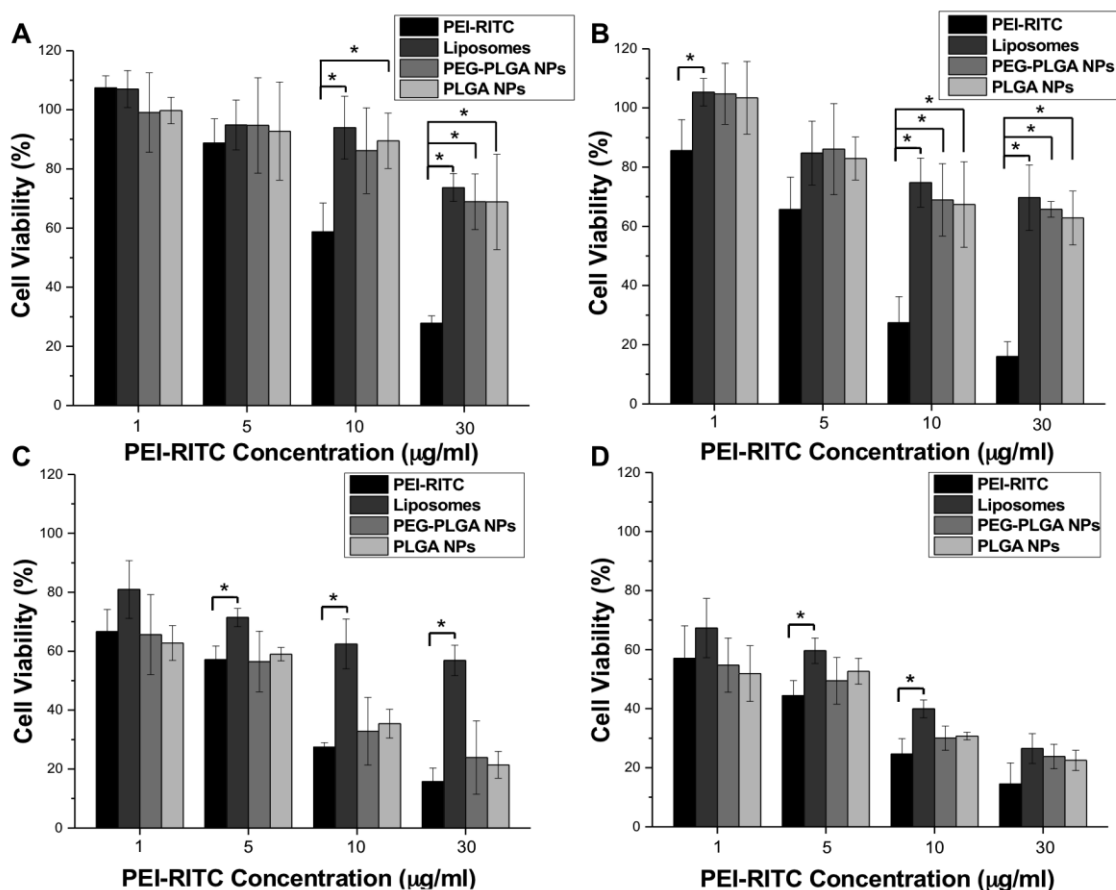


Figure 2.6. Cytotoxicity of PEI-RITC and the three nanohybrids after incubation with MCF-7 cells for (A) 1 h, (B) 4 h, (C) 24 h, and (D) 48 h. PEI-RITC exhibits cytotoxicity in a concentration and incubation time dependent manner whereas all nanohybrids show a marked decrease in cytotoxicity kinetics. After 48 h of treatment, all nanohybrids become comparatively toxic to PEI-RITC. *denotes statistical significance ($p < 0.05$) between PEI-RITC and the three nanohybrids, based on a 1-way ANOVA followed by Tukey's post hoc test.

with cell membranes. As the incubation time increases, more PEI-RITC is released, which in turn increases the amount of PEI-RITC in direct contact with cells, rendering them more susceptible to its toxicity. After 48 h incubation, however, all nanohybrids exhibited similar cytotoxicity (Figure 2.6(D)), indicating that PEI-RITC was almost completely released, internalized into the cells, and induced cytotoxicity. Alternatively,

this may have been due to the proliferation of residual viable cells, which caused the cytotoxic effects of PEI to even out. Interestingly, among the three nanohybrids, the liposome-based one showed the most protective effect against PEI-RITC toxicity, particularly after 4 and 24 h (Figure 2.6(B) and Figure 2.6(C)). This may be attributed to the difference in the internalization mechanism between liposome- and polymeric NP-based systems, since cell internalization of liposomes may occur through endocytosis, membrane fusion, and other mechanisms [15], allowing them to transfer PEI-RITC without direct contact with the cell membrane.

2.3.5 Kinetic control over cellular uptake of PEI-RITC-encapsulated nanohybrids

Next, we investigated how the controlled release of PEI-RITC and the type of the protective layers (either polymeric NPs or liposomes) affect the rate of cellular uptake of the nanohybrids. Throughout this particular study, a low concentration of PEI-RITC and the three nanohybrid systems was used (0.5 $\mu\text{g/mL}$ based on PEI-RITC) to assure that the observations are a result of non-cytotoxic interactions between the nanomaterials and cells, as opposed to cell death.

As demonstrated in Figure 2.7, images obtained using confocal laser scanning microscopy (CLSM) qualitatively reveal that the fastest uptake was observed for unencapsulated PEI-RITC, followed by in order of liposomes, PEG-PLGA NPs, and PLGA NPs. Red, green, and blue fluorescence channels are respectively from PEI-RITC, cell membranes stained by WGA-AF488 conjugate, and nuclei stained by DAPI. The CLSM observation was further supported by quantitative results using a fluorescence activated cell sorter (FACS). As shown in Figure 2.8, following incubation up to 24 h, and in accordance with the CLSM images, the average fluorescence was

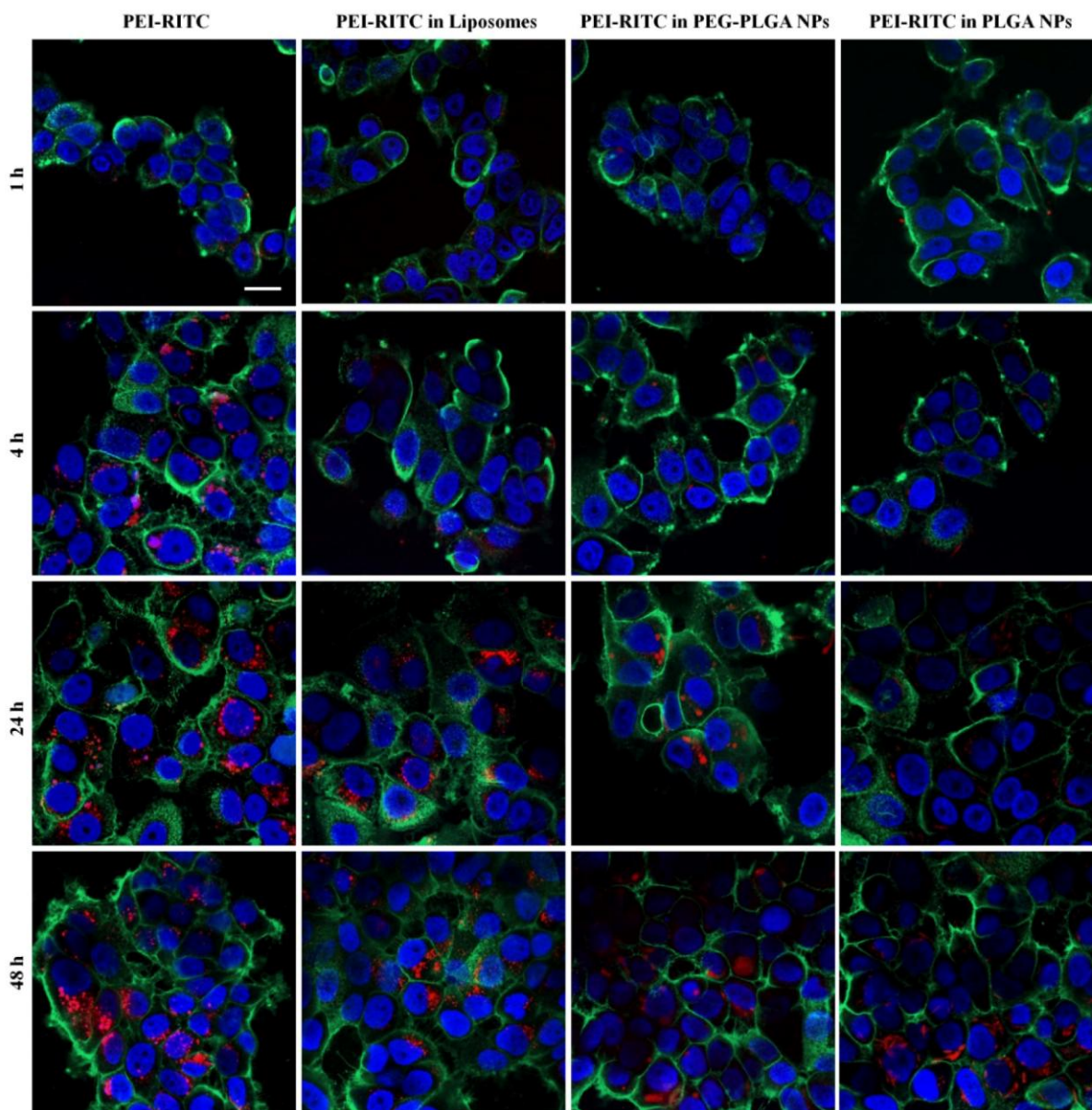


Figure 2.7. CLSM images of MCF-7 cells following treatment with PEI-RITC and the three nanohybrids (PEI-RITC-encapsulated liposomes, PEG-PLGA NPs, and PLGA NPs) all at a concentration of 0.5 $\mu\text{g}/\text{mL}$ based on PEI-RITC for 1 h, 4 h, 24 h, and 48 h (red: PEI-RITC, blue: cell nuclei stained by DAPI, green: cellular membrane stained by WGA-AF 488; scale bar: 20 μm).

highest for unencapsulated PEI-RITC, followed by liposomes, PEG-PLGA NPs, and PLGA NPs. After 48 h of incubation, all of the materials (PEI-RITC and the three

nanohybrids) displayed similar fluorescence intensities, which is consistent with the cytotoxicity (Figure 2.6) and confocal data (Figure 2.7).

The fast uptake of PEI is not surprising, as PEI is known to spontaneously interact with cells via adsorption on the cell surface and internalization into the cells [36]. It has been recently suggested that the biodegradable NPs do not enter cells but rather deliver their cargo via extracellular release or contact-based transfer [38, 39]. This

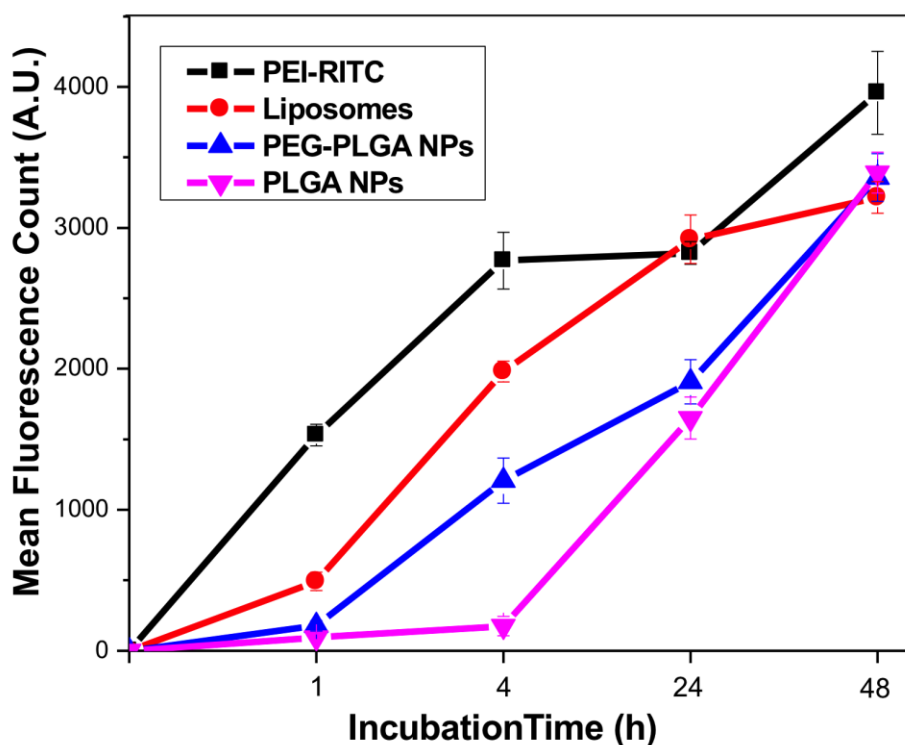


Figure 2.8. Mean fluorescence following treatment of MCF-7 cells with PEI-RITC and the three nanohybrids at a concentration of 0.5 $\mu\text{g}/\text{mL}$ based on PEI-RITC up to 48 h. Kinetic control over PEI-RITC internalization is further confirmed as unencapsulated PEI-RITC shows the fastest uptake, as indicated by having the highest fluorescence count compared to the three nanohybrid formulations. Cell binding and uptake of the nanohybrids occur in the order of liposomes, PEG-PLGA NPs, and PLGA NPs, which is consistent with the confocal data shown in Figure 2.7.

could explain the slow kinetics in PEI-RITC uptake from polymeric NPs observed in this study, since the NP-based nanohybrids would have to go through polymer degradation, release, and subsequent internalization of PEI-RITC into the cell. As for the liposome-based nanohybrid system, liposomes exhibited slowest cytotoxicity kinetics (Figure 2.6), and yet fastest cellular uptake kinetics among the three nanohybrid systems, (Figure 2.7 and Figure 2.8). This set of observations indicates that, unlike the NP-based nanohybrids, cellular internalization of PEI-RITC upon release is not the only mechanism for cell entry of the liposome-based nanohybrid. In fact, upon adsorption onto the cell surface, it is previously reported that liposomes internalize into the cell through membrane fusion and/or endocytosis [15]. The co-existence of the internalization mechanisms likely allows relatively fast uptake kinetics with reduced cytotoxicity at early time points.

Even though they displayed similar release kinetics in buffer, PLGA NPs had a much slower uptake rate than their PEG-PLGA counterparts. Significant uptake of PLGA NPs was only observed after 24 h, with complete internalization after 48 h. This is again probably due to the hydrophobic nature of the PLGA copolymer, which impedes degradation and subsequent PEI-RITC release [28]. The presence of the cellular environment has accentuated the difference between the two types of polymeric NPs, with PEG-PLGA NPs displaying an intermediate uptake rate between the liposome- and PLGA-based nanohybrids. The PEG-PLGA NPs started to show red signals after 4 h of incubation, with complete internalization within 24 h. Although our results indicate that the PEI-RITC internalization from the polymeric NPs largely depends on the degradation and release profiles, it should be noted that other mechanisms such as

endocytosis of the whole NPs may co-exist [40]. As seen in Figure 2.5, degradation of NP-based nanohybrids may not occur within 2 days, and the red fluorescence observed in the CLSM images (Figure 2.7) may partially come from the nanoparticles that have been associated with the cells as an intact form. However, it is obvious that the release kinetics in buffer did not follow the same order or rate observed in the cytotoxicity or the cellular uptake studies (Figures 6, 7 and 8). This could be explained by the difference in the microenvironment surrounding the nanohybrids. For the release test shown in Figure 2.5, all three formulations were suspended in either PBS or acetate buffer only, making the environment markedly different than in the presence of cells, as in the subsequent cytotoxicity and cell uptake experiments (Figures 7, 8 and 9). Due to the presence of enzymes and proteins, as well as the difference in cellular uptake mechanisms, the differences in release kinetics across the nanohybrids were more accentuated when compared to the release in buffers.

One can argue that our results obtained in the absence of therapeutic agents or genetic materials, i.e. pDNA or siRNA, may not directly represent the biological properties of the nanohybrid systems when used for drug or gene delivery. However, the aim of this preliminary work is to establish kinetic control over cytotoxicity and cellular interactions of PEI. The results shown in this paper reflect the highest possible toxicity of PEI, providing a worst-case scenario in terms of potential toxicity of the delivery system itself. In case of active drug compounds, which will be covalently linked to the primary amine groups of PEI, we expect the physicochemical and biological behavior of the system to be very similar to what we have described, since the presence of RITC molecules on PEI also serves as a model for small molecule drugs. As for

complexation with genetic materials, which lowers net positive charges, overall toxicity of PEI would likely be reduced [41, 42]. It is expected that the presence of genetic material will likely affect the overall particle size of the nanohybrid systems. However, with proper optimization of the encapsulation process, it is possible to obtain fine control over the size. Furthermore, given that PEI is known to spontaneously interact with cells, facilitating cellular entry [36, 43, 44], it offers an excellent model system for multifunctional vectors without preparation of complex structures with cytotoxic drugs and targeting agents. Taken together, successful preparation of the three nanohybrid systems (Figure 2.4 and Table 2.1), controlled release of encapsulated PEI (Figure 2.5), kinetically controlled cytotoxicity (Figure 2.6) and cellular internalization (Figure 2.7 and Figure 2.8) all satisfactorily prove that we have successfully achieved the objectives of this study.

2.4 CONCLUSION

Herein we report on PEI-biodegradable polymer and PEI-liposome nanohybrid delivery systems with particle sizes suitable for passive targeting and with temporally controlled cytotoxicity, release and cellular uptake kinetics. This work is the first step towards optimization of a new targeted drug delivery system that can be tailored to achieve the desired release and cellular uptake profiles as a platform for controlled drug delivery applications.

2.5 REFERENCES

1. Nori, A. and J. Kopecek, *Intracellular targeting of polymer-bound drugs for cancer chemotherapy*. Adv. Drug Deliver. Rev., 2005. **57**(4): p. 609-636.
2. Patri, A.K., I.J. Majoros, and J.R. Baker, *Dendritic polymer macromolecular carriers for drug delivery*. Curr. Opin. Chem. Biol., 2002. **6**(4): p. 466-471.
3. Verma, I.M. and N. Somia, *Gene therapy - promises, problems and prospects*. Nature, 1997. **389**(6648): p. 239-242.
4. Boussif, O., et al., *A Versatile vector for gene and oligonucleotide transfer into cells in culture and in vivo - Polyethylenimine* P. Natl. Acad. Sci. USA, 1995. **92**(16): p. 7297-7301.
5. Gebhart, C.L. and A.V. Kabanov, *Evaluation of polyplexes as gene transfer agents*. J. Control. Release, 2001. **73**(2-3): p. 401-416.
6. Akinc, A., et al., *Exploring polyethylenimine-mediated DNA transfection and the proton sponge hypothesis*. J. Gene Med., 2005. **7**(5): p. 657-663.
7. Urban-Klein, B., et al., *RNAi-mediated gene-targeting through systemic application of polyethylenimine (PEI)-complexed siRNA in vivo*. Gene Ther., 2005. **12**(5): p. 461-466.
8. Hong, S., et al., *The role of ganglioside GM(1) in cellular internalization mechanisms of poly(amidoamine) dendrimers*. Bioconjugate Chem., 2009. **20**(8): p. 1503-1513.

9. Hong, S., et al., *Interaction of poly(amidoamine) dendrimers with supported lipid bilayers and cells: Hole formation and the relation to transport*. *Bioconjugate Chem.*, 2004. **15**(4): p. 774-782.
10. Oupicky, D., M. Ogris, and L.W. Seymour, *Development of long-circulating polyelectrolyte complexes for systemic delivery of genes*. *J. Drug Target.*, 2002. **10**(2): p. 93-98.
11. Matsumura, Y. and H. Maeda, *A New concept for macromolecular therapeutics in cancer chemotherapy - Mechanism of tumoritropic accumulation of proteins and the antitumor agent SMANCS*. *Cancer Res.*, 1986. **46**(12): p. 6387-6392.
12. Yuan, F., et al., *Vascular permeability in a human tumor xenograft - molecular size dependence and cutoff size* *Cancer Res.*, 1995. **55**(17): p. 3752-3756.
13. Peer, D., et al., *Nanocarriers as an emerging platform for cancer therapy*. *Nat. Nanotechnol.*, 2007. **2**(12): p. 751-760.
14. Couvreur, P. and C. Vauthier, *Nanotechnology: Intelligent design to treat complex disease*. *Pharm. Res.*, 2006. **23**(7): p. 1417-1450.
15. Torchilin, V.P., *Recent advances with liposomes as pharmaceutical carriers*. *Nat. Rev. Drug Discov.*, 2005. **4**(2): p. 145-160.
16. Ko, Y.T., R. Bhattacharya, and U. Bickel, *Liposome encapsulated polyethylenimine/ODN polyplexes for brain targeting*. *J. Control. Release*, 2009. **133**(3): p. 230-237.

17. Kim, I.S., et al., *Physicochemical characterization of poly(L-lactic acid) and poly(D,L-lactide-co-glycolide) nanoparticles with polyethylenimine as gene delivery carrier*. *Int. J. Pharm.*, 2005. **298**(1): p. 255-262.
18. Son, S. and W.J. Kim, *Biodegradable nanoparticles modified by branched polyethylenimine for plasmid DNA delivery*. *Biomaterials*, 2010. **31**(1): p. 134-143.
19. Yoo, H.S. and T.G. Park, *Biodegradable polymeric micelles composed of doxorubicin conjugated PLGA-PEG block copolymer*. *J. Control. Release*, 2001. **70**(1-2): p. 63-70.
20. Perez, C., et al., *Poly(lactic acid)-poly(ethylene glycol) nanoparticles as new carriers for the delivery of plasmid DNA*. *J. Control. Release*, 2001. **75**(1-2): p. 211-224.
21. Son, S., et al., *Optimized stability retention of a monoclonal antibody in the PLGA nanoparticles*. *Int. J. Pharm.*, 2009. **368**(1-2): p. 178-185.
22. Vauthier, C. and K. Bouchemal, *Methods for the preparation and manufacture of polymeric nanoparticles*. *Pharm. Res.*, 2009. **26**(5): p. 1025-1058.
23. Panyam, J., et al., *Rapid endo-lysosomal escape of poly(DL-lactide-co-glycolide) nanoparticles: implications for drug and gene delivery*. *FASEB J.*, 2002. **16**(10): p. 1217-1226.

24. Crotts, G., H. Sah, and T.G. Park, *Adsorption determines in-vitro protein release rate from biodegradable microspheres: Quantitative analysis of surface area during degradation*. J. Control. Release, 1997. **47**(1): p. 101-111.
25. Fu, Y. and W.J. Kao, *Drug release kinetics and transport mechanisms of non-degradable and degradable polymeric delivery systems*. Expert Opin. Drug Del., 2010. **7**(4): p. 429-444.
26. Polakovic, M., et al., *Lidocaine loaded biodegradable nanospheres II. Modelling of drug release*. J. Control. Release, 1999. **60**(2-3): p. 169-177.
27. Penco, M., et al., *Degradation behaviour of block copolymers containing poly(lactic-glycolic acid) and poly(ethylene glycol) segments*. Biomaterials, 1996. **17**(16): p. 1583-1590.
28. Avgoustakis, K., et al., *PLGA-mPEG nanoparticles of cisplatin: in vitro nanoparticle degradation, in vitro drug release and in Vivo drug residence in blood properties*. J. Control. Release, 2002. **79**(1-3): p. 123-135.
29. Atyabi, F., et al., *Preparation of pegylated nano-liposomal formulation containing SN-38: In vitro characterization and in vivo biodistribution in mice*. Acta Pharmaceut., 2009. **59**(2): p. 133-144.
30. Faisant, N., et al., *Effects of the type of release medium on drug release from PLGA-based microparticles: Experiment and theory*. Int. J. Pharm., 2006. **314**(2): p. 189-197.
31. Jevprasesphant, R., et al., *Transport of dendrimer nanocarriers through epithelial cells via the transcellular route*. J. Control. Release, 2004. **97**(2): p. 259-267.

32. Kopatz, I., J.S. Remy, and J.P. Behr, *A model for non-viral gene delivery: through syndecan adhesion molecules and powered by actin*. J. Gene Med., 2004. **6**(7): p. 769-776.
33. Manunta, M., et al., *Gene delivery by dendrimers operates via different pathways in different cells, but is enhanced by the presence of caveolin*. J. Immunol. Methods, 2006. **314**(1-2): p. 134-146.
34. Seib, F.P., A.T. Jones, and R. Duncan, *Comparison of the endocytic properties of linear and branched PEIs, and cationic PAMAM dendrimers in B16f10 melanoma cells*. J. Control. Release, 2007. **117**(3): p. 291-300.
35. Kitchens, K.M., et al., *Endocytosis inhibitors prevent poly(amidoamine) dendrimer internalization and permeability across Caco-2 cells*. Mol. Pharm., 2008. **5**(2): p. 364-369.
36. Hong, S., et al., *Interaction of polycationic polymers with supported lipid bilayers and cells: Nanoscale hole formation and enhanced membrane permeability*. Bioconjugate Chem., 2006. **17**(3): p. 728-734.
37. Leroueil, P.R., et al., *Nanoparticle interaction with biological membranes: Does nanotechnology present a janus face?* Acc. Chem. Res., 2007. **40**(5): p. 335-342.
38. Chen, H., et al., *Release of hydrophobic molecules from polymer micelles into cell membranes revealed by Forster resonance energy transfer imaging*. P. Natl. Acad. Sci. USA, 2008. **105**(18): p. 6596-6601.
39. Xu, P.S., et al., *Intracellular Drug Delivery by Poly(lactic-co-glycolic acid) Nanoparticles, Revisited*. Mol. Pharm., 2009. **6**(1): p. 190-201.

40. Vasir, J.K. and V. Labhasetwar, *Biodegradable nanoparticles for cytosolic delivery of therapeutics*. *Adv. Drug Deliver. Rev.*, 2007. **59**(8): p. 718-728.
41. Kunath, K., et al., *Low-molecular-weight polyethylenimine as a non-viral vector for DNA delivery: comparison of physicochemical properties, transfection efficiency and in vivo distribution with high-molecular-weight polyethylenimine*. *J. Control. Release*, 2003. **89**(1): p. 113-125.
42. Zhao, Q.Q., et al., *N/P ratio significantly influences the transfection efficiency and cytotoxicity of a polyethylenimine/chitosan/DNA complex*. *Biol. Pharm. Bull.*, 2009. **32**(4): p. 706-710.
43. Neu, M., D. Fischer, and T. Kissel, *Recent advances in rational gene transfer vector design based on poly(ethylene imine) and its derivatives*. *J. Gene Med.*, 2005. **7**(8): p. 992-1009.
44. Fischer, D., et al., *In vitro cytotoxicity testing of polycations: influence of polymer structure on cell viability and hemolysis*. *Biomaterials*, 2003. **24**(7): p. 1121-1131.

CHAPTER 3

TEMPORAL CONTROL OVER CELLULAR TARGETING THROUGH HYBRIDIZATION OF FOLATE-TARGETED DENDRIMERS AND PEG-PLA NANOPARTICLES*

3.1 INTRODUCTION

Polymeric nanocarriers have been widely investigated as a versatile platform for controlled drug delivery to target tissues [1-3]. Among many polymeric materials, poly(amidoamine) (PAMAM) dendrimers hold great promise due to their well-controlled structure and multifunctionality [4-6]. Through conjugation of targeting ligands, dendritic nanodevices (5–10 nm in diameter) have been shown to be effective in achieving selective tumor targeting through specific ligand-receptor interactions, i.e., active targeting [7-9]. On the other hand, larger nanomaterials such as polymeric nanoparticles (NPs) and liposomes are well suited to exploit another targeting strategy termed passive targeting. By utilizing the characteristic tumor biology highlighted by the enhanced permeability and retention (EPR) effect [10, 11], these size-controlled nanocarriers (typically 50-200 nm in diameter) have shown selective accumulation in tumor sites [12, 13].

Each of the two targeting strategies, however, suffers from several limitations [14, 15]. Despite the enhanced active targeting efficacy of dendrimers, due to their

*Reproduced with permission from Sunoqrot, S.; Bae, J. W.; Pearson, R. M.; Shyu, K.; Liu, Y.; Kim, D.; Hong, S. *Biomacromolecules* **2012**, *13*, 1223-1230. Copyright 2012 American Chemical Society.

increased molecular flexibility that facilitates the multivalent binding effect [16, 17], their small size limits their passive targeting capability [18]. Targeted dendrimers with surface-conjugated folic acid (FA) have also been associated with off-target delivery and rapid clearance *in vivo* [19]. In contrast, the relatively large size of the NPs hinders their effective penetration into tumor sites due to limited diffusivity [20]. The rigidity of the actively targeted NPs compared to the flexible dendrimers can also prevent the full utilization of the multivalent binding effect, leading to much lower binding avidities (~100-fold enhancement over free FA) [20] compared to the dendritic nanodevices (up to 170,000-fold enhancement) [16, 21].

Nanocarriers that combine passive targeting based on size control and active targeting through surface-immobilized ligands have been reported for a variety of systems including liposomes [22], micelles [23], and polymeric NPs [24]. However, these approaches do not fully address the issues of decreased circulation times and rapid clearance. For example, studies have shown that the prolonged circulation times achieved by PEGylated nanocarriers are compromised by the addition of targeting ligands to the outer surface [25-27]. These systems also lack the control over the targeting kinetics, due to the surface-exposed targeting ligands. To address these issues, we have designed novel multi-scale hybrid NP systems, or nanohybrids, that combine FA-targeted dendrimer conjugates with polymeric NPs to exploit the strengths and to address the limitations of each individual nanocarrier. This system is based on our previously reported hybrid NPs where poly(ethylenimine)-rhodamine (PEI-RHO) conjugates were encapsulated within protective outer layers of biodegradable polymer-based NPs or biocompatible liposomes [28]. This hybrid design is unique in that the

biologically active polymer conjugates (PEI-RHO) are protected by an outer shell of biodegradable polymers, or biocompatible lipids, allowing precise control over the cellular interaction kinetics of the bioactive polymers.

In this study, the FA-targeted generation 4 (G4) PAMAM dendrimers were encapsulated into biodegradable poly(ethylene glycol)-*b*-poly(*D,L*-lactide) (PEG-PLA) NPs to produce nanohybrids. Through this design, we present a proof-of-concept study where kinetic control over the selective interactions of FA-targeted dendrimers with folate receptor (FR)-overexpressing KB cells (KB FR⁺) was achieved *in vitro*. The design rationale for these nanohybrids is to ultimately achieve sequential utilization of passive and active targeting, i.e., passive accumulation at the tumor site by the controlled size of the nanohybrids, followed by active targeting to individual tumor cells by the dendrimers upon their release from the NPs. This paper progresses by testing three hypotheses: 1) multifunctional G4 PAMAM dendrimers can be successfully encapsulated into biodegradable PEG-PLA copolymers to form nanohybrids; 2) the cellular interaction and targeting kinetics of FA-targeted dendrimers can be temporally controlled through the nanohybrid platform; and 3) the targeting kinetics can be further modulated by controlling the molecular weight (MW) of the biodegradable encapsulating copolymers. Here we report, for the first time to our knowledge, a nanohybrid design that presents a promising delivery platform to enable precise control over its cellular targeting and release kinetics, which has the great potential to overcome the limitations of the existing nanocarrier systems.

3.2 EXPERIMENTAL SECTION

3.2.1 Materials

Generation 4 (G4) PAMAM dendrimer, *N*-hydroxysuccinimide-rhodamine B (NHS-RHO), folic acid (FA), *N*-(3-dimethylaminopropyl)-*N'*-ethylcarbodiimide hydrochloride (EDC), *N*-hydroxysuccinimide (NHS), glycidol, tin(II)2-ethylhexanoate, poly(ethylene glycol) monomethyl ether (mPEG) (MW 5,000 Da), poly(vinyl alcohol) (PVA, 87-89% hydrolyzed, MW 13,000-23,000 Da), and dichloromethane (DCM), were all obtained from Sigma-Aldrich (St. Louis, MO). *D,L*-lactide was purchased from Polysciences Inc. (Warrington, PA). Poly(ethylene glycol)-*b*-poly(lactide) (MW 5,000-*b*-23,000) was obtained from Polymer Source (Quebec, Canada). All other chemicals used in this study were purchased from Sigma-Aldrich unless specified otherwise.

3.2.2 Preparation of a series of G4 PAMAM dendrimer conjugates

G4 PAMAM dendrimers were fluorescently labeled by conjugation with NHS-RHO as described earlier [28]. Amine-terminated G4 (G4-NH₂, 30 mg, 2.0 × 10⁻⁶ mol) was dissolved in 4 mL sodium bicarbonate buffer (pH 9.0), to which 500 μL of NHS-RHO (1.1 × 10⁻⁵ mol) in DMSO was added, and the reaction mixture was vigorously stirred at room temperature (RT) for 24 h. Unreacted NHS-RHO was removed by membrane dialysis using Spectra/Por dialysis membrane (MWCO 3,500, Spectrum Laboratories Inc., Rancho Dominguez, CA) in excess deionized distilled water (ddH₂O) for two days. The purified G4-RHO-NH₂ conjugates were lyophilized over 2 days using a Labconco FreeZone 4.5 system (Kansas City, MO) and stored at -20 °C.

Next, FA was conjugated to G4-RHO-NH₂ as described previously [4, 16]. Briefly, FA (3.1 mg, 7.0 × 10⁻⁶ mol) was activated by EDC (13.4 mg, 7.0 × 10⁻⁵ mol) and NHS (8.0 mg, 7.0 × 10⁻⁵ mol) in 1.5 mL DMSO through vigorous stirring at RT for 1 h. The activated FA solution was added dropwise to 20 mg of G4-RHO-NH₂ (1.4 × 10⁻⁶

mol) in 1 mL of ddH₂O, followed by reaction under vigorous stirring at RT for 24 h. The product was purified by membrane dialysis as described above, resulting in G4-RHO-FA-NH₂. The remaining primary amine groups of both G4-RHO-FA-NH₂ and G4-RHO-NH₂ were hydroxylated to minimize non-specific, electrostatic interactions with cell membranes [29, 30], resulting in fully hydroxylated G4-RHO-FA-OH and G4-RHO-OH.

3.2.3. Synthesis of PEG-PLA copolymers

PEG-PLA was synthesized by ring opening polymerization of *D,L*-lactide as previously described [31]. mPEG (100 mg and 150 mg) was transferred to a 3-neck round bottom flask and dried under vacuum for 2 h. *D,L*-lactide (1.0 g) and tin(II) 2-ethylhexanoate (30 mg) were added to the flask and dried under vacuum for an additional 1 h. The flask was placed in an oil bath that was pre-heated to 120 °C, and the polymerization was carried out under vigorous stirring for 4 h. The flask was then cooled to RT and 10 mL of DCM was added to dissolve the product. DCM was partially evaporated to adjust the solution viscosity, followed by precipitation in cold diethyl ether and vacuum drying overnight. The two feed ratios at 0.1:1 and 0.15:1 of mPEG:*D,L*-lactide resulted in PEG-PLA copolymers with MWs of 5K-45K and 5K-30K, respectively.

3.2.4 Encapsulation of the dendrimer conjugates into PEG-PLA nanoparticles

The hybrid NPs containing the various dendrimer conjugates were prepared using a double emulsion method as we previously described [28]. For example, G4-RHO-FA-OH (100 µL, 1 mg/mL in ddH₂O) was added to 20 mg of either PEG5K-PLA23K, PEG5K-PLA30K, or PEG5K-PLA45K in 1 mL of DCM, and the mixture was sonicated for 1 min using a Misonix XL Ultrasonic Processor (100% duty cycle, 475 W, 1/8" tip, QSonica, LLC, Newtown, CT). Two milliliters of 3% aqueous PVA solution was

then added to the mixture, followed by additional sonication for 1 min. The double emulsion was poured into 20 mL of 0.3% PVA in ddH₂O, and vigorously stirred at RT for 24 h to evaporate DCM. The resulting aqueous solution was transferred to Nalgene high-speed centrifuge tubes (Fisher Scientific, Pittsburg, PA) to remove PVA and unencapsulated G4-RHO-FA-OH by ultracentrifugation at 20,000 rpm for 30 min using a Beckman Avanti J25 Centrifuge (Beckman Coulter, Brea, CA). After washing the NPs five times with ddH₂O, the pellet was resuspended in ddH₂O, lyophilized over 2 days, and stored at -20 °C. All other dendrimer conjugates were encapsulated into PEG5K-PLA45K using the same method.

3.2.5 Structure confirmation and size/surface charge measurements

All dendrimer conjugates and PEG-PLA copolymers were characterized by ¹H NMR using a 400 MHz Bruker DPX-400 spectrometer (Bruker BioSpin Corp., Billerica, MA) as described in our earlier publication [32]. Particle size (diameter, nm) and surface charge (zeta potential, mV) of the conjugates and the nanohybrids were measured in triplicates by quasi-elastic laser light scattering using a Nicomp 380 Zeta Potential/Particle Sizer (Particle Sizing Systems, Santa Barbara, CA) in ddH₂O. The measurements were performed using samples that were suspended in ddH₂O at a concentration of 100 µg/mL, filtered through a 0.45 µm syringe filter, and briefly vortexed prior to each measurement.

3.2.6 Loading efficiencies of the dendrimer-encapsulated nanohybrids

Loading was defined as the dendrimer conjugate content in the nanohybrids [28]. Five milligrams of each nanohybrid formulation were completely dissolved in 1 mL of 0.5 M NaOH, followed by filtration through a 0.45 µm syringe filter. The fluorescence

intensity from the filtrates was then measured using a SpectraMAX GeminiXS microplate spectrofluorometer (Molecular Devices, Sunnyvale, CA). The amount of the dendrimer conjugates in the filtrates was determined from a standard curve of each conjugate's fluorescence versus concentration in 0.5 M NaOH. Loading was expressed as μg dendrimer conjugates per mg copolymer. Loading efficiency was defined as the ratio of the actual loading obtained to the theoretical loading.

3.2.7 Morphology of the nanohybrids: SEM Observation

Surface morphology of the nanohybrids was examined by scanning electron microscopy (SEM) using a JEOL-JSM 6320F field emission microscope (JEOL USA, Peabody, MA) as previously described [28]. Samples were sputter-coated with Pt/Pd at a coating thickness of 6 nm (Polaron E5100 sputter coater system, Polaron, UK) and then visualized at an accelerating voltage of 4.0 mV and 8.0 mm working distance.

3.2.8 Release profiles of the G4-RHO-FA-OH-encapsulated nanohybrids

The release behaviors of G4-RHO-FA-OH from the prepared nanohybrids using different PEG-PLA copolymers (PEG5K-PLA23K (NP23), PEG5K-PLA30K (NP30), and PEG5K-PLA45K (NP45)) were studied in PBS and RPMI 1640 [28]. Five milligrams of each nanohybrid formulation were placed in microcentrifuge tubes and dispersed in 1 mL of either PBS (pH 7.4) or RPMI 1640 medium supplemented with 10% FBS in triplicates, and the solutions were placed in a shaking water bath (37 °C, 100 rpm). At various time points (1, 2, 4, 6, 8, 12, 24, 48 h; every other day thereafter), solutions were centrifuged at 10,000 rpm for 5 min, and the supernatants were collected. The nanohybrids were then redispersed in fresh PBS or RPMI 1640 medium and placed back in the water bath. The fluorescence of the supernatants was measured and the

cumulative amount of G4-RHO-FA-OH released over time was determined from a standard curve of G4-RHO-FA-OH fluorescence versus concentration in PBS or RPMI 1640 medium.

3.2.9 Cellular interactions of the nanohybrids: CLSM and FACS measurements

The KB cell line was obtained from ATCC (Manassas, VA) and grown continuously as a monolayer in FA-deficient GIBCO RPMI 1640 medium (Invitrogen Corporation, Carlsbad, CA) to induce the overexpression of FR, under the same conditions that we previously reported [16]. For confocal imaging, KB FR⁺ cells were seeded in 4-well chamber slides (Millicell EZ Slide, Millipore, Billerica, MA) at a density of 2.0×10^5 cells/well and incubated in FA-deficient RPMI 1640 for 24 h. The cells were treated with G4-RHO-FA-OH, G4-RHO-NH₂, G4-RHO-OH, and the corresponding nanohybrids in the PEG5K-PLA45K shell (NP45) for 1 h and 4 h, at a concentration of 63 nM based on the dendrimer conjugates in PBS with Ca⁺⁺ and Mg⁺⁺ (Mediatech, Inc., Manassas, VA). Another group of KB FR⁺ was pre-incubated with 1 mM FA in PBS with Ca⁺⁺ and Mg⁺⁺ (from a stock solution of 100 mM FA in DMSO) for 30 min before adding G4-RHO-FA-OH and its NP45 formulation. Additionally, KB cells grown in complete RPMI 1640 (Invitrogen), resulting in FR-down-regulated KB (KB FR⁻), were used as a negative control and incubated with G4-RHO-FA-OH and its NP45 formulation. For the cellular interactions of the nanohybrids with different MWs of PLA, cells were similarly treated with G4-RHO-FA-OH and the corresponding nanohybrids prepared with PEG5K-PLA45K (NP45), PEG5K-PLA30K (NP30), and PEG5K-PLA23K (NP23) for 1, 4, and 8 h. After the treatments, cells were washed with PBS three times and fixed in 500 μ L of 4% paraformaldehyde at RT for 10 min. The fixed cells were treated with

antiphotobleaching mounting media with DAPI (Vector Laboratory Inc., Burlingame, CA), and covered with glass cover slips. Cellular binding and uptake were visualized using a Zeiss LSM 510 confocal laser scanning microscope (CLSM, Carl Zeiss, Germany). The 543 nm line of a 1 mW tunable argon laser was used for excitation of RHO, and a 25 mW diode UV 405 nm laser was used for excitation of DAPI. Emission was filtered at 565-595 nm and 420 nm for RHO and DAPI, respectively. Images were captured using a C-Apochromat 63x/1.2 W corr objective, with the pinhole set to 92 μm for the blue channel and 129 μm for the red channel. The detector gain was adjusted to 620 V for the blue channel and 824 V for the red channel.

For the fluorescence activated cell sorter (FACS) analysis, KB FR⁺ were seeded in 12-well plates at a density of 1.0×10^6 cells/well and incubated in FA-deficient RPMI 1640 medium for 24 h. The cells were then treated under the same conditions described in the confocal observation above. After each incubation period, cells were washed with PBS and then suspended with trypsin/EDTA. Cell suspensions were centrifuged at 3500 rpm for 5 min, resuspended in 500 μL of 1% paraformaldehyde for fixation, and transferred to flow cytometry sample tubes. The fluorescence signal intensities from the samples were measured using a MoFlo cell sorter (BD, Franklin Lakes, NJ) and data analysis was performed using Summit v4.3 software (Dako Colorado, Fort Collins, CO).

3.3 RESULTS AND DISCUSSION

In this study, we conducted a series of experiments to develop a nanohybrid system through encapsulation of targeted dendrimers into polymeric NPs. This novel

platform was designed to achieve kinetically controlled receptor-specific interactions of FA-targeted dendrimers, which can be further modulated by varying MWs of PEG-PLA.

3.3.1 Hybridization of multifunctional G4 PAMAM dendrimers and PEG-PLA NPs

A general overview of the preparation of the hybrid NPs is illustrated in Figure 3.1. First, G4 PAMAM dendrimers were functionalized by sequential conjugation with RHO and FA, followed by hydroxylation of the remaining amine groups, resulting in G4-RHO-FA-OH (Figure 10(A)). Note that the full hydroxylation step is critical to eliminate non-specific interactions between amine-terminated dendrimers and cells [7, 29, 33].

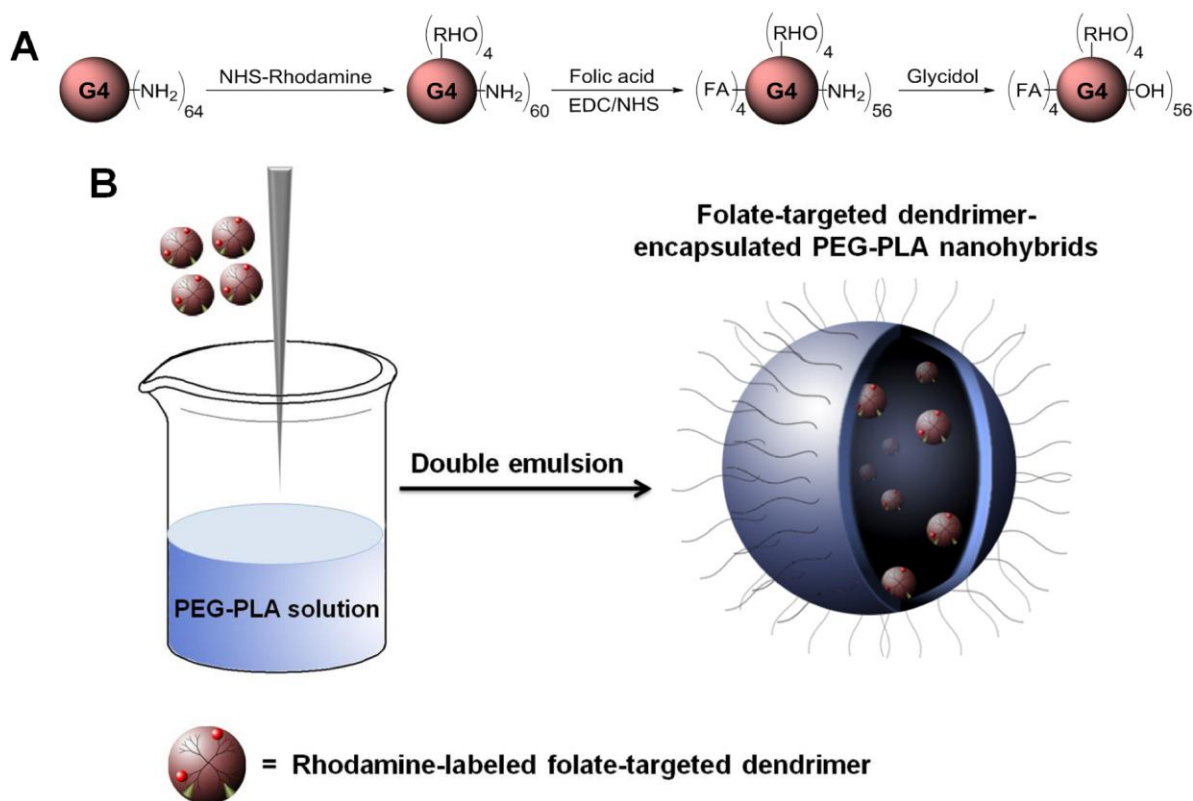


Figure 3.1. Schematic representation of (A) stepwise functionalization of G4 PAMAM dendrimers, and (B) preparation of nanohybrids (*partially contributed by Kevin Shyu*).

The dendrimer conjugates were then encapsulated into PEG-PLA copolymers using the double emulsion method to produce nanohybrids (Figure 10(B)). Conjugation of RHO and FA to the dendrimers and successful end-capping of the amine groups was confirmed using ^1H NMR and zeta potential measurements (Table 3.1 and Figure 3.2).

The ^1H NMR spectra (Figure 3.2) revealed that the conjugates prepared in this study contained approximately 3.9 and 4.3 RHO and FA molecules per dendrimer, respectively. Through various reactions, we prepared G4-RHO-NH₂, G4-RHO-FA-OH, and the control conjugate G4-RHO-OH, to be hybridized with the PEG-PLA copolymers.

PEG-PLA copolymers were synthesized by bulk polymerization of lactide using mPEG5K as the initiator [31]. ^1H NMR was used to confirm the chemical structure of the PEG-PLA copolymers and to estimate the MWs of the PLA block (Figure 3.3). By varying the mPEG:lactide feed ratio, two copolymers with different MWs of PLA were prepared. When the feed ratio of mPEG:lactide was 0.15:1, the MW of PLA was calculated to be 29,800 g/mol, based on the relative integration ratios of peak b around 3.62 ppm (the protons of the ethylene oxide repeating units) to peak c around 5.15 ppm (the lactide repeating units). This copolymer is referred to PEG5K-PLA30K throughout this paper. When the feed ratio of mPEG:lactide was 0.10:1, the MW of PLA was calculated to be 44,900 g/mol, which is referred to as PEG5K-PLA45K. A commercially available PEG5K-PLA23K was also used as a third copolymer for this study.

The first hypothesis was validated through the nanohybrid formation by double emulsion. The encapsulation process yielded nanohybrids with controlled particle sizes around 100 nm in diameter and with high loading efficiencies (69 – 85%) (Table 3.1 and Figure 3.4). The significant differences in zeta potential for the prepared nanohybrids (-

7.0 – -17.3 mV) from those of the dendrimer conjugates before encapsulation (3.4 –

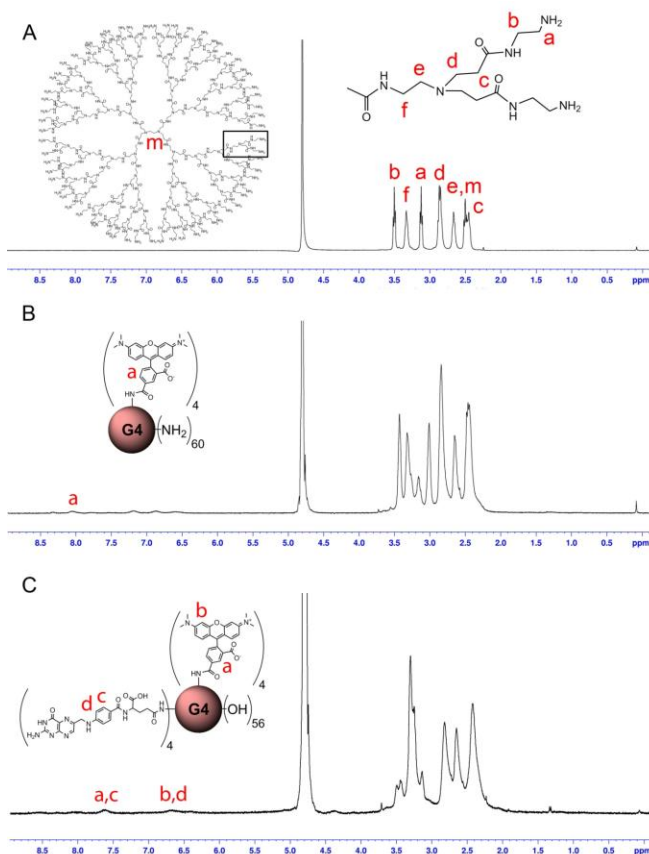


Figure 3.2. ¹H NMR spectra of (A) G4 PAMAM dendrimer, (B) G4-RHO-NH₂, and (C) G4-RHO-FA-OH. The ¹H NMR spectrum of G4 PAMAM dendrimers (A) shows 6 characteristic peaks at 2.46, 2.65, 2.84, 3.01, 3.32, and 3.43 ppm. After conjugation with RHO, new peaks between 6.50 and 8.50 ppm corresponding to the aromatic protons of RHO were observed (B). Based on the relative integration values at 8.04 ppm and the dendrimer peaks, it was calculated that each dendrimer has approximately 3.9 RHO molecules. For G4-RHO-FA-OH (C), an increase in the integration values at 6.68 and 7.76 ppm, compared to G4-RHO, indicated the successful FA conjugation. Based upon the difference in the relative integration values of the characteristic RHO and FA peaks, it was calculated that approximately 4.3 FA molecules were attached to a dendrimer molecule (*acquired by Ryan M. Pearson*).

28.1 mV) confirmed the successful encapsulation (Table 3.1). The results highlighted in

Figure 13 and Table 3.1 support hypothesis (1) and clearly indicate that the encapsulation of the dendrimer conjugates into the polymeric NPs was successfully achieved.

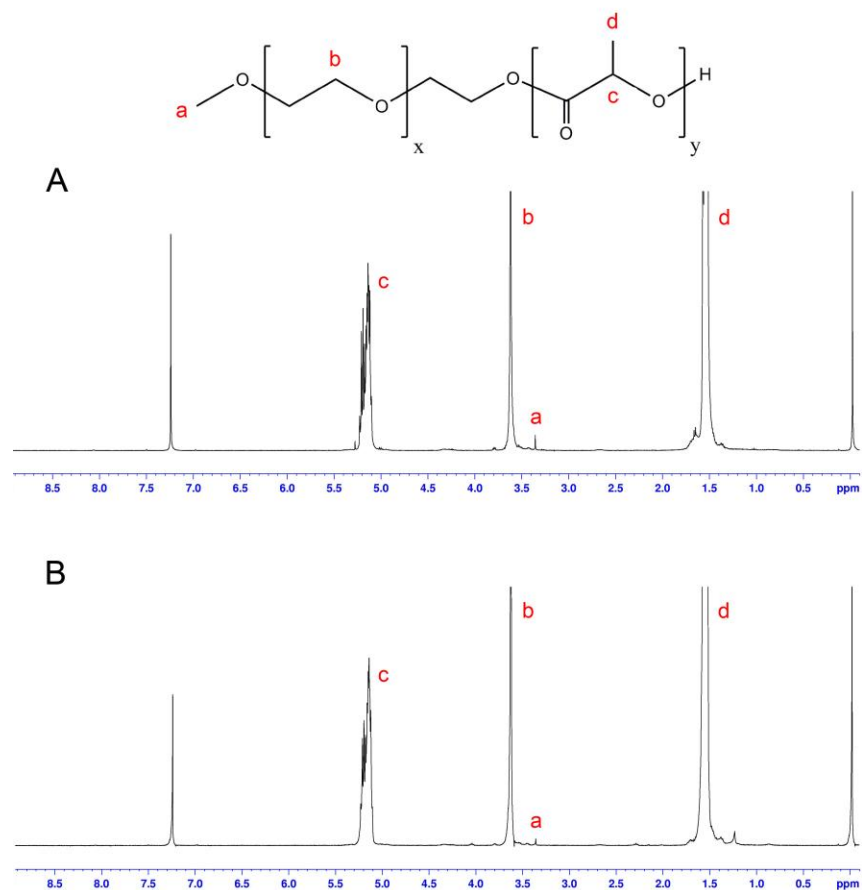
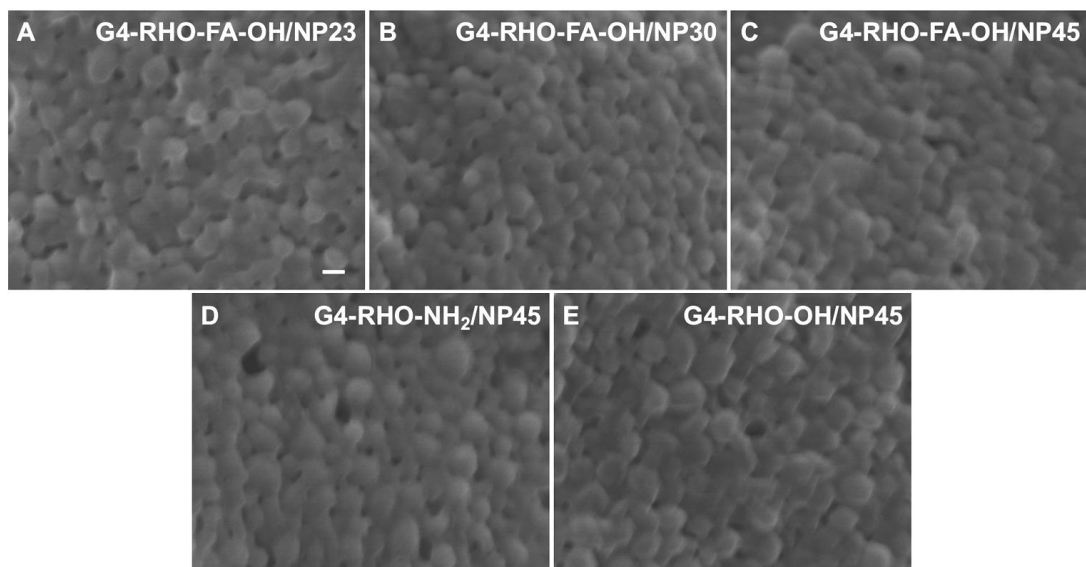


Figure 3.3. ¹H NMR spectra of (A) PEG(5K)-PLA(30K), and (B) PEG(5K)-PLA(45K). The ¹H NMR spectra of PEG-PLA shows two characteristic peaks of PLA at 5.15 and 1.55 ppm (c and d), corresponding to the protons of methine and methylene groups, respectively. As for mPEG, two characteristic peaks corresponding to the methoxy group (a) and the ethylene glycol repeating units (b) were observed at 3.62 and 3.35 ppm, respectively. The MWs of PEG-PLA were estimated using the relative integration ratios of peak b and c, based on the the integral value for the methoxy group of mPEG which was set to 3 (*acquired by Jin Woo Bae*).

Table 3.1. Characterization of the G4 PAMAM dendrimer-based nanohybrids

	Particle size (nm)	Zeta potential (mV)	Loading efficiency (%)
G4-RHO-NH ₂	16.7 ± 2.4	28.1 ± 1.8	N/A
G4-RHO-OH	12.1 ± 7.3	4.2 ± 1.7	N/A
G4-RHO-FA-OH	19.6 ± 7.8	3.4 ± 1.6	N/A
G4-RHO-NH ₂ /NP45	103.3 ± 5.2	-12.5 ± 4.2	79.2
G4-RHO-OH/NP45	121.5 ± 9.6	-9.8 ± 6.3	72.0
G4-RHO-FA-OH/NP23	97.6 ± 11.9	-11.0 ± 2.7	85.4
G4-RHO-FA-OH/NP30	146.9 ± 2.2	-7.0 ± 2.4	79.6
G4-RHO-FA-OH/NP45	115.5 ± 13.2	-17.3 ± 3.5	81.8

**Figure 3.4.** Scanning electron microscopy (SEM) images of the nanohybrids prepared in this study showing controlled particle sizes around 100 nm in diameter. Scale bar: 100 nm.

3.3.2 Temporally controlled cellular targeting of the nanohybrids and its implication for targeted drug delivery

For the second hypothesis, we tested if FR specificity of the FA-targeted dendrimer conjugates could be kinetically controlled by our nanohybrid design. The cellular interactions of the dendrimer conjugates and their respective nanohybrids were studied in KB FR⁺ cells using CLSM and FACS. Nanohybrids prepared with PEG5K-PLA45K (NP45) were employed for this experiment. Confocal images of KB FR⁺ cells after 1 h incubation (Figure 3.5) clearly show that only the targeted dendrimers (G4-RHO-FA-OH: red fluorescence) bind to the cell surface, which is in agreement with the FACS measurements (Figure 3.6) and a previous report [16]. This interaction was completely blocked when the cells were pre-incubated with an excess amount of free FA (Figures 3.5 and Figure 3.6), confirming that the observed dendrimer-cell interactions are a result of selective binding and uptake between FA on the dendrimers and FR on the cell surfaces.

In the case of the G4-RHO-FA-OH-based nanohybrids, we hypothesized that they will also bind specifically to the FR, but with a time delay as the targeted dendrimers are protected by the PEG-PLA NP shell. Indeed, receptor-specific binding was observed with the FA-targeted nanohybrids (G4-RHO-FA-OH/NP45) after 4 h incubation only. This interaction was comparable to that of the unencapsulated G4-RHO-FA-OH in terms of fluorescence intensity from the dendrimers in and/or on the cells. Furthermore, the dendrimer internalization was blocked upon pre-incubation with excess FA (Figures 3.5 and Figure 3.6) and was negligible in KB FR⁻ cells (Figure 3.7), confirming that the observed dendrimer interactions are FR-specific.

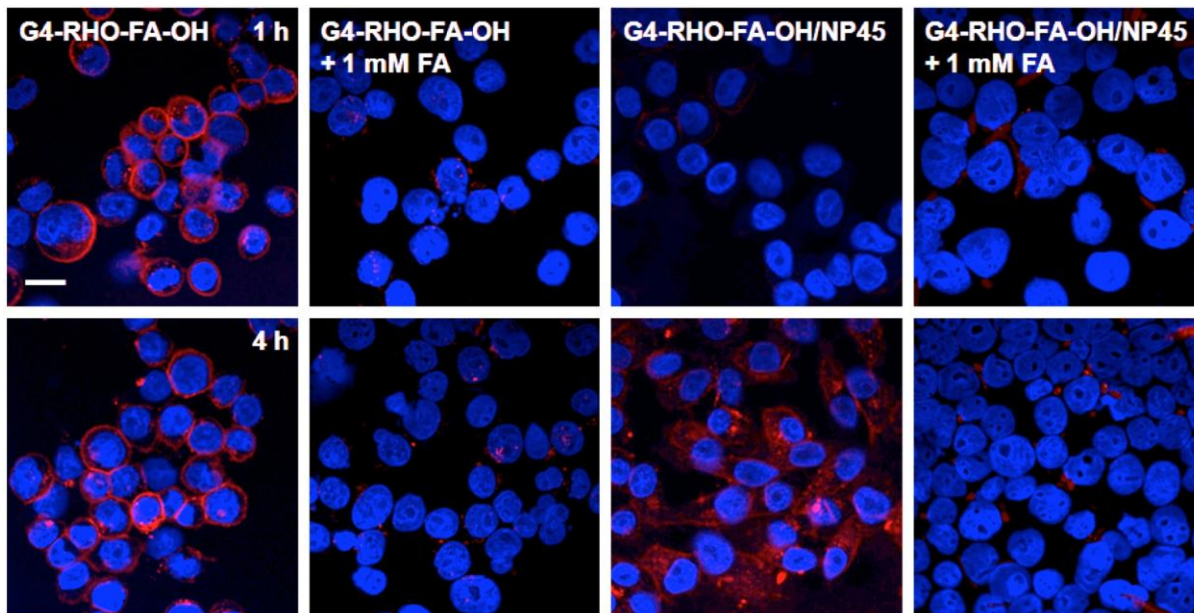


Figure 3.5. CLSM images of KB FR⁺ cells after incubation with G4-RHO-FA-OH and its corresponding NP45 nanohybrids at a concentration of 63 nM (based on the dendrimer conjugates) for 1 h (upper row) and 4 h (lower row) (red: dendrimer conjugates, blue: cell nuclei stained by DAPI, scale bar: 20 μ m). The receptor targeting of the dendrimer-FA conjugates is confirmed by significant binding of the unencapsulated conjugates to the cell surface within 1 h (1st column), which was blocked by pre-incubating the cells with 1 mM of free FA (2nd column). Temporal control over targeting is demonstrated using G4-RHO-FA-OH-encapsulated nanohybrids that do not interact with cells until 4 h (3rd column), and the interaction was also blocked by free FA (4th column).

As shown in Figure 3.6, the control, non-targeted nanohybrids (G4-RHO-NH₂/NP45 and G4-RHO-OH/NP45) showed a significantly lower, if not negligible, degree of cellular interaction. G4-RHO-NH₂ exhibited a degree of non-specific interactions after 4 hr incubation likely due to electrostatic interactions [29, 33, 34]. The significance of these results is two-fold: (1) FA-targeted dendrimers maintain selectivity to KB FR⁺ cells after the encapsulation and release process; and (2) the nanohybrid

design allows for temporal control over the receptor targeting of the dendrimer-FA conjugates.

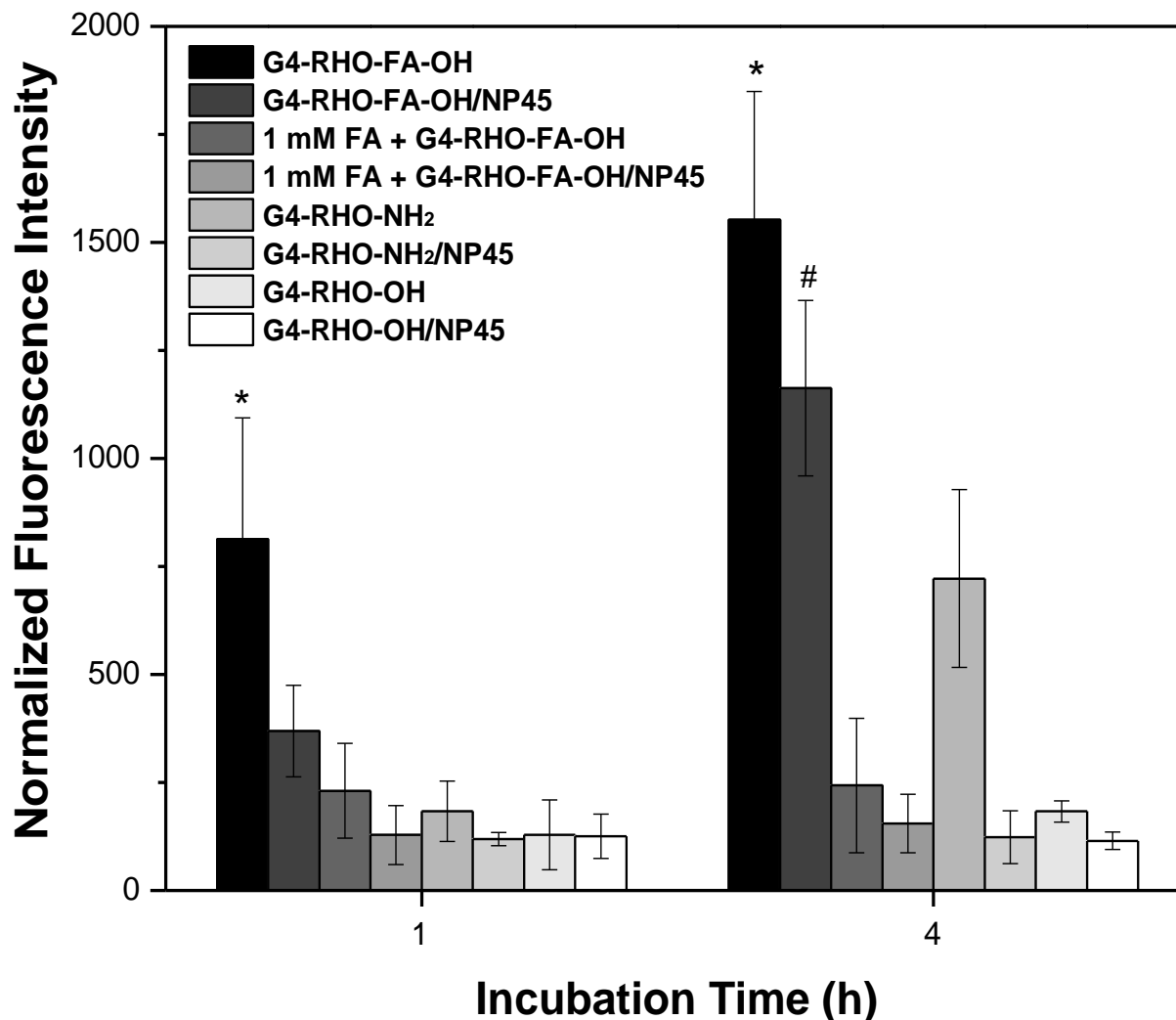


Figure 3.6. Mean fluorescence intensities measured by FACS after the treatment of FR⁺ KB cells with G4-RHO-FA-OH and its NP45 nanohybrid formulation under the same conditions described in Figure 3.5. * denotes statistical significance ($p < 0.05$) between G4-RHO-FA-OH and the control conjugate groups, and # denotes statistical significance ($p < 0.05$) between G4-RHO-FA-OH/NP45 and the control nanohybrids, based on a 1-way ANOVA followed by Tukey's post hoc test. G4-RHO-NH₂ shows the interactions with the cells after 4 h due to non-specific electrostatic interactions.

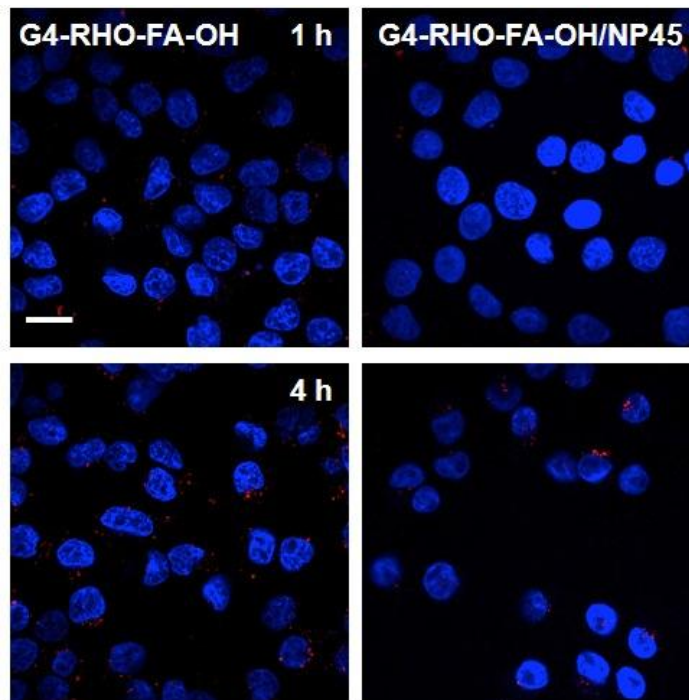


Figure 3.7. CLSM images of KB FR⁻ cells after incubation with G4-RHO-FA-OH and its corresponding NP45 nanohybrids at a concentration of 63 nM (based on the dendrimer conjugates) for 1 h (upper row) and 4 h (lower row) (red: dendrimer conjugates, blue: cell nuclei stained by DAPI, scale bar: 20 μ m).

These observations highlight the potential of our nanohybrid system to control the selective cellular interaction kinetics of actively targeted polymer conjugates. This in turn would help address some of the challenges encountered with the currently available nanocarriers. We expect that by encapsulating the targeted dendrimers into a biodegradable polymeric shell, the conjugates would likely be shielded from immediate undesirable interactions with the receptors that are present in normal tissues. We also anticipate that through nanohybridization, the polymer conjugates would not be cleared from the circulation as rapidly as what has been previously observed with targeted polymers with surface-exposed FA [25]. Current strategies that have been investigated

to overcome the rapid clearance of dendrimer-drug conjugates include PEGylation to achieve steric stabilization, and surface modification by acetylation [18, 19, 35]. However, with proper optimization, the added advantage of our nanohybrid system is the possibility of exploiting two systems with different scales. That is, by encapsulating the dendrimer conjugates into polymeric NPs, the particle size of the system becomes large enough (~100 nm compared to 5-10 nm for the dendrimers) to potentially enable passive accumulation in the tumor tissues through the EPR effect. Furthermore, the targeted dendrimers upon release would likely penetrate into the solid tumors more effectively than the larger NPs, due to their small size [36, 37]. The *in vivo* validation of this nanohybrid design will be the subject of our future publications.

3.3.3 Controlled release of FA-targeted dendrimers from the nanohybrids enables tailored targeting kinetics

We tested the third hypothesis by encapsulating G4-RHO-FA-OH into PEG-PLA copolymers with various MWs of PLA, to produce three types of nanohybrids: G4-RHO-FA-OH/NP23, G4-RHO-FA-OH/NP30, and G4-RHO-FA-OH/NP45 prepared using PEG5K-PLA23K, PEG5K-PLA30K, and PEG5K-PLA45K, respectively. The release profiles of the dendrimer conjugates in PBS buffer and in serum-containing RPMI 1640 (Figure 3.8) were biphasic, consisting of a relatively fast release within the first 8 h, most probably due to surface desorption of the dendrimer conjugates [38]. This early release can also indicate that some conjugates may not have been completely encapsulated within the NP core. The profile became slow and sustained afterward, likely resulting from the gradual degradation of the copolymer matrix and diffusion of the dendrimer conjugates [39]. The MW of the PLA block was inversely proportional to the release

rate of the dendrimer conjugates regardless of the release medium, which is similar to previous reports [40]. The higher PEG:PLA ratio in the smaller MW PLA copolymers also results in increased hydrophilicity, greater water uptake, and faster degradation compared to copolymers with a smaller PEG:PLA ratio [31, 41]. The smaller MW and the more hydrophilic surface are expected to contribute to the faster release profile of the G4-RHO-FA-OH/NP23 nanohybrids than that of the NP30 and NP45 nanohybrids. The degradation kinetics of PEG-PLA copolymers themselves are reportedly slower than the release kinetics observed in this study [42, 43]. This suggests that the release of the dendrimer conjugates is not only governed by degradation of the PLA block, but by diffusion as well, similar to what was observed for proteins with comparable MW [44-47].

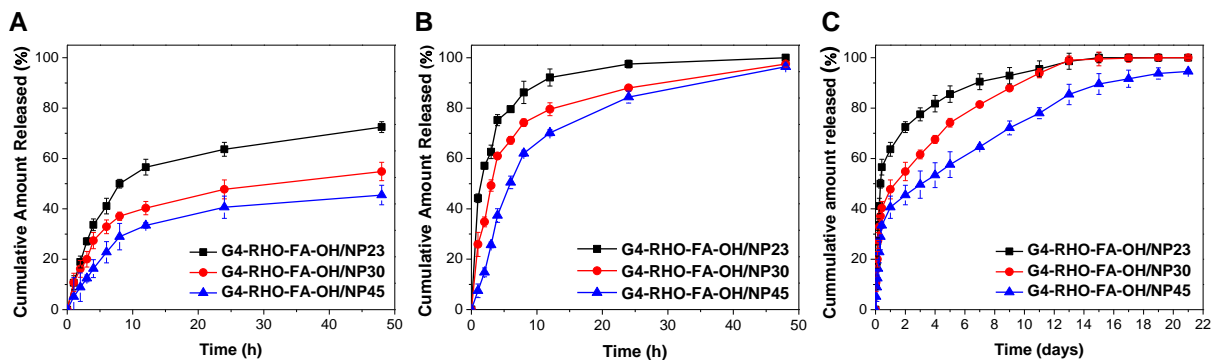


Figure 3.8. Release tests of G4-RHO-FA-OH nanohybrids conducted in (A) PBS buffer and (B) RPMI 1640 medium with 10% FBS for the first 48 h of incubation, and (C) PBS buffer up to 21 days. Nanohybrids with the smallest PLA MW (NP23) show the fastest release in both release media, followed by NP30, and lastly NP45. The release rates of all three nanohybrids in RPMI 1640 are much faster than those in PBS.

We observed much faster release profiles in serum-containing RPMI 1640 compared to PBS, (Figure 3.8(B)), likely attributed to the presence of serum proteins such as albumin in the RPMI 1640. Serum albumin has been shown to exhibit esterase-like activity that accelerates the hydrolysis of the PLA chains [41, 48, 49]. Regardless of the release medium, the overall release profiles demonstrate that the release kinetics of the targeted dendrimers can be controlled by varying the MW of the encapsulating copolymers, which would in turn affect the cellular targeting and interaction kinetics.

In order to achieve kinetic control over FR targeting, each of the G4-RHO-FA-OH/NP23, G4-RHO-FA-OH/NP30, and G4-RHO-FA-OH/NP45 nanohybrids was incubated with KB FR⁺ cells up to 8 h. After 1 h incubation (Figures 3.9 and Figure 3.10), only the G4-RHO-FA-OH/NP23 nanohybrids showed noticeable receptor interactions, which were comparable to unencapsulated G4-RHO-FA-OH. NP30 and NP45 nanohybrids exhibited slower cellular interaction and targeting kinetics. After 4 h incubation, they started to show significant receptor binding, but these interactions were still lower than those observed with the NP23 nanohybrids. After 8 h of incubation, the FACS results demonstrate that all nanohybrids show similar degrees of cellular binding/uptake to unencapsulated G4-RHO-FA-OH (Figure 3.10). The observed temporal delay in the cellular interactions of the NP30 and NP45 nanohybrids can be attributed to the increase in the MW of the PLA block, which delays the release of the FA-conjugates to interact with FR on the cell surface. The larger differences in the release kinetics (Figure 3.8) compared to the differences in cellular interaction kinetics (Figures 3.9 and 3.10) could be due to the rapid desorption of G4-RHO-FA-OH located

near the nanohybrid surfaces and the facilitated degradation in the presence of KB cells [50]. Overall, it is obvious that the kinetics of the cellular interactions of the nanohybrids

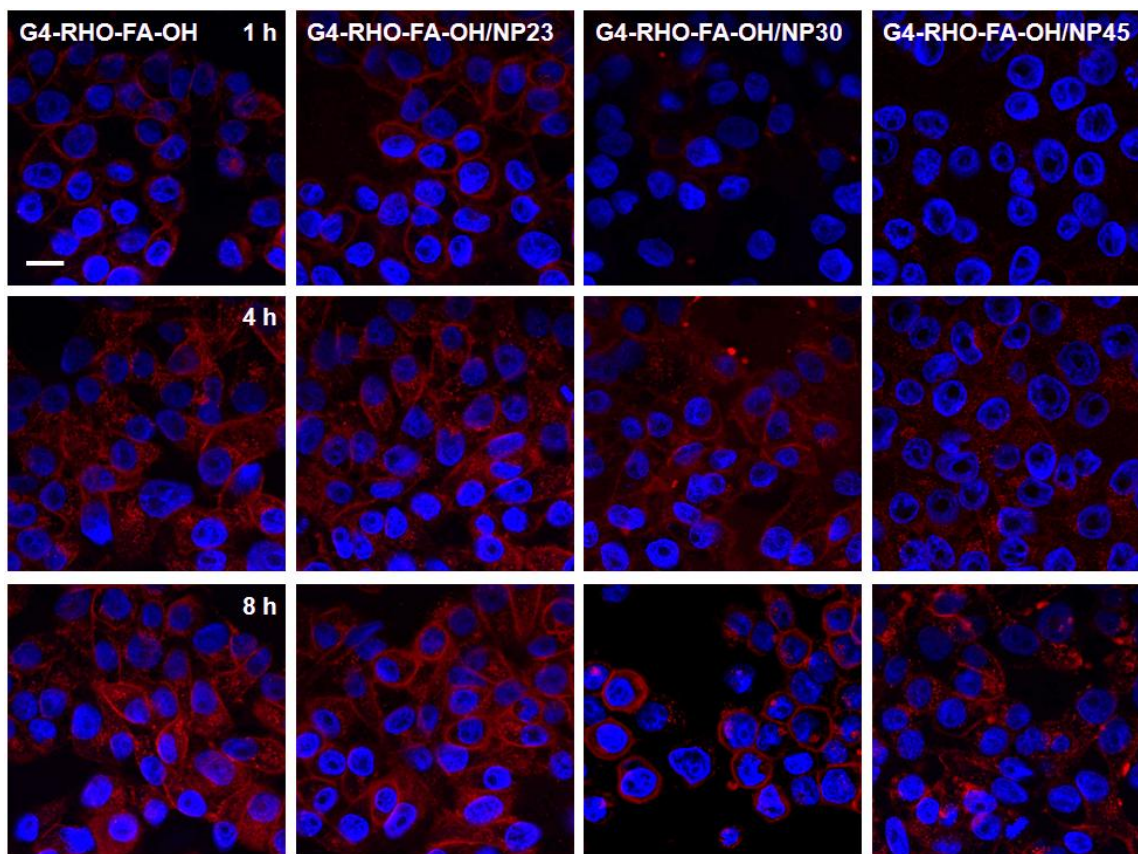


Figure 3.9. CLSM images of KB FR⁺ cells following incubation with G4-RHO-FA-OH and three types of nanohybrids prepared using PEG-PLA with different PLA MW: NP23, NP30, and NP45, at a concentration of 63 nM based on dendrimer conjugates for 1 h (top row), 4 h (middle row), and 8 h (bottom row) (red: dendrimer conjugates, blue: cell nuclei stained by DAPI, scale bar: 20 μ m). Temporal control over targeting is further demonstrated using G4-RHO-FA-OH-encapsulated nanohybrids with different PLA MW. Nanohybrids with the smallest PLA (NP23) (2nd column) show the fastest receptor binding that is comparable to unencapsulated G4-RHO-FA-OH (1st column). NP30 (3rd column) and NP45 (4th column) nanohybrids do not show interaction with the cells until after 4 h incubation. After 8 h incubation, all nanohybrids are either bound to the surface or internalized into the cells.

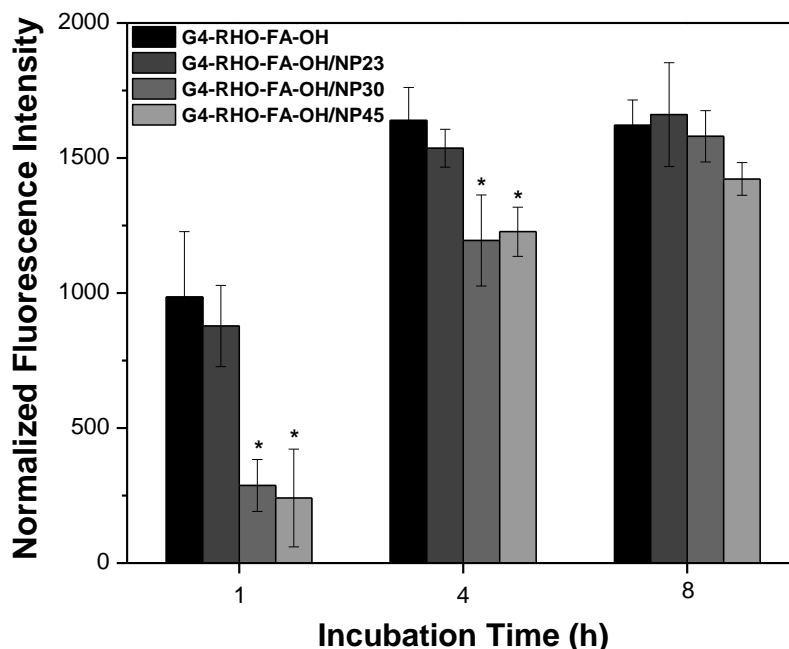


Figure 3.10. Mean fluorescence intensities measured by FACS ($n = 2$) after the treatment of KB FR⁺ cells with G4-RHO-FA-OH and three types of nanohybrids with different PLA MW: NP23, NP30, and NP45, under the same conditions used for Figure 6. Temporal control over FR targeting is observed using the nanohybrids with different PLA MW. The nanohybrids with the smallest PLA (NP23) showed the highest fluorescence count that is comparable to unencapsulated G4-RHO-FA-OH over the time course of the experiment. The NP30 and NP45 nanohybrids start to show a significant increase in fluorescence after 4 h incubation. After 8 h incubation, all nanohybrids exhibit similar fluorescence intensities. Even though the release profiles in buffer and serum-containing medium are markedly different, no significant difference in the cellular interaction kinetics is observed between NP30 and NP45 nanohybrids. * denotes statistical significance ($p < 0.05$) between G4-RHO-FA-OH and the nanohybrids based on a 1-way ANOVA followed by Tukey's post hoc test.

are primarily governed by the controlled release profiles of the different MW PLAs, further supporting our third hypothesis.

3.4 CONCLUSION

Taken together, the results from this study support the three hypotheses stated earlier. For hypothesis (1), both targeted and non-targeted dendrimer conjugates were encapsulated into PEG-PLA NPs with controlled sizes at high encapsulation efficiencies (Table 3.1 and Figure 3.4). Hypothesis (2) was validated by the FR specificity and temporally controlled targeting of the FA-targeted dendrimer-containing nanohybrids (Figures 3.5 and Figure 3.6). The release tests and the cellular interaction studies using CLSM and FACS (Figures 3.8, Figure 3.9, and Figure 3.10) demonstrated that the targeting kinetics of the dendrimers can be controlled by altering the MW of the biodegradable components of the nanohybrid systems, thereby supporting hypothesis (3). This control over the targeting kinetics further emphasizes the versatility and flexibility of our nanohybrid design, which can be tailored to achieve the desired targeting kinetics and release rates of multifunctionalized polymer-drug conjugates. Our novel nanohybrids demonstrate a great potential to enable precise control over the targeting kinetics of the nanocarrier to tumor cells, which can potentially minimize premature elimination and off-target delivery of the conventional nanocarriers that have targeting agents being exposed on the surface. The flexibility of the nanohybrid design can also be exploited to achieve temporally controlled ligand presentations for targeting inflammatory diseases [51]. In addition, the staged, temporally controlled targeting to multiple ligands (e.g. selectins, IL-6, STAT3) would effectively block the inflammatory responses that frequently accompany various cancers [52, 53].

3.5 REFERENCES

1. Peer, D., et al., *Nanocarriers as an emerging platform for cancer therapy*. Nat. Nanotechnol., 2007. **2**(12): p. 751-760.
2. Kim, J., Y. Piao, and T. Hyeon, *Multifunctional nanostructured materials for multimodal imaging, and simultaneous imaging and therapy*. Chem. Soc. Rev., 2009. **38**(2): p. 372-390.
3. Barreto, J.A., et al., *Nanomaterials: Applications in cancer imaging and therapy*. Adv. Mater., 2011. **23**(12): p. H18-H40.
4. Majoros, I.J., et al., *Poly(amidoamine) dendrimer-based multifunctional engineered nanodevice for cancer therapy*. J. Med. Chem., 2005. **48**(19): p. 5892-5899.
5. Majoros, I.J., et al., *PAMAM dendrimer-based multifunctional conjugate for cancer therapy: Synthesis, characterization, and functionality*. Biomacromolecules, 2006. **7**(2): p. 572-579.
6. Myc, A., et al., *Preclinical antitumor efficacy evaluation of dendrimer-based methotrexate conjugates*. Anti-Cancer Drug., 2008. **19**(2): p. 143-149.
7. Kukowska-Latallo, J.F., et al., *Nanoparticle targeting of anticancer drug improves therapeutic response in animal model of human epithelial cancer*. Cancer Res., 2005. **65**(12): p. 5317-5324.
8. Duncan, R., *Polymer conjugates as anticancer nanomedicines*. Nat. Rev. Cancer, 2006. **6**(9): p. 688-701.

9. Myc, A., et al., *Targeting the efficacy of a dendrimer-based nanotherapeutic in heterogeneous xenograft tumors in vivo*. *Anti-Cancer Drug.*, 2010. **21**(2): p. 186-192.
10. Matsumura, Y. and H. Maeda, *A New concept for macromolecular therapeutics in cancer chemotherapy - Mechanism of tumoritropic accumulation of proteins and the antitumor agent SMANCS*. *Cancer Res.*, 1986. **46**(12): p. 6387-6392.
11. Gu, F.X., et al., *Targeted nanoparticles for cancer therapy*. *Nano Today*, 2007. **2**(3): p. 14-21.
12. Maeda, H., *Tumor-selective delivery of macromolecular drugs via the EPR effect: Background and future prospects*. *Bioconjugate Chem.*, 2010. **21**(5): p. 797-802.
13. Torchilin, V., *Tumor delivery of macromolecular drugs based on the EPR effect*. *Adv. Drug Deliver. Rev.*, 2011. **63**(3): p. 131-135.
14. Riehemann, K., et al., *Nanomedicine-Challenge and perspectives*. *Angew. Chem. Int. Ed.*, 2009. **48**(5): p. 872-897.
15. Ruenraroengsak, P., J.M. Cook, and A.T. Florence, *Nanosystem drug targeting: Facing up to complex realities*. *J. Control. Release*, 2010. **141**(3): p. 265-276.
16. Hong, S., et al., *The binding avidity of a nanoparticle-based multivalent targeted drug delivery platform*. *Chem. Biol.*, **2007**. **14**(1): p. 107-115.
17. Myung, J., et al., *Dendrimer-mediated multivalent binding for the enhanced capture of tumor cells*. *Angew. Chem. Int. Ed.*, 2011. **50**(49): p. 11769-11772.
18. Lee, C.C., et al., *Designing dendrimers for biological applications*. *Nat. Biotechnol.*, 2005. **23**(12): p. 1517-1526.

19. Singh, P., et al., *Folate and folate-PEG-PAMAM dendrimers: Synthesis, characterization, and targeted anticancer drug delivery potential in tumor bearing mice*. *Bioconjugate Chem.*, 2008. **19**(11): p. 2239-2252.
20. Danhier, F., O. Feron, and V. Preat, *To exploit the tumor microenvironment: Passive and active tumor targeting of nanocarriers for anti-cancer drug delivery*. *J. Control. Release*, 2010. **148**(2): p. 135-146.
21. Stella, B., et al., *Design of folic acid-conjugated nanoparticles for drug targeting*. *J. Pharm. Sci.*, 2000. **89**(11): p. 1452-1464.
22. Gabizon, A., et al., *Tumor cell targeting of liposome-entrapped drugs with phospholipid-anchored folic acid-PEG conjugates*. *Adv. Drug Deliver. Rev.*, 2004. **56**(8): p. 1177-1192.
23. Bae, Y., et al., *Multifunctional polymeric micelles with folate-mediated cancer cell targeting and pH-triggered drug releasing properties for active intracellular drug delivery*. *Mol. Biosyst.*, 2005. **1**(3): p. 242-250.
24. Zhang, Z.P., S.H. Lee, and S.S. Feng, *Folate-decorated poly(lactide-co-glycolide)-vitamin E TPGS nanoparticles for targeted drug delivery*. *Biomaterials*, 2007. **28**(10): p. 1889-1899.
25. Gabizon, A., et al., *In vivo fate of folate-targeted polyethylene-glycol liposomes in tumor-bearing mice*. *Clin. Cancer Res.*, 2003. **9**(17): p. 6551-6559.
26. McNeeley, K.M., A. Annapragada, and R.V. Bellamkonda, *Decreased circulation time offsets increased efficacy of PEGylated nanocarriers targeting folate receptors of glioma*. *Nanotechnology*, 2007. **18**(38).

27. McNeeley, K.M., et al., *Masking and triggered unmasking of targeting ligands on nanocarriers to improve drug delivery to brain tumors*. *Biomaterials*, 2009. **30**(23-24): p. 3986-3995.
28. Sunoqrot, S., et al., *Kinetically controlled cellular interactions of polymer-polymer and polymer-liposome nanohybrid systems*. *Bioconjugate Chem.*, 2011. **22**(3): p. 466-474.
29. Hong, S., et al., *Interaction of poly(amidoamine) dendrimers with supported lipid bilayers and cells: Hole formation and the relation to transport*. *Bioconjugate Chem.*, 2004. **15**(4): p. 774-782.
30. Leroueil, P.R., et al., *Nanoparticle interaction with biological membranes: Does nanotechnology present a janus face?* *Acc. Chem. Res.*, 2007. **40**(5): p. 335-342.
31. Avgoustakis, K., et al., *PLGA-mPEG nanoparticles of cisplatin: in vitro nanoparticle degradation, in vitro drug release and in Vivo drug residence in blood properties*. *J. Control. Release*, 2002. **79**(1-3): p. 123-135.
32. Bae, J.W., et al., *Dendron-mediated self-assembly of highly PEGylated block copolymers: a modular nanocarrier platform*. *Chem. Commun.*, 2011. **47**(37): p. 10302-10304.
33. Hong, S., et al., *The role of ganglioside GM(1) in cellular internalization mechanisms of poly(amidoamine) dendrimers*. *Bioconjugate Chem.*, 2009. **20**(8): p. 1503-1513.
34. Hong, S., et al., *Interaction of polycationic polymers with supported lipid bilayers and cells: Nanoscale hole formation and enhanced membrane permeability*. *Bioconjugate Chem.*, 2006. **17**(3): p. 728-734.

35. Gillies, E.R., et al., *Biological evaluation of polyester dendrimer: Poly(ethylene oxide) "bow-tie" hybrids with tunable molecular weight and architecture*. Mol. Pharm., 2005. **2**(2): p. 129-138.
36. Jain, R.K. and T. Stylianopoulos, *Delivering nanomedicine to solid tumors*. Nat. Rev. Clin. Oncol., 2010. **7**(11): p. 653-664.
37. Wong, C., et al., *Multistage nanoparticle delivery system for deep penetration into tumor tissue*. P. Natl. Acad. Sci. USA, 2011. **108**(6): p. 2426-2431.
38. Li, Y.P., et al., *PEGylated PLGA nanoparticles as protein carriers: synthesis, preparation and biodistribution in rats*. Journal of Controlled Release, 2001. **71**(2): p. 203-211.
39. Xiao, R.Z., et al., *Recent advances in PEG-PLA block copolymer nanoparticles*. Int. J. Nanomed., 2010. **5**: p. 1057-1065.
40. Giannavola, C., et al., *Influence of preparation conditions on acyclovir-loaded poly-D,L-lactic acid nanospheres and effect of PEG coating on ocular drug bioavailability*. Pharm. Res., 2003. **20**(4): p. 584-590.
41. Ishihara, T., et al., *Polymeric nanoparticles encapsulating betamethasone phosphate with different release profiles and stealthiness*. Int. J. Pharm., 2009. **375**(1-2): p. 148-154.
42. Belbella, A., et al., *In vitro degradation of nanospheres from poly(D,L-lactides) of different molecular weights and polydispersities*. Int. J. Pharm., 1996. **129**(1-2): p. 95-102.

43. Li, Y., et al., *PEG-PLA diblock copolymer micelle-like nanoparticles as all-trans-retinoic acid carrier: in vitro and in vivo characterizations*. *Nanotechnology*, 2009. **20**(5): p. 055106.
44. Mukherjee, B., et al., *Preparation, characterization and in-vitro evaluation of sustained release protein-loaded nanoparticles based on biodegradable polymers*. *Int. J. Nanomed.*, 2008. **3**(4): p. 487-496.
45. Polakovic, M., et al., *Lidocaine loaded biodegradable nanospheres II. Modelling of drug release*. *J. Control. Release*, 1999. **60**(2-3): p. 169-177.
46. Soppimath, K.S., et al., *Biodegradable polymeric nanoparticles as drug delivery devices*. *J. Control. Release*, 2001. **70**(1-2): p. 1-20.
47. Panyam, J., et al., *Polymer degradation and in vitro release of a model protein from poly(-lactide-co-glycolide) nano- and microparticles*. *J. Control. Release*, 2003. **92**(1-2): p. 173-187.
48. Catiker, E., M. Gumusderelioglu, and A. Guner, *Degradation of PLA, PLGA homo- and copolymers in the presence of serum albumin: a spectroscopic investigation*. *Polym. Int.*, 2000. **49**(7): p. 728-734.
49. Lockridge, O., et al., *Pseudo-esterase activity of human albumin - Slow turnover on tyrosine 411 and stable acetylation of 82 residues including 59 lysines*. *J. Biol. Chem.*, 2008. **283**(33): p. 22582-22590.
50. Vasir, J.K. and V. Labhasetwar, *Biodegradable nanoparticles for cytosolic delivery of therapeutics*. *Adv. Drug Deliver. Rev.*, 2007. **59**(8): p. 718-728.
51. Thomas, T.P., et al., *Folate-targeted nanoparticles show efficacy in the treatment of inflammatory arthritis*. *Arthritis Rheum.*, 2011. **63**(9): p. 2671-2680.

52. Yu, H., M. Kortylewski, and D. Pardoll, *Crosstalk between cancer and immune cells: role of STAT3 in the tumour microenvironment*. Nat. Rev. Immunol., 2007. **7**(1): p. 41-51.
53. Barthel, S.R., et al., *Targeting selectins and selectin ligands in inflammation and cancer*. Expert Opin. Ther. Targets, 2007. **11**(11): p. 1473-1491.

CHAPTER 4

IN VITRO EVALUATION OF DENDRIMER-POLYMER HYBRID NANOPARTICLES ON THEIR CONTROLLED CELLULAR TARGETING KINETICS*

4.1 INTRODUCTION

Nanocarriers such as polymer-drug conjugates, dendrimers, polymeric nanoparticles (NPs), micelles, and liposomes have demonstrated great potential to achieve targeted therapy for cancer treatments [1-6]. Targeting strategies using those nanocarriers include passive targeting based on size control and active targeting via ligand conjugation [7-9]. To increase the targeting efficacy, integration of the two targeting approaches within a single nanocarrier has been widely attempted using a variety of nanomaterials such as ligand-conjugated polymeric NPs [10], micelles [11], and liposomes [12, 13]. However, the single-scale size of these nanocarriers has limitations to optimize their biological properties in terms of biodistribution, tumor targeting, penetration, and cellular uptake, largely because of the different size requirements associated with each of those properties [14, 15].

The dense tumor interstitial matrix and abnormal vasculature can lead to inefficient distribution of the drug payloads throughout the tissue [16]. Specifically, the relatively large size of the nanocarriers (50-200 nm to exploit the enhanced permeability and retention (EPR) effect) and targeting moieties exposed on their surfaces can retard tumor penetration due to limited diffusivity and high binding affinity to the superficial

*Reproduced with permission from Sunoqrot, S.; Liu, Y.; Kim, D.-H.; Hong, S. *Mol. Pharm.* **2013**, *ASAP Article*, DOI: 10.1021/mp300560n. Copyright 2013 American Chemical Society.

tumor cells, respectively [16]. In contrast, smaller NPs (<10 nm) have been shown to achieve enhanced tissue permeation and penetration [15-17]. In particular, folate (FA)-targeted poly(amidoamine) (PAMAM) dendrimers have previously shown high targeting efficacy to FA receptor (FR)-overexpressing tumor xenografts [18-20]. However, their small size (~5 nm in diameter) and the surface-exposed targeting ligands have resulted in rapid renal clearance and significant liver uptake, respectively.^{13, 23} Therefore, to maximize the targeting efficacy of drug payloads, a multi-scale nanocarrier, one that combines two or more nanocarriers with different size scales, would be highly desirable. One of the promising ways to achieve the multi-scale system would be to combine actively targeted nanocarriers with favorable tissue penetration and cellular internalization properties, together with larger NPs with a controlled size for passive targeting and long circulation.

Previously, we designed a multi-scale nanocarrier platform by combining linear polymers or targeted dendrimers with larger polymeric NPs [21, 22]. Generation 4 (G4) PAMAM dendrimers were conjugated with folic acid (FA) as a targeting ligand and encapsulated within poly(ethylene glycol)-*b*-poly(*D,L*-lactide) (PEG-PLA) copolymers to produce the hybrid NPs, or nanohybrids, with controlled sizes (~100 nm). The design rationale of the nanohybrid system was to combine the controlled release and larger size of polymeric NPs with the targeting efficacy and favorable tissue penetration of targeted dendrimers. The resulting nanohybrids selectively interacted with FR-overexpressing KB cells (KB FR⁺) in a temporally controlled manner due to the presence of the PEG-PLA shell. Our multi-scale hybrid NPs successfully combined polymeric NPs and targeted dendrimers, allowing precise control over the targeting

kinetics by tuning the release profile of the actively targeted dendrimers [22].

The dendrimers in the core and polymeric NP shell impart dual properties to the nanohybrid system. This led us to set up a hypothesis that the biological properties of the system may be dictated by one component or the other at a given time, which is dependent upon the dissociation kinetics of the two components. In this paper, we tested this hypothesis by a series of experiments using nanohybrid systems labeled with different fluorophores for the outer shell and dendrimers in the core. First, the effect of incubation time on the selective cellular uptake of the nanohybrids was investigated at various incubation hours (up to 48 h) and compared to free dendrimers and empty polymeric NPs. The cellular association kinetics was also correlated with the release kinetics of the dendrimers in a cell-conditioned culture medium in order to examine the effect of the cellular microenvironment on dendrimer release. Secondly, the cellular uptake mechanisms of the nanohybrids were investigated by employing metabolic inhibitors, such as methyl- β -cyclodextrin (M β CD) and fillipin, which block clathrin- and caveolae-mediated endocytic pathways, respectively. These experiments were designed to elucidate the dominant uptake mechanism(s) of the nanohybrids at various incubation hours. Thirdly, to simulate *in vivo* tumor penetration, multicellular tumor spheroids (MCTS) were used as a 3D *in vitro* model mimicking *in vivo* tumor tissues, allowing evaluation of the penetration ability of the nanohybrids as a function of incubation time. Lastly, the potential of the nanohybrids as a drug carrier was assessed using nanohybrids containing methotrexate (MTX). Our study herein provides fundamental understanding on the kinetically controlled biological properties of the newly developed nanohybrids, which is a key step for further development for *in vivo*

applications.

4.2 EXPERIMENTAL SECTION

4.2.1 Materials

Generation 4 (G4) PAMAM dendrimer, *N*-hydroxysuccinimide-rhodamine B (NHS-RHO), folic acid (FA), methotrexate (MTX), *N*-(3-dimethylaminopropyl)-*N'*-ethylcarbodiimide hydrochloride (EDC), *N*-hydroxysuccinimide (NHS), fluorescein isothiocyanate (FITC), filipin, M β CD, glycidol, tin(II)2-ethylhexanoate, poly(ethylene glycol) monomethyl ether (mPEG) (MW 5,000 Da), poly(vinyl alcohol) (PVA, 87-89% hydrolyzed, MW 13,000-23,000 Da), trifluoroacetic acid (TFA), dimethyl sulfoxide (DMSO), dimethylformamide (DMF), and dichloromethane (DCM) were all obtained from Sigma-Aldrich (St. Louis, MO). *D,L*-lactide and Boc-NH-PEG5K-OH were purchased from Polysciences Inc. (Warrington, PA) and Jenkem Technology (Beijing, China), respectively. All other chemicals used in this study were purchased from Sigma-Aldrich unless specified otherwise.

4.2.2 Preparation of G4 PAMAM dendrimer conjugates

Fully hydroxylated RHO-labeled FA-targeted G4 PAMAM dendrimer conjugates (G4-RHO-FA-OH) containing 3.9 RHO and 4.3 FA molecules per dendrimer were prepared and characterized by ¹H NMR as reported in our earlier publication [22, 23]. MTX was conjugated to the hydroxylated dendrimer conjugates by an ester bond as previously described [23]. Briefly, MTX (1.3 mg, 2.8×10^{-6} mol) was dissolved in 200 μ L DMSO, and EDC (5.4 mg, 2.8×10^{-5} mol) and NHS (3.2 mg, 2.8×10^{-5} mol) in 1 mL DMSO were added dropwise under vigorous stirring at RT for 1 h. The activated MTX

solution was added dropwise to 10 mg of either G4-RHO-FA-OH or G4-RHO-OH (7.0×10^{-7} mol) dissolved in 5 mL of ddH₂O, followed by vigorous stirring at RT for 24 h. The solution was then dialyzed in a 3,500 MWCO dialysis membrane (Spectrum Laboratories Inc., Rancho Dominguez, CA) against ddH₂O for 2 days, lyophilized for two days, and stored at -20 °C.

4.2.3 Synthesis of FITC-PEG-PLA

PEG-PLA and Boc-NH-PEG-PLA were prepared by ring opening polymerization of *D,L*-lactide as previously described [22]. FITC-PEG-PLA was then prepared following deprotection of Boc-NH-PEG-PLA [24]. Briefly, Boc-NH-PEG-PLA was deprotected by dissolving 200 mg in 4 mL of DCM, and 4 mL of TFA was added into the solution dropwise under vigorous stirring for 15 min. TFA and DCM were evaporated under vacuum at 70°C using a rotary evaporator. The product was redissolved in 1 mL DCM, precipitated using cold diethyl ether, vacuum filtered, and dried overnight. H₂N-PEG-PLA was conjugated to FITC by dissolving 50 mg (1.2×10^{-3} mmol) in 2 mL DMF. FITC (0.6 mg, 1.5×10^{-3} mmol) in 500 μ L DMF was added into the polymer/DMF solution under vigorous stirring at RT overnight. Excess FITC was removed by membrane dialysis against ddH₂O using a 3,500 MWCO dialysis membrane for two days. The final product was then lyophilized over 2 days and stored at -20 °C.

4.2.4 Encapsulation of the dendrimer conjugates into FITC-labeled PEG-PLA NPs

FITC-labeled hybrid NPs containing targeted or non-targeted dendrimer conjugates (G4-RHO-FA-OH or G4-RHO-OH) were prepared using a double emulsion method [21, 22]. For example, G4-RHO-FA-OH (100 μ L, 1 mg/mL in ddH₂O) was

added to 1 mL of 20 mg/mL solution of PEG-PLA/FITC-PEG-PLA (10:1 w/w) in DCM, and the mixture was sonicated for 1 min using a Misonix XL Ultrasonic Processor (100% duty cycle, 475 W, 1/8" tip, QSonica, LLC, Newtown, CT). Two milliliters of 3% aqueous PVA solution was then added to the mixture, followed by additional sonication for 1 min. The double emulsion was poured into 20 mL of 0.3% PVA in ddH₂O, and vigorously stirred at RT for 24 h to evaporate DCM. The resulting nanohybrid solution was transferred to Nalgene high-speed centrifuge tubes (Fisher Scientific, Pittsburg, PA) to remove PVA and unencapsulated G4-RHO-FA-OH by ultracentrifugation at 20,000 rpm (48,384 × g) for 30 min using a Beckman Avanti J25 Centrifuge (Beckman Coulter, Brea, CA). After washing the nanohybrids five times with ddH₂O, the pellet was resuspended in ddH₂O, lyophilized over 2 days, and stored at -20 °C. G4-RHO-OH was also encapsulated into FITC-labeled NPs using the same method. Empty FITC-NPs were prepared by adding 100 µL ddH₂O instead of the dendrimer solution.

4.2.5 Structure confirmation and size/surface charge measurements

The dendrimer conjugates and PEG-PLA copolymers were characterized by ¹H NMR using a 400 MHz Bruker DPX-400 spectrometer (Bruker BioSpin Corp., Billerica, MA) as described in our earlier publication [22]. The MW of PEG-PLA was also measured by Gel Permeation Chromatography (GPC) based on polystyrene standards as previously described [24]. Measurements were carried out using a 600 HPLC pump, 717plus Autosampler, and 2414 Refractive Index detector (Waters, Milford, MA, USA) using THF as the mobile phase at 1 mL/min with a Waters Styragel® HR2 column at 30°C. The structure of G4-RHO-FA-OH-MTX and G4-RHO-OH-MTX was confirmed by UV/Vis using a DU800 UV/Vis Spectrophotometer (Beckman Coulter, CA). The number

of MTX molecules attached to each dendrimer was calculated based on a standard curve of MTX absorbance versus concentration in ddH₂O at 373 nm. Particle size (diameter, nm) and surface charge (zeta potential, mV) of the conjugates and the nanohybrids were measured in triplicates by quasi-elastic laser light scattering using a Nicomp 380 Zeta Potential/Particle Sizer (Particle Sizing Systems, Santa Barbara, CA) in ddH₂O. The measurements were performed using samples that were suspended in ddH₂O at a concentration of 100 µg/mL, filtered through a 0.45 µm syringe filter, and briefly vortexed prior to each measurement.

4.2.6 Loading efficiencies of the dendrimer-encapsulated nanohybrids

Loading was defined as the dendrimer conjugate content in the nanohybrids. Five milligrams of each nanohybrid formulation were dissolved in 1 mL of 0.5 M to degrade the PEG-PLA and completely release the loaded dendrimers, followed by filtration through a 0.45 µm syringe filter. The fluorescence intensity from the filtrates was then measured using a SpectraMAX GeminiXS microplate spectrofluorometer (Molecular Devices, Sunnyvale, CA). The amount of the dendrimer conjugates in the filtrates was determined from a standard curve of each conjugate's fluorescence versus concentration in 0.5 M NaOH at 544 nm excitation and 576 nm emission wavelengths. Loading was expressed as µg dendrimer conjugates per mg copolymer. Loading efficiency was defined as the ratio of the actual loading obtained to the theoretical loading.

4.2.7 Scanning Electron Microscopy (SEM) observations

Surface morphology of the nanohybrids was examined by scanning electron microscopy (SEM) using a JEOL-JSM 6320F field emission microscope (JEOL USA,

Peabody, MA) as previously described [22, 24]. Samples were sputter-coated with Pt/Pd at a coating thickness of 6 nm (Polaron E5100 sputter coater system, Polaron, UK) and then visualized at an accelerating voltage of 4.0 mV and 8.0 mm working distance.

4.2.8 Cell culture

The KB cell line was purchased from the American Type Tissue Collection (ATCC, Manassas, VA) and grown continuously as a monolayer at 37 °C, 5% CO₂ in GIBCO RPMI 1640 medium (Invitrogen Corporation, Carlsbad, CA), resulting in FR-downregulated KB cells (KB FR⁻). The RPMI 1640 medium was supplemented with penicillin (100 units/mL), streptomycin (100 mg/mL), and 10% heat-inactivated fetal bovine serum (FBS) (Invitrogen) before use. Some of the cells were cultured in FA-deficient RPMI 1640 media (Invitrogen) for at least 4 days before experiments, resulting in FR-overexpressing KB (KB FR⁺) cells [22, 25].

4.2.9 Dendrimer release kinetics in cell-conditioned culture media

KB FR⁺ cells were seeded in 12-well plates at a density of 2×10^5 cells/well in complete FA-deficient RPMI 1640 for 24 h. The complete medium was then replaced with basal FA-deficient RPMI 1640, and the cells were incubated up to 48 h. At 1, 4, 24, and 48 h, the media were withdrawn and used to dissolve the nanohybrids in triplicate to achieve a concentration equivalent to 100 nM G4-RHO-FA-OH. The nanohybrids were then incubated for 1, 4, 24, and 48 h. At the end of each incubation time, the solutions were centrifuged at 14,000 rpm ($23,708 \times g$) for 5 min to precipitate intact nanohybrids, and the fluorescence intensities of the supernatants were measured. The

amounts of the dendrimer conjugates released over time were determined based on a standard curve of G4-RHO-FA-OH fluorescence versus concentration in basal FA-deficient RPMI 1640, as described above.

4.2.10 Cellular interactions of the nanohybrids labeled with two dyes (RHO and FITC)

KB FR⁺ cells were seeded in 4-well chamber slides (Millicell EZ Slide, Millipore, Billerica, MA) at a density of 1.0×10^5 cells/well and incubated in FA-deficient RPMI 1640 for 24 h. The cells were then treated with G4-RHO-FA-OH, G4-RHO-OH, the corresponding FITC-labeled nanohybrids, and empty FITC-NPs for 30 min (G4-RHO-FA-OH only), 1, 4, 24, and 48 h, at a concentration of 100 nM based on the dendrimer conjugates in basal FA-deficient RPMI 1640. Additionally, KB FR⁻ cells were also used as a negative control and incubated with G4-RHO-FA-OH and its nanohybrid formulation. After each incubation time, cells were washed twice with PBS with Ca⁺⁺/Mg⁺⁺ (Mediatech, Inc., Manassas, VA), fixed in 4% paraformaldehyde for 10 min, and washed again. The slides were then mounted with antiphotobleaching mounting media with DAPI and covered with glass coverslips for confocal observations.

4.2.11 Cellular interactions of the nanohybrids in the presence of endocytic inhibitors

KB FR⁺ cells were seeded in 4-well chamber slides as described above, and then treated with filipin (1 μ g/mL) [26], M β CD (5 mM) [27], or a mixture of filipin and M β CD in FA-deficient basal RPMI 1640 for 1 h. Cells were washed once with PBS with Ca⁺⁺/Mg⁺⁺, followed by adding G4-RHO-FA-OH (100 nM), the corresponding

nanohybrids, and empty FITC-NPs. The treatment was carried out for 4 and 24 h, after which the confocal samples were prepared as described above.

4.2.12 Penetration assay using multicellular tumor spheroids (MCTS)

MCTS formation was performed using the liquid overlay method [28]. KB FR⁺ cells from a confluent T-75 flask were detached using trypsin-EDTA and resuspended in FA-deficient RPMI 1640 at a concentration of 6×10^3 cells/mL. Five hundred microliters of the cell suspension were transferred to 8-well chamber slides (Millicell EZ Slide, Millipore, Billerica, MA) coated with 1% agarose in complete FA-deficient RPMI 1640. The cells were then incubated on agarose for 7 days to allow the formation of MCTS. After 7 days, 250 μ L of the media in each well were removed, and MCTS were treated with 250 μ L of 200 nM G4-RHO-FA-OH, an equivalent concentration of the nanohybrids, or empty FITC-NPs, for 1, 4, 24, and 48 h. After each treatment, MCTS were carefully washed twice with PBS with Ca⁺⁺/Mg⁺⁺, fixed in paraformaldehyde for 10 min, and washed again. The chamber gasket was then removed, and the pieces of agarose were transferred to glass cover slips for confocal observation.

4.2.13 Confocal microscopy observation

Cells incubated with various nanomaterials as described above were visualized using a Zeiss LSM 510 Meta confocal laser scanning microscope (CLSM, Carl Zeiss, Germany). A 25 mW diode UV 405 nm laser was used for excitation of DAPI, the 543 nm line of a 1 mW tunable HeNe laser was used for excitation of RHO, and the 488 nm line of a 30 mW tunable Ar laser was used for the excitation of FITC. Emission was filtered at 420 nm, 565-595 nm, and 505-530 nm for DAPI, RHO and FITC, respectively. Images were captured using a 63x/1.2 Water DIC C-Apochromat objective. Z-stack

images for the 2D cell culture experiments were taken at 1 μm intervals for a total slice thickness of 8 μm . For the penetration assay, MCTS were viewed using a 10x/0.25 Ph1 A-Plan objective, and Z-stack images were taken at 20 μm intervals for a total slice thickness of 140 μm .

4.2.14 Cytotoxicity assay of the MTX-conjugated dendrimers and nanohybrids

Each of G4-RHO-FA-OH-MTX, G4-RHO-OH-MTX, or free MTX was encapsulated into PEG-PLA NPs using the double emulsion method as described above. KB FR⁺ cells were seeded in 96-well plates at a density of 5×10^3 cells/well for 24 h. The cells ($n = 4$) were then treated with 1 μM free MTX or an equivalent concentration of the dendrimer conjugates, nanohybrids, or MTX-encapsulated NPs in basal FA-deficient RPMI 1640 for 1, 4, 24, 48, and 72 h. After each incubation time, the media was replaced with complete FA-deficient RPMI 1640 and the cells were further incubated for 72 h to allow them to proliferate, while changing the media after 48 h. At 72 h post-treatment, the media was replaced, and the MTS assay reagent (CellTiter 96 AQueous One Solution (MTS) Assay, Promega, Madison, WI) was added to each well. The cells were incubated for 2 h, and the plates were read at 492 nm absorbance wavelength. Cell viability was expressed as % proliferation relative to untreated cells and plotted against incubation time. A similar experiment was conducted with the control conjugates without MTX (G4-RHO-FA-OH and G4-RHO-OH and their nanohybrids) and empty NPs.

4.3 RESULTS AND DISCUSSION

4.3.1 Preparation of the G4 PAMAM dendrimer conjugates and nanohybrids

A general overview of the preparation of the nanohybrids is illustrated in Figure 4.1. RHO-labeled, FA-targeted G4 PAMAM dendrimers were prepared by sequential conjugation with RHO and FA, followed by hydroxylation of the remaining amine groups, resulting in G4-RHO-FA-OH (Figure 4.1(A)). The hydroxylation step was performed to eliminate non-specific interactions between amine-terminated dendrimers and cell membranes as well as to enable subsequent conjugation with MTX through an ester bond [23]. Conjugation of RHO and FA to the dendrimers and successful end-capping of the amine groups was confirmed using ^1H NMR and zeta potential measurements (Table 4.1 and Figure 4.2). The ^1H NMR spectra (Figure 4.2) revealed that the conjugates prepared in this study contained approximately 3.9 and 4.3 RHO and FA molecules per dendrimer, respectively. Since the characteristic proton peaks of MTX were overlapping with those of FA and RHO, the no. of MTX molecules present could

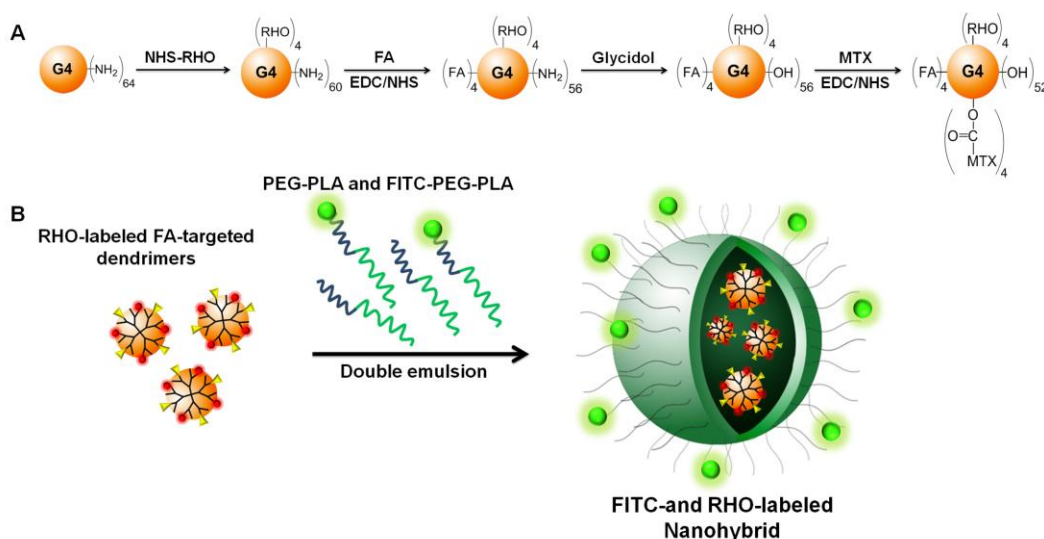


Figure 4.1. Overview of nanohybrid preparation. (A) Sequential preparation of the targeted dendrimer conjugates, (B) Encapsulation of the dendrimer conjugates into PEG-PLA copolymers to produce the nanohybrids.

not be estimated by ^1H NMR. For this reason, MTX conjugation was confirmed using UV/Vis (Figure 4.3), which revealed that there are approximately 4.7 and 5.6 MTX molecules attached to G4-RHO-FA-OH and G4-RHO-OH, respectively. PEG-PLA and FITC-PEG-PLA copolymers were synthesized by bulk polymerization of *D,L*-lactide using mPEG5K and Boc-NH-PEG5K-OH as initiators. ^1H NMR was used to confirm the

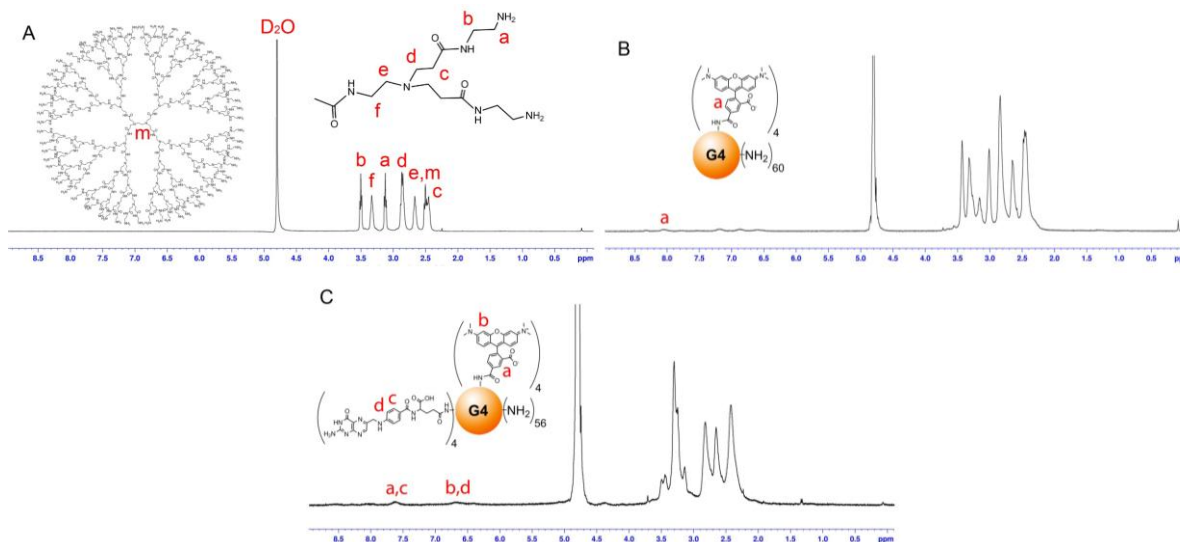


Figure 4.2. ^1H NMR spectra of (A) G4 PAMAM dendrimer, (B) G4-RHO-NH₂, and (C) G4-RHO-FA-NH₂. The ^1H NMR spectrum of G4 PAMAM dendrimers (A) shows 6 characteristic peaks at 2.46, 2.65, 2.84, 3.01, 3.32, and 3.43 ppm. After conjugation with RHO, new peaks between 6.50 and 8.50 ppm corresponding to the aromatic protons of RHO were observed (B). Based on the relative integration values at 8.04 ppm and the dendrimer peaks, it was calculated that each dendrimer has approximately 3.9 RHO molecules. For G4-RHO-FA-NH₂ (C), an increase in the integration values at 6.68 and 7.76 ppm, compared to G4-RHO, indicated successful FA conjugation. Based upon the difference in the relative integration values of the characteristic RHO and FA peaks, it was calculated that approximately 4.3 FA molecules were attached to the dendrimer.

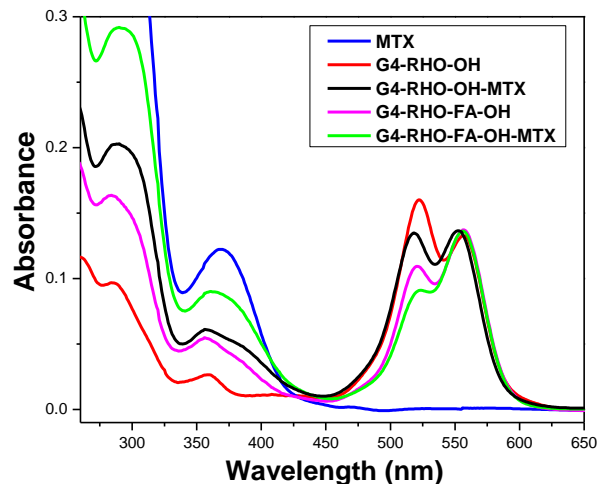


Figure 4.3. UV/Vis spectra of MTX, MTX-dendrimer conjugates, and the control dendrimers in ddH₂O. Based on the absorbance of the conjugates at 373 nm, G4-RHO-FA-OH-MTX and G4-RHO-OH-MTX each contain 4.7 and 5.6 MTX molecules per dendrimer, respectively.

chemical structure of the copolymers and to estimate the MW of the PLA block (Figure 4.4). This was calculated to be 44,900 g/mol for PEG-PLA (M_n : 37,500, M_w : 45,521, PDI: 1.2 as measured by GPC) and 48,800 g/mol for Boc-NH-PEG-PLA based on the relative integration ratios of peak b around 3.62 ppm (the protons of the ethylene oxide repeating units) to peak c around 5.15 ppm (the lactide repeating units). Following deprotection of Boc-NH-PEG-PLA, H₂N-PEG-PLA was obtained and conjugated to FITC, which was also confirmed using ¹H NMR (Figure 4.4).

The various dendrimer conjugates were then encapsulated into PEG-PLA copolymers using the double emulsion method to produce the nanohybrids as we described earlier (Figure 4.1(B)). Dendrimer encapsulation was performed using double emulsion to prepare nanohybrids with controlled particle sizes around 100 nm in diameter (Figure 4.5) and at high loading efficiencies (67 – 83%) (Table 4.1). The change in zeta potential values for the nanohybrids (-11.6 – -18.6 mV) compared to

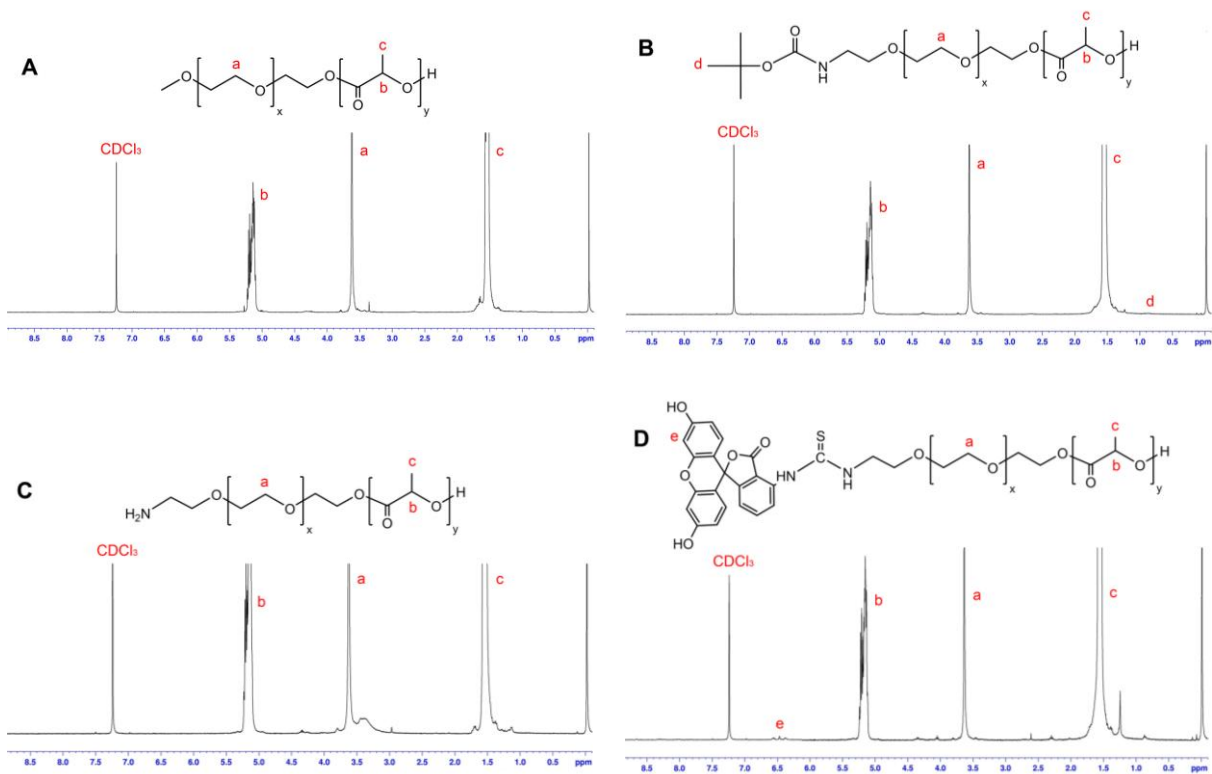


Figure 4.4. ^1H NMR spectra of (A) PEG-PLA, (B) Boc-NH-PEG-PLA, (C) deprotected H_2N -PEG-PLA, and (D) FITC-PEG-PLA. The ^1H NMR spectrum of PEG-PLA shows two characteristic peaks of PLA at 5.15 and 1.55 ppm (b and c), corresponding to the protons of the methine and methylene groups, respectively. As for mPEG, the characteristic peak corresponding to the ethylene glycol repeating units (b) was observed at 3.62 ppm. The MWs of PEG-PLA were estimated using the relative integration ratios of peaks b and c, based on the integral value for peak a of mPEG. This was calculated to be 44,900 g/mol for PEG-PLA and 48,800 g/mol for Boc-NH-PEG-PLA. Deprotection of Boc-NH-PEG-PLA was confirmed by the disappearance of peak d (0.85 ppm) corresponding to the Boc group. Conjugation of FITC to H_2N -PEG-PLA was confirmed by the appearance of peak e at 6.45 ppm corresponding to the aromatic protons of FITC, and it was calculated that 0.8 FITC molecules were attached to the polymer based on the relative integration ratio of peaks a and e.

Table 4.1. Characterization of the G4 PAMAM dendrimers and nanohybrids

	Particle size (nm)	Zeta potential (mV)	Loading efficiency (%)
G4-RHO-NH ₂	16.7 ± 2.4	28.1 ± 1.8	N/A
G4-RHO-OH	12.1 ± 7.3	4.2 ± 1.7	N/A
G4-RHO-OH-MTX	15.2 ± 3.2	2.5 ± 0.7	N/A
G4-RHO-FA-OH	19.6 ± 7.8	3.4 ± 1.6	N/A
G4-RHO-FA-OH-MTX	13.4 ± 5.3	3.2 ± 1.1	N/A
FITC-NP	114.7 ± 5.7	-13.5 ± 4.2	N/A
G4-RHO-OH/FITC-NP	101.5 ± 8.5	-11.6 ± 3.3	69.0
G4-RHO-OH-MTX/NP	89.8 ± 12.5	-18.6 ± 3.5	83.1
G4-RHO-FA-OH/FITC-NP	125.5 ± 10.2	-15.3 ± 6.5	72.5
G4-RHO-FA-OH-MTX/NP	79.8 ± 5.4	-14.4 ± 5.7	67.2

those of the dendrimer conjugates before encapsulation (3.4 – 28.1 mV) indicated successful encapsulation.

4.3.2 Selective cellular interactions of the nanohybrids containing targeted dendrimers

Non-targeted polymeric NPs have been reported to exhibit a degree of non-specificity when incubated with cells [21, 29]. Targeted dendrimers on the other hand have shown excellent receptor selectivity with minimal non-specific uptake after neutralization of the surface groups [22, 25]. Our design strategy is based on

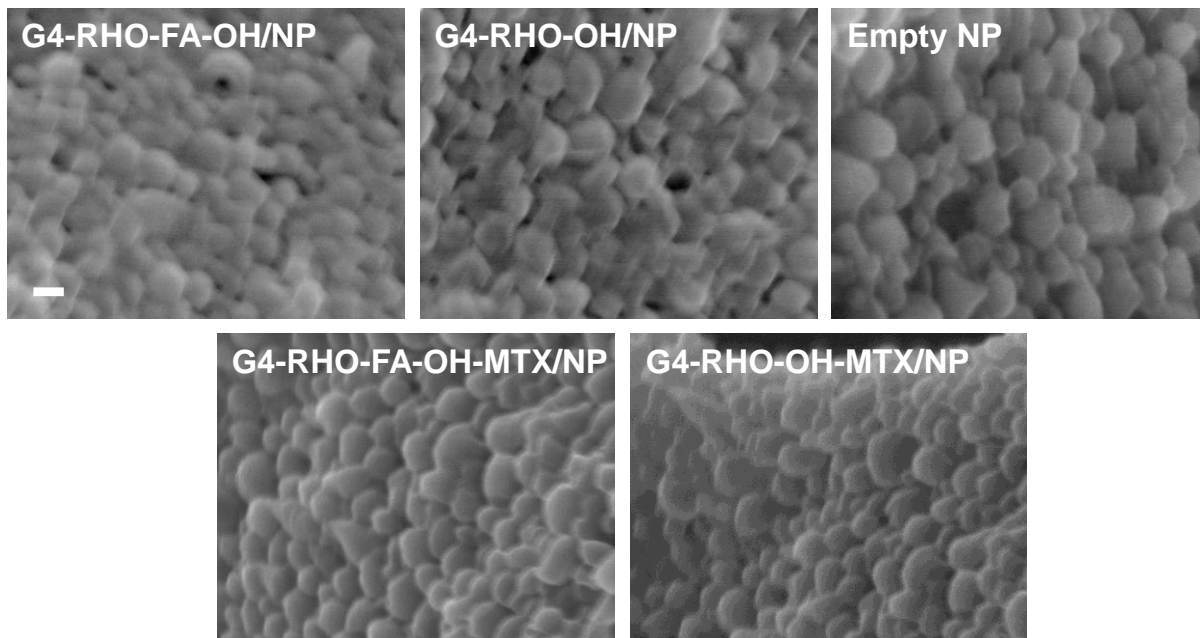


Figure 4.5. SEM images of the nanohybrids prepared in this study showing controlled particle sizes around 100 nm in diameter (scale bar: 100 nm).

hybridization of the two nanocarriers, which is hypothesized to impart both dendrimer- and NP-like attributes to the nanohybrid system. To test this hypothesis, we first investigated whether the targeting efficiency of the system is more affected by the dendrimers (highly selective) or by the polymeric NPs (non-specific). We previously monitored the cellular uptake of the FA-targeted nanohybrids based on RHO conjugated to the dendrimers, showing high selectivity of the nanohybrids to KB FR⁺ cells up to 4 h of incubation [22]. In this paper, we conducted a similar experiment using a two-dye system, i.e., FITC-labeled NPs encapsulating RHO-labeled dendrimers, and observed the cellular interactions of the nanohybrids up to 48 h of incubation.

As similarly observed in our previous report, after 1 h of incubation, only the free targeted dendrimers (G4-RHO-FA-OH) showed significant cellular binding and uptake into KB FR⁺ (Figure 4.6). The targeted nanohybrids (G4-RHO-FA-OH/FITC-NP) started

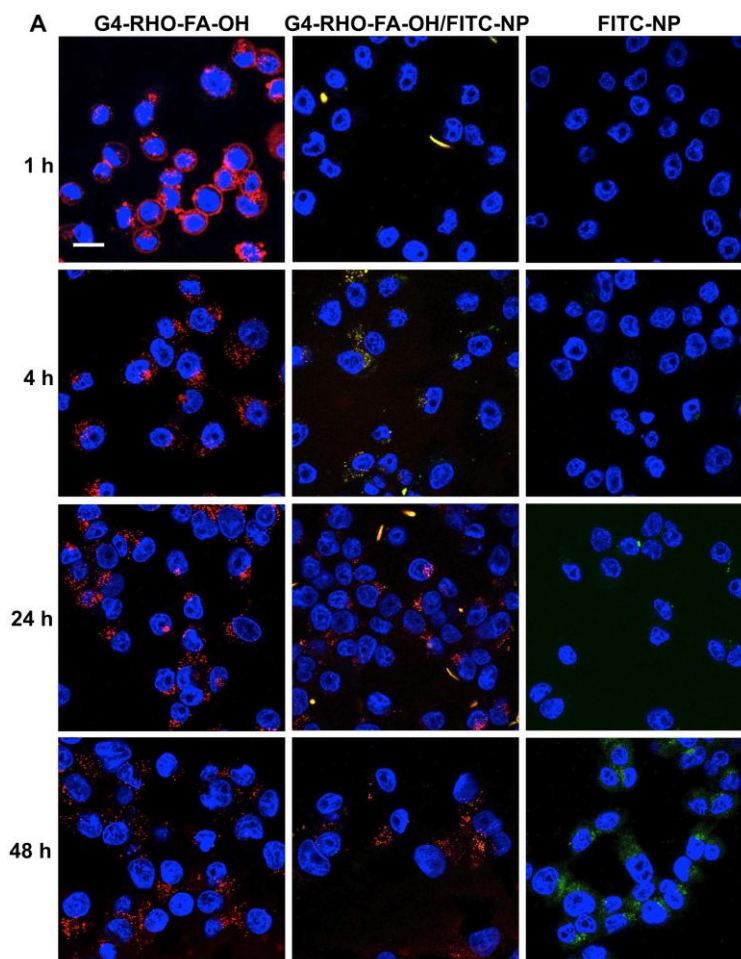


Figure 4.6. CLSM images of KB FR⁺ cells upon incubation with G4-RHO-FA-OH (left column), G4-RHO-FA-OH-encapsulated nanohybrids (middle column), and empty FITC-NPs (right column) up to 48 h. Red: RHO-labeled dendrimers, green: FITC-labeled NPs, blue: cell nuclei stained by DAPI, scale bar: 20 μ m.

to selectively interact with the cells after 4 h, likely due to the protective effect of the polymeric shell (Figure 4.6 and Figure 4.7). The overlap in the red and green fluorescence signals in those images shows the co-localization of the dendrimers with the nanohybrid shell, indicating that the nanohybrids interacted with cells intact. This interaction was seemingly specific, as the fluorescence from the targeted nanohybrids was significantly higher than that of the non-targeted nanohybrids (G4-RHO-OH/FITC-

NP) and that from KB FR⁺ cells (Figure 4.8). Green fluorescence signals from empty FITC-NPs were also negligible (Figure 4.6 and Figure 4.7). Our observations indicate that the targeted dendrimers, particularly those near the surface of the nanohybrids, may act as a driving force that contributes to the selective association with FR on the

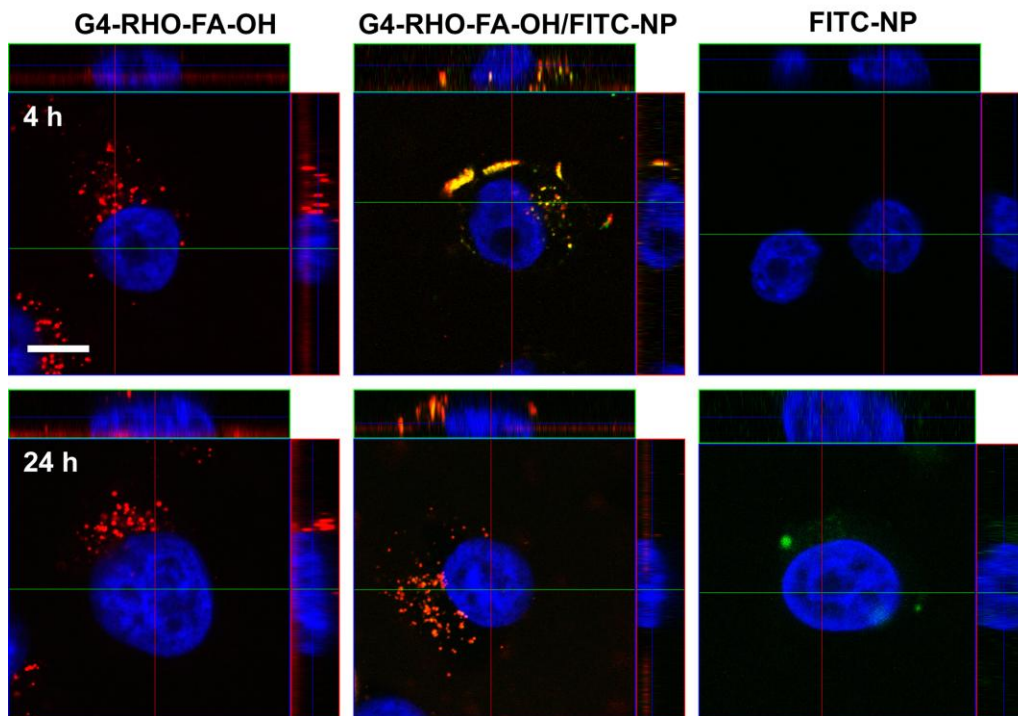


Figure 4.7. Ortho view of Z-stack images of KB FR⁺ cells upon incubation with G4-RHO-FA-OH (left column), G4-RHO-FA-OH-encapsulated nanohybrids (middle column), and empty FITC-NPs (right column) at 4 and 24 h. Red: RHO-labeled dendrimers, green: FITC-labeled NPs, blue: cell nuclei stained by DAPI, scale bar: 10 μm . The targeted dendrimers show specific interaction with KB FR⁺ throughout the incubation period. The targeted nanohybrids start to selectively interact with the cells after 4 h as the overlapping red and green fluorescence signals are observed. At longer incubation hours (24 h and Figure 25), the red signals become predominant, indicating that the released dendrimers selectively interact with the KB FR⁺ cells. The empty NPs start to interact with the cells after 24 h likely due to non-specific interactions.

cells. After 24 h, the targeted nano hybrids still showed a degree of overlap in the red

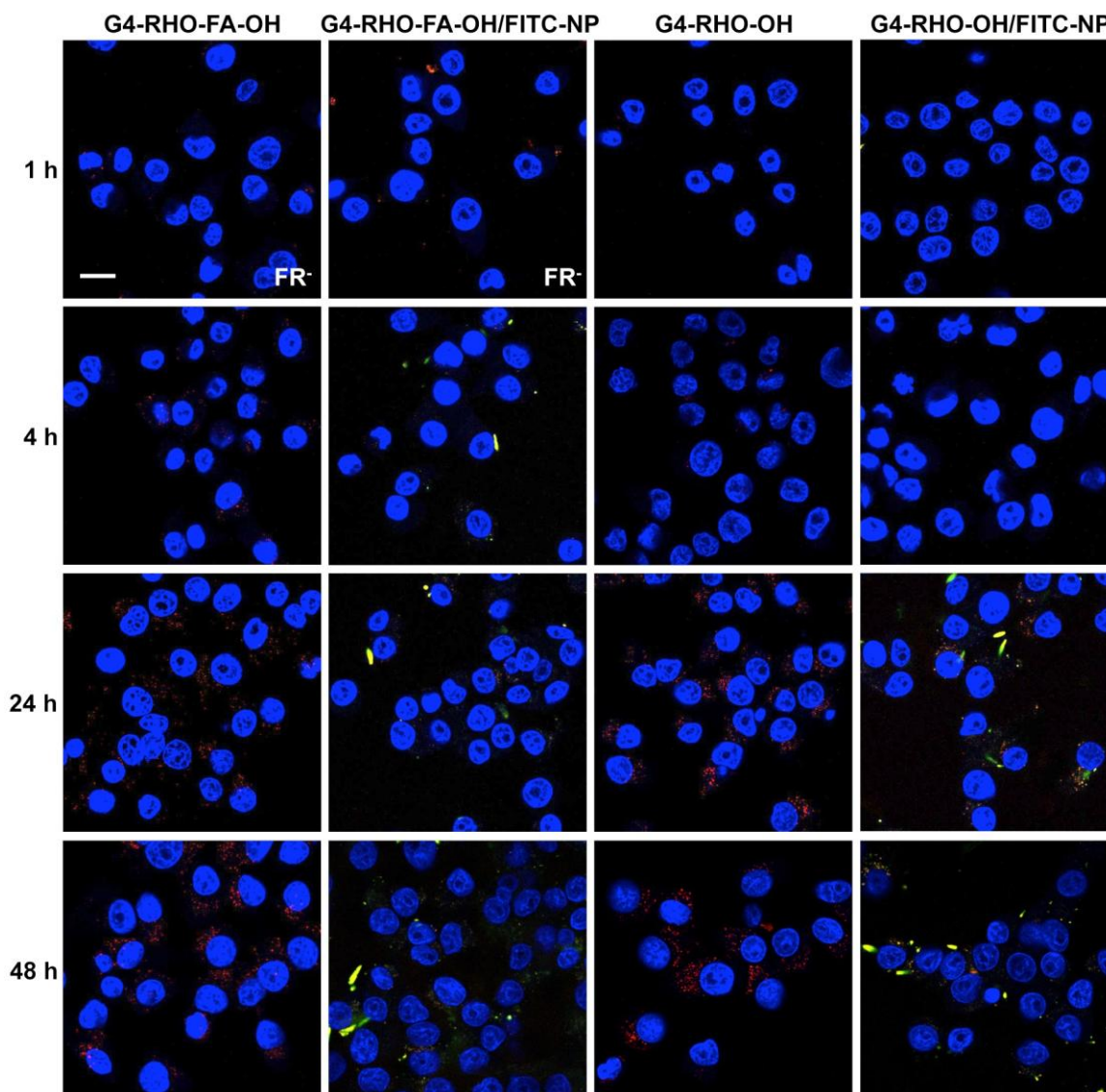


Figure 4.8. CLSM images of (L to R): KB FR⁻ cells incubated with G4-RHO-FA-OH, KB FR⁻ cells incubated with G4-RHO-FA-OH/FITC-NPs, KB FR⁺ cells incubated with G4-RHO-OH, and KB FR⁺ cells incubated with G4-RHO-OH/FITC-NPs up to 48 h. G4-RHO-FA-OH and its corresponding nano hybrids show limited interactions with KB FR⁻ cells. Nontargeted dendrimer conjugates (G4-RHO-OH) and their corresponding nano hybrids show a significantly lower degree of interactions with KB FR⁺ cells compared to the FA-targeted systems (Figure 25). Red: RHO-labeled dendrimers, green: FITC-labeled NPs, blue: DAPI, scale bar: 20 μ m.

and green signals; however, an increase in the red fluorescence intensity relative to the green signal was observed from the cells when compared to that at 4 h. The separation of the red signal from the green fluorescence is a clear indication of the dendrimer release from the nanohybrids after 24 h of incubation, which became predominantly observed from the cells at the longer incubation hours (24-48 h). After 48 h of incubation, non-specific cellular interactions were observed as non-targeted systems and the empty FITC-NPs started to interact with the cells (Figure 4.6 and Figure 4.8).

4.3.3 The cellular microenvironment facilitates dendrimer release from the nanohybrids

Release kinetics of macromolecules from polymeric NPs with similar MW to the PEG-PLA copolymers used in this study are typically slow and can take up to several days to weeks to complete the release. For example, we have previously conducted a release study of the dendrimers from the nanohybrids in PBS and found that only 18% and 38% of the dendrimer conjugates are released after 4 and 24 h, respectively [22]. Unexpectedly, Figure 4.6 shows that the cellular uptake kinetics were much faster and completed within 48 h, which is likely due to the presence of cells that accelerate the release kinetics. We thus investigated the effect of the cellular microenvironment on the dissociation and release of the dendrimer conjugates from the nanohybrids. The release medium used for this experiment was the same culture medium used for the cellular uptake studies after conditioning in the presence of cells for various incubation hours. As shown in Figure 4.9, the release kinetics in conditioned culture medium was significantly faster (38% and 60% release after 4 and 24 h, respectively) compared to that obtained using PBS. This accelerated release profile confirmed that the selective

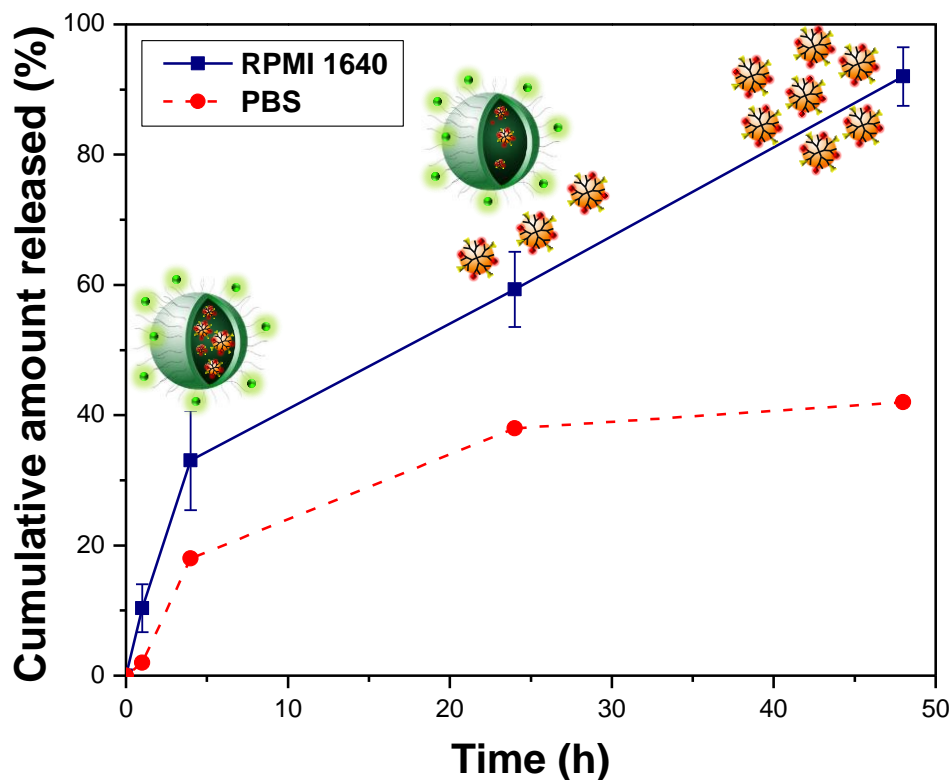


Figure 4.9. Release kinetics of G4-RHO-FA-OH/FITC-NP in cell-conditioned basal FA-deficient RPMI 1640 media. Faster release kinetics were obtained compared to the release profile in PBS (red dotted line, adapted from Figure 17), with ~90% of the dendrimer conjugates released after 48 h of incubation.

cellular interaction observed in Figure 4.6 is primarily a result of the release of the targeted dendrimers from the nanohybrids at longer incubation hours. Thus, by conducting the release test in the conditioned media, we can better understand the effect of the cellular microenvironment on the release kinetics of the nanohybrids. This serves as a valuable *in vitro* tool that can help predict the *in vivo* behavior of the nanohybrids.

4.3.4 Dual properties in cellular interactions of the nanohybrids revealed by endocytic inhibitors

Nanocarriers (both targeted and non-targeted) are known to be associated with various internalization mechanisms such as endocytosis (clathrin-, caveolae-mediated, or non-specific adsorptive endocytosis), energy-independent cell entry, and macropinocytosis [29-31]. Although controversial, polymeric NPs have been reported to internalize into cells through non-specific pathways that are frequently associated with clathrin-mediated endocytosis, whereas FA-targeted dendrimers reportedly utilize caveolae-mediated endocytosis similar to other FA-targeted systems [32]. M β CD is a commonly used agent for cellular uptake studies and is known to extract cholesterol from membranes, which inhibits clathrin-coated pit formation and subsequent endocytosis [27]. Filipin on the other hand is known to inhibit caveolae-mediated endocytosis [26].

We compared the cellular uptake mechanism of the FA-targeted nanohybrids to that of free FA-targeted dendrimers and non-targeted empty FITC-NPs under the presence of filipin, M β CD, or a combination of the two agents, at various incubation times. As shown in Figure 4.10, cellular uptake of G4-RHO-FA-OH was inhibited by filipin and filipin/M β CD, but not affected by M β CD alone up to 24 h. In contrast, the internalization of the nanohybrids was inhibited by both M β CD and filipin/M β CD at 4 h but only by filipin/M β CD after 24 h. These observations indicate that the cellular interaction of the nanohybrids follows a similar pathway to polymeric NPs at early incubation times. After 24 h, as more dendrimers are released, the nanohybrids exhibit characteristics of both dendrimers and NPs, requiring the blockade of the two pathways to inhibit their internalization.

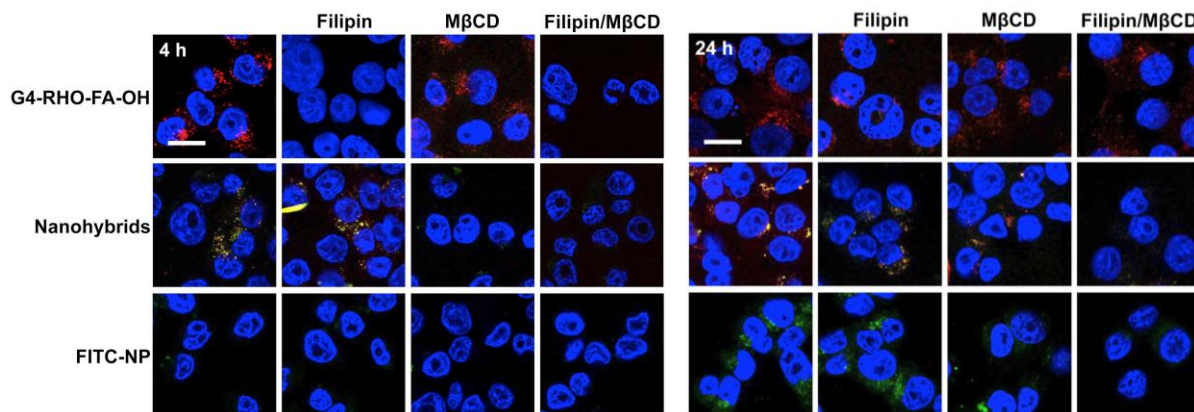


Figure 4.10. Effect of endocytic inhibitors on cellular interactions of the nanohybrids observed using CLSM. KB FR⁺ cells were incubated with G4-RHO-FA-OH, nanohybrids (G4-RHO-FA-OH/FITC-NP), and empty FITC-NPs for 4 h and 24 h. Red: RHO-labeled dendrimers, green: FITC-labeled NPs, blue: cell nuclei stained by DAPI, scale bar: 20 μ m. Cellular uptake of the targeted dendrimers is fully inhibited at 4 h by filipin and filipin/M β CD, but not affected by M β CD alone. The uptake of the targeted nanohybrids is inhibited by M β CD and filipin/M β CD at 4 h, exhibiting polymeric NP-like behavior. However, at 24 h, only filipin/M β CD blocks the interaction of the nanohybrids, and yet limited effect of M β CD is observed, indicating the selective cellular interactions by the released dendrimers (red fluorescence). As expected, non-specific uptake of the empty FITC-NPs at 24 h is inhibited by M β CD and filipin/M β CD.

The cellular uptake inhibition of empty FITC-NPs at 4 h was not as obvious since the incubation time may not have been enough to achieve significant non-specific internalization of the NPs. However, inhibition was observed at 24 h by M β CD and filipin/M β CD, confirming that the cellular uptake of NPs was dependent on non-specific clathrin-mediated mechanism. Even though the inhibitory effect of filipin and M β CD was partially reversed by 24 h, resulting in incomplete inhibition for some groups (G4-RHO-FA-OH at 24 h), these results confirm that the nanohybrids possess both NP-like and dendrimer-like characteristics in an incubation time-dependent manner.

4.3.5 Targeted dendrimers penetrate tumor spheroids following their release from the nanohybrids

Tumor spheroids generated by the liquid overlay method can serve as a reliable *in vitro* 3D tumor model. Their multicellular organization represents not only cell aggregates, but has also been reported to contain an organized extracellular matrix resembling that of tumors *in vivo* [33, 34]. The small size, molecular flexibility, and deformability of dendrimers have been shown to contribute to their highly efficient tissue penetration through tumors and 3D tumor models such as MCTS [35, 36].

Using MCTS, we assessed tumor penetration of the FA-targeted dendrimers and nanohybrids up to 48 h incubation. Figure 4.11 shows confocal images taken at a depth of 80 μm into each spheroid. Free G4-RHO-FA-OH starts to penetrate into the spheroids within 1 h. For the nanohybrids, a delay up to 4 h in spheroid penetration was observed, followed by substantially increased red signals, representing that the released dendrimers have reached the core of the spheroids. The absence of green signals in the core of the spheroids treated with the nanohybrids strongly indicates that only the released dendrimers were able to penetrate as deep as free dendrimers, while the intact nanohybrids remained at the periphery. A similar observation, with more nanohybrids clustered at the MCTS periphery, was obtained at 24 and 48 h. As expected, empty FITC-NPs were not able to penetrate the spheroids, remaining on top or at the periphery. The results highlighted in Figure 30 serve as *in vitro* validation for the design rationale of our multi-scale nanohybrid system, where efficient tumor penetration can be achieved by the smaller, highly flexible dendrimers upon release from the NP shell that has suitable size for passive targeting to tumors.

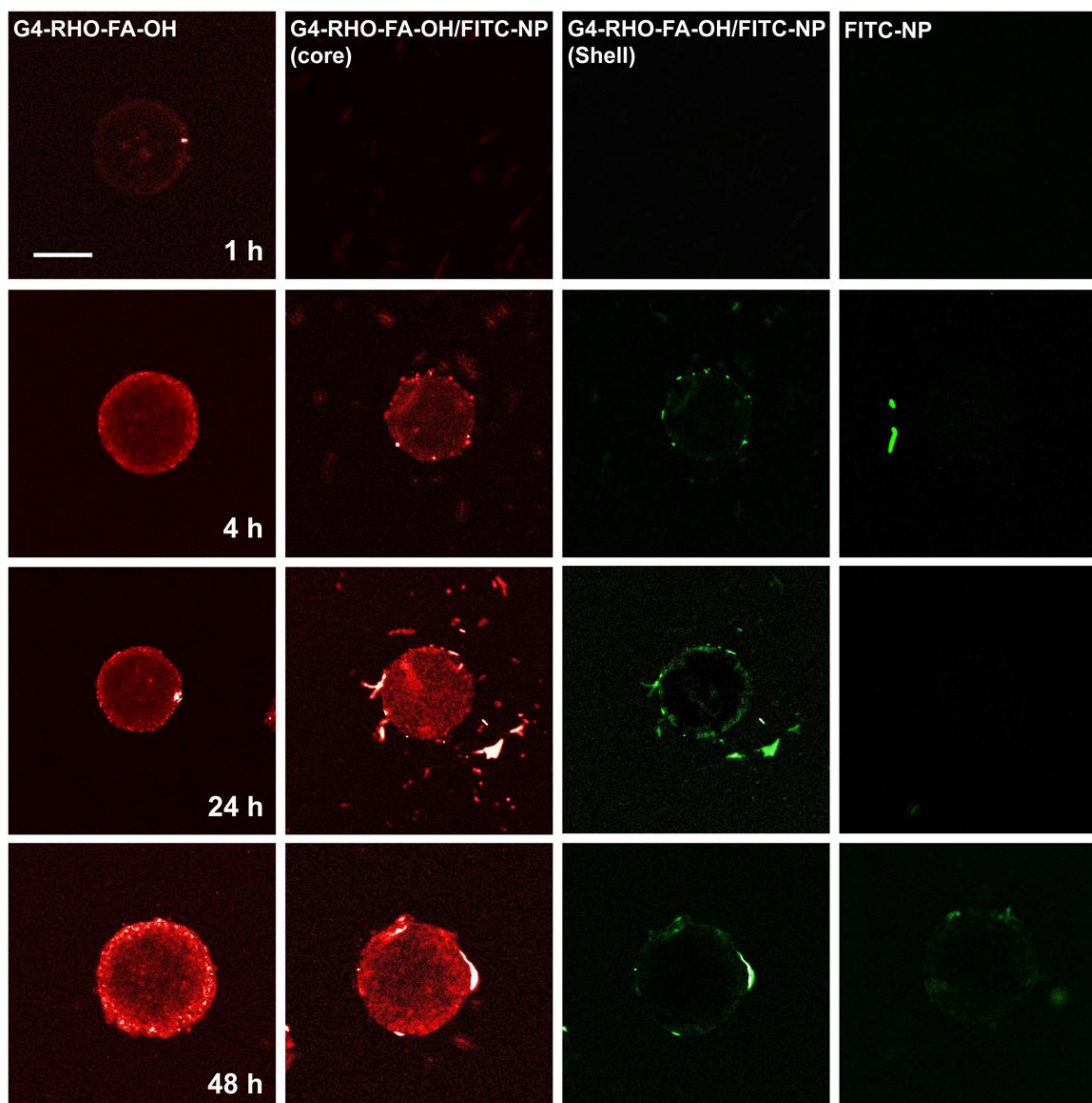


Figure 4.11. (A) CLSM images of KB FR⁺ MCTS upon incubation with G4-RHO-FA-OH, G4-RHO-FA-OH/FITC-NP, and empty FITC-NPs up to 48 h. Red: RHO-labeled dendrimers, green: FITC-labeled NPs. Images shown were taken at a depth of 80 μm into each spheroid, scale bar: 100 μm . Only the free dendrimers and those released from the nanohybrids are able to penetrate deep into the spheroids. Empty FITC-NPs and intact nanohybrids accumulate at the periphery of the spheroids even after 48 h.

4.3.6 The nanohybrid platform enables temporal control over cytotoxicity

In order to validate the drug delivery potential of the nanohybrids, we employed MTX as a model chemotherapeutic drug [18, 19]. For this experiment, MTX was

conjugated to the targeted and non-targeted dendrimer conjugates, followed by encapsulation into PEG-PLA, resulting in the MTX-containing nanohybrids. As shown in Figure 4.12, no significant inhibition in cell proliferation was observed within the first 4 h of incubation, which can be attributed to the incomplete release of the drug and drug

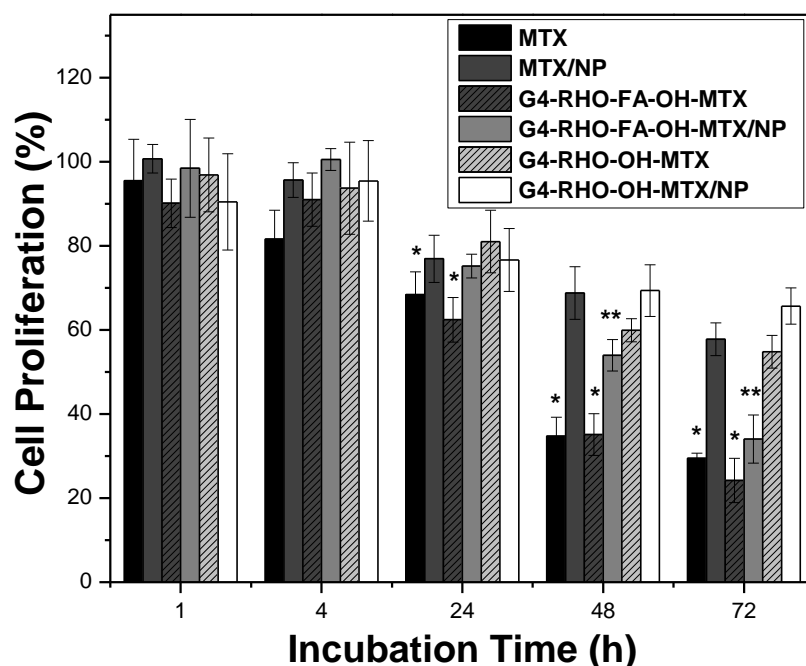


Figure 4.12. Cell proliferation kinetics of KB FR⁺ (n = 4) after treatment with MTX-conjugated dendrimers and nanohybrids at a concentration equivalent to 1 μ M MTX over 72 h. The MTS assay was performed after additional 72 h to allow the cells to proliferate. Free MTX and the MTX-conjugated FA-targeted dendrimers start to exhibit cytotoxicity after 24 h, as indicated by the reduction in cell proliferation (<80%) relative to untreated controls. G4-RHO-FA-OH-MTX-encapsulated nanohybrids show a similar effect on cell growth at the 72 h time point but with a time delay of 48 h due to the controlled release of the dendrimer conjugates. * and ** denote significant difference in cell proliferation relative to the non-targeted dendrimer conjugates (G4-RHO-OH-MTX) and nanohybrids (G4-RHO-OH-MTX/NP), respectively. Statistical analysis was performed using OriginPro 8.5 using 1-way ANOVA followed by Tukey's post hoc test at $p < 0.05$.

conjugates from the various systems. After 24 h, free MTX and the targeted dendrimer-MTX conjugates (G4-RHO-FA-OH-MTX) showed a significant inhibition in cell proliferation, and a less but obvious anti-proliferation effect was observed from the group treated with the targeted nanohybrids (G4-RHO-FA-OH-MTX/NP). The targeted nanohybrids showed a delay in the cellular uptake of the drug conjugates, which translated into a delay in the cytotoxic effect of MTX, while maintaining the similar receptor selectivity as the free targeted dendrimers. After 72 h of incubation, the targeted nanohybrids maintained their selectivity as shown in the significantly higher cytotoxic effect compared to the non-targeted nanohybrids containing G4-RHO-OH-MTX and MTX-encapsulated NPs.

These results provide a promising starting point for future *in vivo* translation of this system. The controlled release of the targeted dendrimer-drug conjugates from the nanohybrids is expected to protect against premature elimination from the circulation, while improving their tumor accumulation and penetration through sequential passive and active targeting.

4.4 CONCLUSION

Taken together, the results highlighted herein demonstrate the temporally controlled, dual nature of the multi-scale nanohybrid platform. Through a series of *in vitro* experiments that simulate *in vivo* situations, our results indicate that the dendrimer-polymer nanohybrid system combines the characteristics of free dendrimers, such as high receptor selectivity and efficient tumor penetration, with the controlled release properties and larger size of the polymeric NPs. Co-localization of the dendrimers and the polymeric NP shell of the nanohybrids showed the selective uptake of the intact

nanohybrids at 4 h of incubation (Figure 25 and Figure 26). The release of free dendrimers, which was facilitated in the culture medium (Figure 28), enhanced the selective uptake of the nanohybrids up to 24 h, as supported by the increased red fluorescence signals from KB FR⁺ observed at longer incubation times (Figure 25). Inhibition of different endocytic pathways revealed that the uptake mechanism of the nanohybrids closely resembles polymeric NPs at earlier time points, and follows both dendrimers- and NP-like pathways at longer incubation times (Figure 29). MCTS served as an effective 3D *in vitro* model for tumor penetration and showed the released dendrimers from the nanohybrids can still achieve efficient penetration similar to free dendrimers (Figure 30). Finally, the *in vitro* cytotoxicity results (Figure 31) demonstrate the high FR selectivity of the FA-targeted dendrimer-MTX conjugates and their nanohybrids. In addition to the selective toxicity, the targeted nanohybrids also exhibited the controlled cellular uptake kinetics that is attributed to the nanohybrid design. These results will be further validated *in vivo* to demonstrate the tumor targeting efficacy of the nanohybrids through a combination of longer circulation time and enhanced tumor selectivity and penetration.

4.5 REFERENCES

1. Duncan, R., *Polymer conjugates as anticancer nanomedicines*. Nat. Rev. Cancer, 2006. **6**(9): p. 688-701.
2. Gref, R., et al., *Biodegradable long-circulating polymeric nanospheres*. Science, 1994. **263**(5153): p. 1600-1603.
3. Jin, S.-E., J.W. Bae, and S. Hong, *Multiscale observation of biological interactions of nanocarriers: From nano to macro*. Microsc. Res. Techniq., 2010. **73**(9): p. 813-823.
4. Nasongkla, N., et al., *Multifunctional polymeric micelles as cancer-targeted, MRI-ultrasensitive drug delivery systems*. Nano Lett., 2006. **6**(11): p. 2427-2430.
5. Pearson, R.M., et al., *Dendritic nanoparticles: the next generation of nanocarriers? Therapeutic delivery*, 2012. **3**(8): p. 941-59.
6. Torchilin, V.P., *Recent advances with liposomes as pharmaceutical carriers*. Nat. Rev. Drug Discov., 2005. **4**(2): p. 145-160.
7. Matsumura, Y. and H. Maeda, *A New concept for macromolecular therapeutics in cancer chemotherapy - Mechanism of tumoritropic accumulation of proteins and the antitumor agent SMANCS*. Cancer Res., 1986. **46**(12): p. 6387-6392.
8. Peer, D., et al., *Nanocarriers as an emerging platform for cancer therapy*. Nat. Nanotechnol., 2007. **2**(12): p. 751-760.
9. Danhier, F., O. Feron, and V. Preat, *To exploit the tumor microenvironment: Passive and active tumor targeting of nanocarriers for anti-cancer drug delivery*. J. Control. Release, 2010. **148**(2): p. 135-146.

10. Hu, C.M.J., et al., *Half-antibody functionalized lipid-polymer hybrid nanoparticles for targeted drug delivery to carcinoembryonic antigen presenting pancreatic cancer cells*. Mol. Pharm., 2010. **7**(3): p. 914-920.
11. Bae, Y., et al., *Multifunctional polymeric micelles with folate-mediated cancer cell targeting and pH-triggered drug releasing properties for active intracellular drug delivery*. Mol. Biosyst., 2005. **1**(3): p. 242-250.
12. Eavarone, D.A., X.J. Yu, and R.V. Bellamkonda, *Targeted drug delivery to C6 glioma by transferrin-coupled liposomes*. J. Biomed. Mater. Res., 2000. **51**(1): p. 10-14.
13. Gabizon, A., et al., *In vivo fate of folate-targeted polyethylene-glycol liposomes in tumor-bearing mice*. Clin. Cancer Res., 2003. **9**(17): p. 6551-6559.
14. Lee, H., et al., *The Effects of particle size and molecular targeting on the intratumoral and subcellular distribution of polymeric nanoparticles*. Mol. Pharm., 2010. **7**(4): p. 1195-1208.
15. Huang, K., et al., *Size-dependent localization and penetration of ultrasmall gold nanoparticles in cancer cells, multicellular spheroids, and tumors in vivo*. ACS Nano, 2012. **6**(5): p. 4483-4493.
16. Wong, C., et al., *Multistage nanoparticle delivery system for deep penetration into tumor tissue*. P. Natl. Acad. Sci. USA, 2011. **108**(6): p. 2426-2431.
17. Tang, L., et al., *Synthesis and biological response of size-specific, monodisperse drug-silica nanoconjugates*. ACS Nano, 2012. **6**(5): p. 3954-3966.

18. Myc, A., et al., *Targeting the efficacy of a dendrimer-based nanotherapeutic in heterogeneous xenograft tumors in vivo*. *Anti-Cancer Drug.*, 2010. **21**(2): p. 186-192.
19. Kukowska-Latallo, J.F., et al., *Nanoparticle targeting of anticancer drug improves therapeutic response in animal model of human epithelial cancer*. *Cancer Res.*, 2005. **65**(12): p. 5317-5324.
20. Singh, P., et al., *Folate and folate-PEG-PAMAM dendrimers: Synthesis, characterization, and targeted anticancer drug delivery potential in tumor bearing mice*. *Bioconjugate Chem.*, 2008. **19**(11): p. 2239-2252.
21. Sunoqrot, S., et al., *Kinetically controlled cellular interactions of polymer-polymer and polymer-liposome nanohybrid systems*. *Bioconjugate Chem.*, 2011. **22**(3): p. 466-474.
22. Sunoqrot, S., et al., *Temporal control over cellular targeting through hybridization of folate-targeted dendrimers and PEG-PLA nanoparticles*. *Biomacromolecules*, 2012. **13**: p. 1223-1230.
23. Majoros, I.J., et al., *Poly(amidoamine) dendrimer-based multifunctional engineered nanodevice for cancer therapy*. *J. Med. Chem.*, 2005. **48**(19): p. 5892-5899.
24. Bae, J.W., et al., *Dendron-mediated self-assembly of highly PEGylated block copolymers: a modular nanocarrier platform*. *Chem. Commun.*, 2011. **47**(37): p. 10302-10304.
25. Hong, S., et al., *The binding avidity of a nanoparticle-based multivalent targeted drug delivery platform*. *Chem. Biol.*, **2007**. **14**(1): p. 107-115.

26. Schnitzer, J.E., et al., *Filipin-sensitive caveolae-mediated transport in endothelium - Reduced transcytosis, scavenger endocytosis, and capillary permeability of select macromolecules*. J. Cell Biol., 1994. **127**(5): p. 1217-1232.
27. Rodal, S.K., et al., *Extraction of cholesterol with methyl-beta-cyclodextrin perturbs formation of clathrin-coated endocytic vesicles*. Mol. Biol. Cell, 1999. **10**(4): p. 961-974.
28. Friedrich, J., et al., *Spheroid-based drug screen: considerations and practical approach*. Nat. Protoc., 2009. **4**(3): p. 309-324.
29. Hillaireau, H. and P. Couvreur, *Nanocarriers' entry into the cell: relevance to drug delivery*. Cell. Mol. Life Sci., 2009. **66**(17): p. 2873-2896.
30. Hong, S., et al., *The role of ganglioside GM(1) in cellular internalization mechanisms of poly(amidoamine) dendrimers*. Bioconjugate Chem., 2009. **20**(8): p. 1503-1513.
31. Leroueil, P.R., et al., *Nanoparticle interaction with biological membranes: Does nanotechnology present a janus face?* Acc. Chem. Res., 2007. **40**(5): p. 335-342.
32. Rothberg, K.G., et al., *The glycopospholipid-linked folate receptor internalizes folate without entering the clathrin-coated pit endocytic pathway*. J. Cell Biol., 1990. **110**(3): p. 637-649.
33. Davies, C.D., et al., *Comparison of extracellular matrix in human osteosarcomas and melanomas growing as xenografts, multicellular spheroids, and monolayer cultures*. Anticancer Res., 1997. **17**(6D): p. 4317-4326.
34. Paulus, W., C. Huettner, and J.C. Tonn, *Collagens, integrins and the mesenchymal drift in glioblastomas: a comparison of biopsy*

- specimens, spheroid and early monolayer cultures.* Int. J. Cancer, 1994. **58**(6): p. 841-846.
35. Waite, C.L. and C.M. Roth, *PAMAM-RGD conjugates enhance siRNA delivery through a multicellular spheroid model of malignant glioma.* Bioconjugate Chem., 2009. **20**(10): p. 1908-1916.
36. Dhanikula, R.S., et al., *Methotrexate loaded polyether-copolyester dendrimers for the treatment of gliomas: Enhanced efficacy and intratumoral transport capability.* Mol. Pharm., 2008. **5**(1): p. 105-116.

CHAPTER 5

PROLONGED BLOOD CIRCULATION TIME AND ENHANCED TUMOR RETENTION OF FOLATE-TARGETED DENDRIMER-POLYMER NANOHYBRID SYSTEMS

5.1 INTRODUCTION

Over the last few decades, nanotechnology-based platforms have shown great promise in reducing the toxic side effects of anti-neoplastic drugs [1]. The controlled size of nanoparticles (NPs) such as liposomes, biodegradable polymeric NPs, and micelles allows their passive accumulation at tumor tissues through the enhanced permeability and retention (EPR) effect, while minimizing their uptake by normal tissues [2-6]. For example, FDA-approved anti-cancer NPs such as Doxil® and Abraxane® are associated with significant reduction in adverse effects compared to conventional chemotherapy due to their particle size (~100 nm) [7-9]. To increase the targeting efficacy, ligand conjugation on the surface of these NPs has also been attempted to achieve active targeting to tumors [10-15]. However, the therapeutic benefit of these NPs and the majority of nanocarriers under investigation is limited by inadequate tumor delivery. The dense tumor interstitial matrix hinders the diffusion of NPs larger than 60 nm despite their ability to cross the leaky tumor vessels, causing them to accumulate in perivascular regions and exert only local effects [16, 17].

On the other hand, smaller NPs can achieve better and interstitial transport and tumor penetration [18-22]. However, their small size is often associated with a shorter

blood half-life and nonspecific uptake by organs of the reticuloendothelial system (RES). In particular, folate (FA)-targeted poly(amidoamine) (PAMAM) dendrimers have previously shown high targeting efficacy to FA receptor (FR)-overexpressing tumor xenografts [23-27]. Unfortunately, their small size (~ 5 nm in diameter) and the surface exposure of the targeting ligands has been the cause of their short circulation time and significant liver uptake [27, 28].

To maximize the targeting efficacy of existing nanocarriers, there is an emerging requirement to develop a multi-scale system. The ideal properties of this system are to combine actively-targeted smaller NPs that possess favorable tissue penetration and diffusivity, with larger NPs with a controlled size for passive targeting and longer blood circulation times. Previously, we have designed a multi-scale hybrid NP platform that combines targeted dendrimers with larger polymeric NPs [29, 30]. Using FA-targeted generation 4 (G4) PAMAM dendrimers encapsulated within poly(ethylene glycol)-*b*-poly(*D,L*-lactide) (PEG-PLA) copolymers, we were able to produce hybrid NPs, or nanohybrids with controlled sizes around 100 nm. The nanohybrids combined the highly selective cellular interactions of FA-targeted dendrimers with the larger size and controlled release properties of polymeric NPs, which dictated their cellular interaction kinetics and uptake pathways by FA receptor (FR)-overexpressing KB cells (KB FR⁺). Simulated penetration assays in multicellular tumor spheroids (MCTS) also revealed that the targeted dendrimers can penetrate deep into the spheroids upon their release from the nanohybrids, imparting favorable penetration properties as opposed to the polymeric NPs alone.

These preliminary findings highlight the potential of the nanohybrid system to enhance the targeting efficacy of the individual nanocarriers *in vivo*. The encapsulation of targeted dendrimers within the protective matrix of PEG-PLA produced nanohybrids with controlled release and cellular targeting kinetics, while maintaining efficient penetration *in vitro*. This led us to hypothesize that this platform can address the limitations facing FA-targeted dendrimers and polymeric NPs. For example, the short blood circulation times and significant liver uptake of FA-targeted dendrimers due to surface exposure of FA molecules, and the limited tissue diffusivity of polymeric NPs due to their large size. As illustrated in Figure 5.1, by controlling the release of the dendrimer conjugates, the nanohybrid platform can prolong the circulation time of free dendrimers and protect against premature systemic elimination. At the same time, the controlled size of the nanohybrids allows them to passively target tumors through the EPR effect. As the nanohybrids accumulate at the tumor site, actively targeted dendrimers are gradually released from the biodegradable PEG-PLA matrix, enabling selective targeting to individual cancer cells, with more efficient tumor distribution and penetration (Figure 5.1).

Previously, the targeting efficacy of FA-targeted G5 PAMAM dendrimers has been extensively evaluated *in vitro* and has shown great promise in enhancing targeted drug delivery to tumors *in vivo* [25-27]. Throughout our previous studies, we have employed FA-targeted G4 PAMAM dendrimers, possessing a smaller size (MW 14kDa) compared to G5 dendrimers (28kDa), with sufficient surface functional groups for attachment of imaging agents and targeting ligands. In order to validate the choice of dendrimer generation for *in vivo* biodistribution studies, we compared the penetration

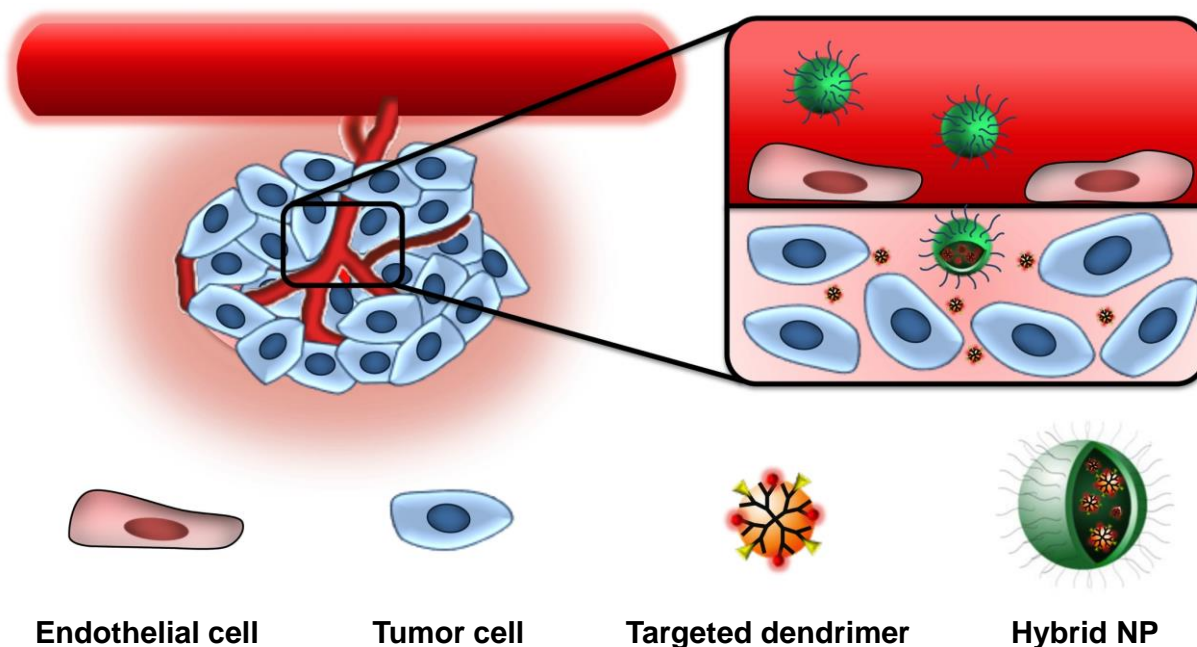


Figure 5.1. Overview of the sequential passive and active targeting enabled by the nanohybrid system. The PEGylated larger NP allows the nanohybrids to be long circulating and passively accumulate at the tumor site through the EPR effect. Once there, actively-targeted dendrimers are gradually released and able to penetrate deep within the tumor tissue, ultimately resulting in enhanced targeting efficacy (*partially contributed by Kevin Shyu*).

efficiency of G4 and G5 dendrimers in MCTS. We then conducted a biodistribution study in healthy mice to investigate the *in vivo* fate of nanohybrids encapsulating nontargeted G4 dendrimers compared to free dendrimer conjugates and empty NPs following a single IV injection up to 24 h. In order to validate the targeting efficacy of FA-targeted nanohybrids, a similar study was carried out in athymic nude mice carrying xenografts of KB FR⁺ tumors using FA-targeted dendrimers and nanohybrids, as well as empty NPs.

5.2 EXPERIMENTAL SECTION

5.2.1 Materials

G4 and G5 PAMAM dendrimers, rhodamine B isothiocyanate (RITC), folic acid (FA), glycidol, tin(II)2-ethylhexanoate, poly(ethylene glycol) monomethyl ether (mPEG) (MW 5,000 Da), poly(vinyl alcohol) (PVA, 87-89% hydrolyzed, MW 13,000-23,000 Da), dimethyl sulfoxide (DMSO), dimethylformamide (DMF), and dichloromethane (DCM) were all obtained from Sigma-Aldrich (St. Louis, MO). *D,L*-lactide and Boc-NH-PEG5K-OH were purchased from Polysciences Inc. (Warrington, PA) and Jenkem Technology (Beijing, China), respectively. All other chemicals used in this study were purchased from Sigma-Aldrich unless specified otherwise.

5.2.2 Preparation of G4 and G5 PAMAM dendrimer conjugates

Fully hydroxylated RITC-labeled FA-targeted G4 and G5 PAMAM dendrimer conjugates (G4-RITC-FA-OH and G5-RITC-FA-OH) were prepared and characterized by UV/Vis (DU800 UV/Vis Spectrophotometer, Beckman Coulter, CA) and ¹H NMR (400 MHz Bruker DPX-400 spectrometer, Bruker BioSpin Corp., Billerica, MA) as reported in our earlier publications [29, 30]. Briefly, 20 mg of G4 PAMAM (1.4×10^{-3} mmol) and G5 PAMAM (6.9×10^{-3} mmol) were each dissolved in 4 mL methanol, to which TEA (4.1 μ L, 3.0×10^{-2} mmol for G4, and 6.4 μ L, 4.5×10^{-2} mmol for G5) was added, followed by adding acetic anhydride (2.6 μ L, 2.7×10^{-2} mmol for G4, and 3.6 μ L, 3.8×10^{-2} mmol for G5). The reactions were carried out under vigorous stirring at RT overnight. The products were diluted with deionized distilled water (ddH₂O) and purified by ultrafiltration using an Amicon Ultra-15 Centrifugal Filter Unit (MWCO 3000, Millipore, Billerica, MA), at 4000 rpm and 4 °C for 20 min, with repeated washing with ddH₂O five times. The dendrimers were then re-dissolved in ddH₂O and lyophilized.

For conjugation of RITC, 15 mg of G4 (1.1×10^{-3} mmol) and G5 (5.2×10^{-4} mmol) was dissolved in 3 mL ddH₂O, to which RITC (2.3 mg, 4.2×10^{-3} mmol for G4, and 1.4 mg, 2.6×10^{-3} mmol for G5) dissolved in 200 μ L DMSO was added under vigorous stirring at RT overnight. Excess RITC was removed by ultrafiltration as described above, by washing with ddH₂O ten times. The products were then diluted in ddH₂O and lyophilized, resulting in G4-RITC-NH₂ and G5-RITC-NH₂.

FA conjugation was performed by reacting FA (1.6 mg, 3.5×10^{-3} mmol for G4, and 1.2 mg, 2.8×10^{-3} mmol for G5) with EDC (6.7 mg, 3.5×10^{-2} mmol for G4, and 5.3 mg, 2.8×10^{-2} mmol for G5) and NHS (4.1 mg, 3.5×10^{-2} mmol for G4, and 3.2 mg, 2.8×10^{-2} mmol for G5) in 500 μ L DMSO under vigorous stirring at RT for 30 min. Activated FA was then added to G4-RITC-NH₂ (10 mg, 7.0×10^{-4} mmol) and G5-RITC-NH₂ (10 mg, 3.5×10^{-4} mmol) each dissolved in 2 mL ddH₂O under vigorous stirring at RT overnight. The products were purified by ultrafiltration as described above, diluted in ddH₂O, and lyophilized, resulting in G4-RITC-FA-NH₂ and G5-RITC-FA-NH₂.

The remaining amine groups on the dendrimer conjugates were hydroxylated by dissolving 5 mg of each conjugate in 2 mL ddH₂O, to which glycidol (200% molar excess relative to the number of primary amines) was added under vigorous stirring at RT for 3 h. The final products were purified by ultrafiltration as described above, diluted in ddH₂O, and lyophilized, resulting in G4-RITC-FA-OH, G4-RITC-OH, G5-RITC-FA-OH, and G5-RITC-OH.

5.2.3 Synthesis of PEG-PLA and RITC-PEG-PLA

PEG-PLA and Boc-NH-PEG-PLA were prepared by ring opening polymerization of *D,L*-lactide as previously described [29, 30]. RITC-PEG-PLA was then prepared

following deprotection of Boc-NH-PEG-PLA. Briefly, Boc-NH-PEG-PLA was deprotected by dissolving 200 mg in 4 mL of DCM, and 4 mL of TFA was added into the solution dropwise under vigorous stirring for 15 min. TFA and DCM were evaporated under vacuum at 70°C using a rotary evaporator. The product was redissolved in 1 mL DCM, precipitated using cold diethyl ether, vacuum filtered, and dried overnight. H₂N-PEG-PLA was conjugated to RITC by dissolving 50 mg (1.2×10^{-3} mmol) in 2 mL DMF. RITC (0.6 mg, 1.5×10^{-3} mmol) in 500 μ L DMF was added into the polymer/DMF solution under vigorous stirring at RT overnight. Excess RITC was removed by membrane dialysis against ddH₂O using a 3,500 MWCO dialysis membrane for two days. The final product was then lyophilized over 2 days and stored at -20 °C.

5.2.4 Encapsulation of the dendrimer conjugates into PEG-PLA NPs

Nanohybrids containing targeted or non-targeted dendrimer conjugates (G4-RITC-FA-OH or G4-RITC-OH) were prepared using a double emulsion method [29-31]. For example, G4-RITC-FA-OH (1 mL, 3 mg/mL in ddH₂O) was added to 5 mL of 10 mg/mL solution of PEG-PLA in DCM, and the mixture was sonicated for 1 min using a Misonix XL Ultrasonic Processor (100% duty cycle, 475 W, 1/8" tip, QSonica, LLC, Newtown, CT). Ten milliliters of 3% aqueous PVA solution was then added to the mixture, followed by additional sonication for 1 min. The double emulsion was poured into 20 mL of 0.3% PVA in ddH₂O, and vigorously stirred at RT for 24 h to evaporate DCM. Unencapsulated dendrimers and PVA were removed by ultracentrifugation, with repeated washing with ddH₂O fifteen times. The resulting nanohybrid solution was redissolved in ddH₂O, lyophilized over 2 days, and stored at -20 °C. G4-RITC-OH was also encapsulated into PEG-PLA NPs using the same method. Empty RITC-NPs (50%

w/w RITC-PEG-PLA) were prepared by adding ddH₂O instead of the dendrimer solution.

5.2.5 Structure confirmation and size/surface charge measurements

The dendrimer conjugates and PEG-PLA copolymers were characterized by ¹H NMR as previously described [29-31]. The structure of G4-RITC-FA-OH and G5-RITC-FA-OH was also confirmed by UV/Vis. The number of RITC and FA molecules attached to each dendrimer was calculated based on a standard curve of RITC and FA absorbance versus concentration in ddH₂O at 556 nm and 275 nm, respectively. Particle size (diameter, nm) and surface charge (zeta potential, mV) of the conjugates and the nanohybrids were measured in triplicates by quasi-elastic laser light scattering using a Nicomp 380 Zeta Potential/Particle Sizer (Particle Sizing Systems, Santa Barbara, CA) in ddH₂O. The measurements were performed using samples that were suspended in ddH₂O at a concentration of 100 µg/mL, filtered through a 0.45 µm syringe filter, and briefly vortexed prior to each measurement.

5.2.6 Loading efficiencies of G4 dendrimer-encapsulated nanohybrids

Two milligrams of lyophilized nanohybrids was dissolved in 1 mL of 0.5 M NaOH to degrade the PEG-PLA and completely release the loaded dendrimers, followed by filtration through a 0.45 µm syringe filter. The fluorescence intensity from the filtrates was then measured using a BioTek Synergy 4 microplate spectrofluorometer (Winooski, VT). The amount of the dendrimer conjugates in the filtrates was determined from a standard curve of each conjugate's fluorescence versus concentration in 0.5 M NaOH at 540 nm excitation and 590 nm emission wavelengths. Loading was expressed as mg

dendrimer conjugates per mg copolymer. Loading efficiency was defined as the ratio of the actual loading obtained to the theoretical loading.

5.2.7 Cell culture

The KB cell line was purchased from the American Type Tissue Collection (ATCC, Manassas, VA) and grown continuously as a monolayer at 37 °C, 5% CO₂ in GIBCO FA-deficient RPMI 1640 medium (Invitrogen Corporation, Carlsbad, CA) supplemented with penicillin (100 units/mL), streptomycin (100 mg/mL), and 10% heat-inactivated fetal bovine serum (FBS) (Invitrogen), resulting in FR-overexpressing KB (KB FR⁺) cells.

5.2.8 Penetration assay using multicellular tumor spheroids (MCTS)

MCTS formation was performed using the liquid overlay method as previously reported [30]. KB FR⁺ cells from a confluent T-75 flask were detached using trypsin-EDTA and resuspended in FA-deficient RPMI 1640 at a concentration of 6×10^3 cells/mL. Five hundred microliters of the cell suspension were transferred to 8-well chamber slides (Millicell EZ Slide, Millipore, Billerica, MA) coated with 1% agarose in complete FA-deficient RPMI 1640. The cells were then incubated on agarose for 5 days to allow the formation of MCTS. After 5 days, 250 μ L of the media in each well were removed, and MCTS were treated with 250 μ L of 200 nM G4-RITC-FA-OH, G5-RITC-FA-OH, and the control conjugates G4-RITC-OH and G5-RITC-OH, for 1, 4, and 24 h. After each treatment, MCTS were carefully washed twice with PBS with Ca⁺⁺/Mg⁺⁺, fixed in paraformaldehyde for 10 min, and washed again. The chamber gasket was then removed, and the pieces of agarose were transferred to glass cover slips for confocal observation.

5.2.9 Confocal microscopy observations

Tumor spheroids were visualized using a Zeiss LSM 510 Meta confocal laser scanning microscope (CLSM, Carl Zeiss, Germany). The 543 nm line of a 1 mW tunable HeNe laser was used for the excitation of RITC, and emission was filtered at 565-595 nm. Images were captured using a 10x/0.25 Ph1 A-Plan objective, and Z-stack images were taken at 20 μm intervals for a total slice thickness of 200 μm .

5.2.10 Animals

Female BALB/c healthy and BALB/c athymic nude mice (6-8 weeks old) were obtained from Harlan Laboratories (Indianapolis, IN). Animals were treated in accordance with the National Institutes of Health Guide for the Care and Use of Laboratory Animals and the established Institutional Animal Care and Use protocol at the University of Illinois at Chicago. Animals were housed in a temperature and light-controlled environment (12 h light: 12 h darkness) and were provided food and water *ad libitum*.

5.2.11 Biodistribution of nontargeted dendrimers and nanohybrids in healthy animals

Female BALB/c mice ($n = 5$) were anesthetized with an IP injection of ketamine/xylazine (50 mg/kg and 5 mg/kg, respectively) prior to each injection. Each animal was injected with 3.7 mg/kg of the nontargeted dendrimer conjugates (G4-RITC-OH) (in ~ 200 μL normal saline) or an equivalent dose of the nanohybrids or RITC-NPs (~ 80 mg/kg in ~ 200 μL normal saline) via the tail vein. At 1, 8, and 24 h post-injection, animals were given a high dose of ketamine/xylazine (100 mg/kg and 10 mg/kg,

respectively) IP. Blood was collected from the dorsal vein into heparin-coated BD Vacutainer® tubes (Franklin Lakes, NJ). After blood collection, cervical dislocation was performed to ensure death, and organs were harvested (heart, lung, liver, kidneys, spleen, ovaries) for analysis.

5.2.12 Biodistribution of FA-targeted dendrimers and nanohybrids in a KB FR⁺ xenograft model

Six- to eight-week-old female BALB/c athymic nude mice (n = 3) were kept on a FA-deficient diet upon arrival and throughout the study. KB FR⁺ cells from confluent T-150 flasks were suspended in PBS at a concentration of 2.5×10^7 cells/mL, and ~200 μ L of the cell suspension was injected subcutaneously using a 30g needle into the right flank of each mouse. The tumors were allowed to grow for 2 weeks until reaching ~1 cm³ in size. Each animal was then anesthetized as described above and injected with 3.7 mg/kg G4-RITC-FA-OH (in ~200 μ L normal saline) or an equivalent dose of the nanohybrids or RITC-NPs (~80 mg/kg in ~200 μ L normal saline) via the tail vein. At 1 and 24 h post-injection, animals were given a high dose of ketamine/xylazine (100 mg/kg and 10 mg/kg, respectively) IP. Blood was collected from the dorsal vein into heparin-coated BD Vacutainer® tubes. After blood collection, cervical dislocation was performed to ensure death, and tumors and organs were harvested (heart, lung, liver, kidneys, spleen, ovaries) for analysis.

5.2.13 Blood and tissue analysis

For analysis of the blood collected from animals treated with the free dendrimer conjugates, blood collected from each animal was centrifuged at 13200 rpm (5 min, 4 °C) and the concentration of dendrimer conjugates was calculated from plasma by

measuring the fluorescence of the supernatant at 540 nm excitation and 590 nm emission wavelengths based on a standard curve of dendrimer fluorescence versus concentration in plasma collected from saline-treated controls. For the analysis of the blood collected from animals treated with the nanohybrids and NPs, 100 μ L of whole blood was incubated with an equal volume of 1 N NaOH to ensure degradation of the nanohybrids and NPs overnight in a shaking incubator (100 rpm, 37 °C). One hundred microliters of each sample were then taken to measure the fluorescence as above. The amount of dendrimer conjugates in the nanohybrids and the amount of RITC-NP in the blood samples was calculated based on standard curves of dendrimer conjugates and RITC-NP in NaOH-treated whole blood.

For the analysis of tumor and tissue samples, approximately 100 mg of each tissue was massed into microcentrifuge tubes, to which 300 μ L of ddH₂O was added. The samples were homogenized on ice using a manual tissue homogenizer. In order to ensure NP degradation, tissue homogenates from animals treated with the nanohybrids and RITC-NPs were incubated with an equal volume of 1 N NaOH overnight in a shaking incubator (100 rpm, 37 °C). Tissue homogenates were centrifuged at 13200 rpm (30 min, 4°C). Supernatants were then collected and the fluorescence was measured at 540 nm excitation and 590 nm emission wavelengths using a fluorescence plate reader. The amount of dendrimer conjugates (free or encapsulated) and RITC-NPs in each sample was calculated based on standard curves of each material in supernatants of tissues and KB FR⁺ tumors collected from saline controls, and expressed as % injected dose (ID)/g tissue.

5.3 RESULTS AND DISCUSSION

5.3.1 Preparation of the G4 and G5 PAMAM dendrimer conjugates and nanohybrids

RITC-labeled, FA-targeted G4 and G5 PAMAM dendrimers were prepared by sequential conjugation with RITC and FA, followed by hydroxylation of the remaining amine groups, resulting in G4-RHO-FA-OH and G5-RITC-FA-OH. Conjugation of RITC and FA to the dendrimers and successful end-capping of the amine groups was confirmed using ^1H NMR, UV/Vis, and zeta potential measurements (Table 5.1, Figure 5.2, Figure 5.3, and Figure 5.4). UV/Vis spectra revealed that the conjugates prepared in this study contained approximately 3.4 RITC and 5.8 FA molecules per G4 dendrimer, and 2.8 RITC and 5.9 FA molecules per G5 dendrimer.

PEG-PLA and RITC-PEG-PLA copolymers were synthesized by ring-opening polymerization of *D,L*-lactide using mPEG5K and Boc-NH-PEG5K-OH as initiators [29,

Table 5.1. Characterization of G4 and G5 PAMAM dendrimers and nanohybrids

	Particle size (nm)	Zeta potential (mV)	Loading efficiency (%)
G4-RITC-OH	12.1 \pm 7.3	4.2 \pm 1.7	N/A
G4-RITC-FA-OH	16.3 \pm 7.8	2.7 \pm 1.5	N/A
G5-RITC-OH	13.1 \pm 2.8	8.3 \pm 4.6	N/A
G5-RITC-FA-OH	14.0 \pm 2.9	2.8 \pm 1.2	N/A
G4-RITC-OH/NP	71.6 \pm 14.2	-16.6 \pm 0.8	59.2
G4-RITC-FA-OH/NP	60.8 \pm 10.3	-12.5 \pm 2.4	83.8
RITC-NP	62.4 \pm 14.1	-16.5 \pm 1.5	N/A

30]. ^1H NMR was used to confirm the chemical structure of the copolymers and to estimate the MW of the PLA block (Figure 5.5). This was calculated to be 44,900 g/mol for PEG-PLA and 48,800 g/mol for Boc-NH-PEG-PLA based on the relative integration ratios of peak b around 3.62 ppm (the protons of the ethylene oxide repeating units) to peak c around 5.15 ppm (the lactide repeating units). Following deprotection of Boc-

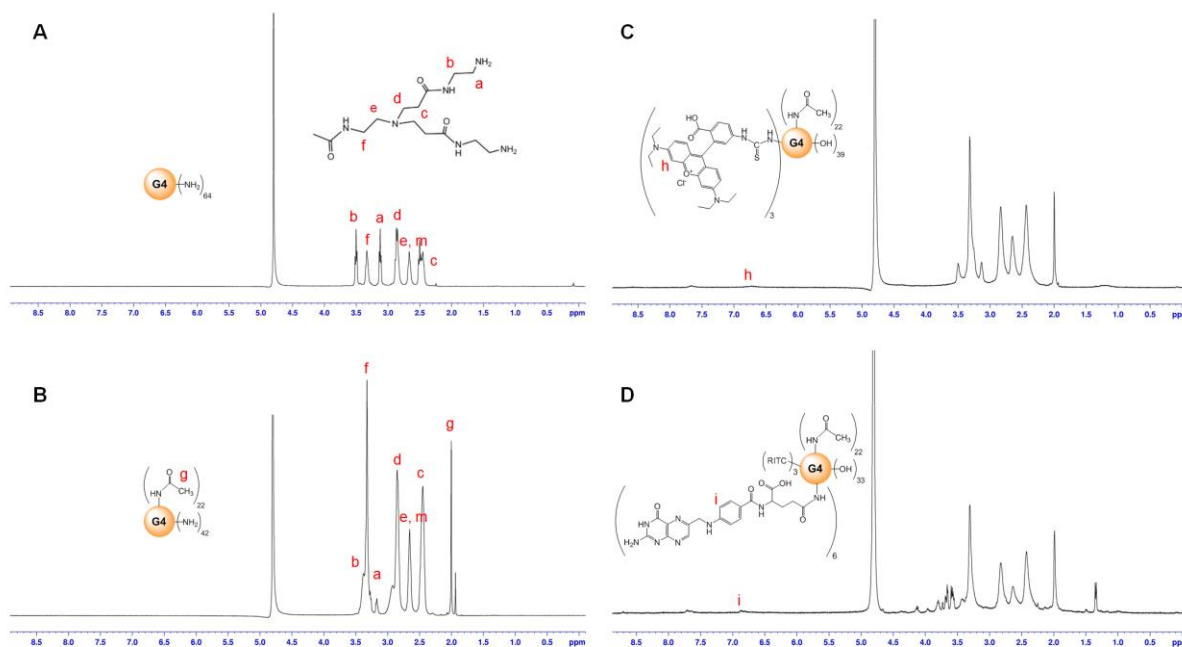


Figure 5.2. ^1H NMR spectra of (A) G4 PAMAM dendrimer, (B) partially acetylated G4, (C) RITC conjugated, fully hydroxylated G4-RITC-OH, and (D) fully hydroxylated, RITC and FA conjugated G4-RITC-FA-OH. The ^1H NMR spectrum of G4 PAMAM dendrimers (A) has 6 characteristic peaks corresponding to the protons of the internal methylene groups and those adjacent to the surface amino groups at 2.46, 2.65, 2.84, 3.01, 3.32, and 3.43 ppm. After partial acetylation, a new peak appeared at 1.95 ppm corresponding to the acetamide protons. The dendrimer was 30% acetylated based on the integration ratio between peak g and peaks a-f (B). RITC conjugation resulted in new peaks corresponding to the aromatic protons between 6.75 – 7.65 ppm (C). FA conjugation also resulted in peaks around 6.55 – 7.85 which overlapped with the RITC peaks (D).

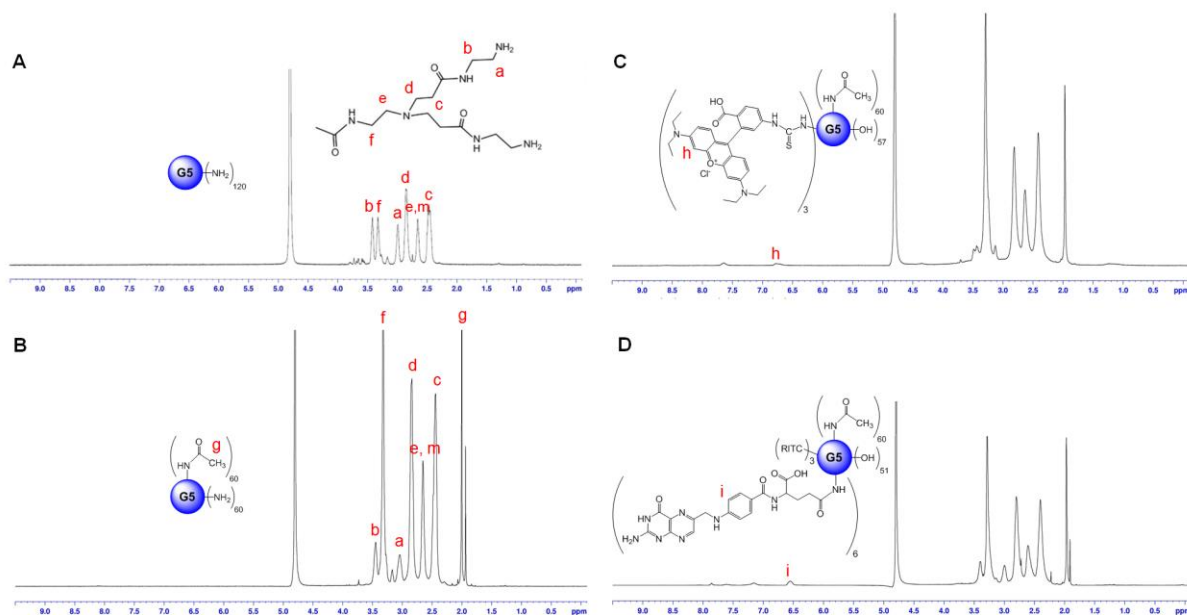


Figure 5.3. ^1H NMR spectra of (A) G5 PAMAM dendrimer, (B) partially acetylated G5, (C) RITC conjugated, fully hydroxylated G5-RITC-OH, and (D) fully hydroxylated, RITC and FA conjugated G5-RITC-FA-OH. The ^1H NMR spectrum of G5 PAMAM dendrimers (A) has 6 characteristic peaks corresponding to the protons of the internal methylene groups and those adjacent to the surface amino groups at 2.46, 2.65, 2.84, 3.01, 3.32, and 3.43 ppm. After partial acetylation, a new peak appeared at 1.95 ppm corresponding to the acetamide protons. The dendrimer was 50% acetylated based on the integration ratio between peak g and peaks a-f (B). RITC conjugation resulted in new peaks corresponding to the aromatic protons between 6.75 – 7.65 ppm (C). FA conjugation also resulted in peaks around 6.55 – 7.85 which overlapped with the RITC peaks (D).

NH-PEG-PLA, H_2N -PEG-PLA was obtained and conjugated to RITC, which was also confirmed using ^1H NMR (Figure 5.5).

G4 dendrimer conjugates were then encapsulated into PEG-PLA copolymers to produce the nanohybrids as we described earlier [29, 30]. Dendrimer encapsulation was performed using double emulsion to prepare nanohybrids with controlled particle

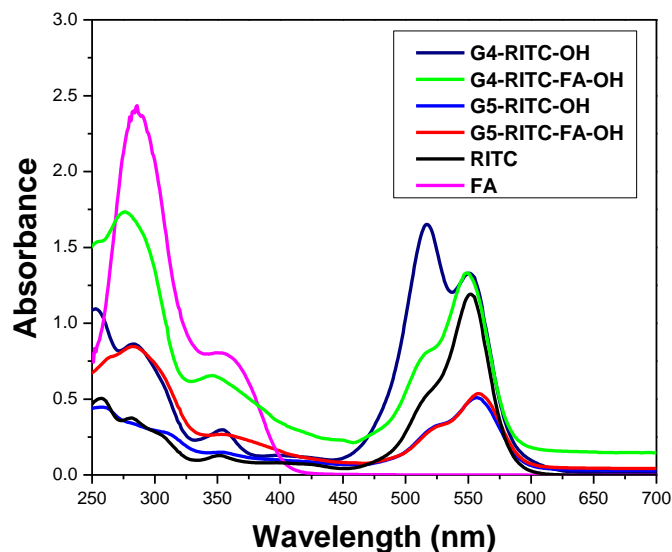


Figure 5.4. UV/Vis spectra of G4 and G5 PAMAM dendrimer conjugates prepared in this study compared to RITC and FA. The number of RITC and FA molecules attached to each dendrimer was calculated based on the absorbance of the conjugates at 556 nm and 275 nm, respectively. UV/Vis spectra revealed that the conjugates prepared in this study contained approximately 3.4 RITC and 5.8 FA molecules per G4 dendrimer, and 2.8 RITC and 5.9 FA molecules per G5 dendrimer.

sizes around 70 nm in diameter and at high loading efficiencies (59 – 84%) (Table 5.1). The change in zeta potential values for the dendrimer conjugates before encapsulation (2.7 – 4.2 mV) compared to the nanohybrids (-12.5 – -16.6 mV) indicated successful encapsulation. Empty, RITC-labeled PEG-PLA NPs (RITC-NPs) were also prepared and characterized by measuring the particle size and zeta potential (Table 5.1).

5.3.2 Penetration efficiency of FA-targeted G4 and G5 PAMAM dendrimers

The penetration efficiency of G4 dendrimer conjugates was validated and compared to FA-targeted G5 dendrimers, which have been extensively investigated *in vitro* and *in vivo* for targeted drug delivery to tumors [24, 26, 27, 32]. As shown in

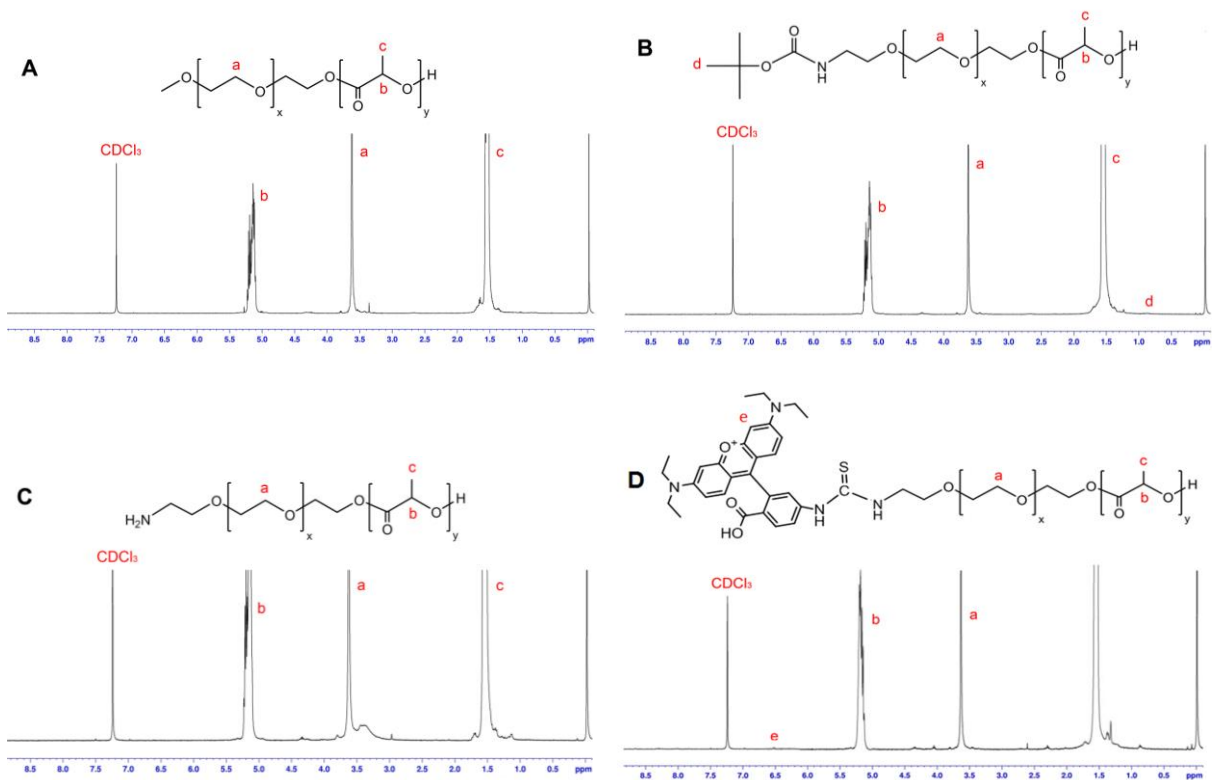


Figure 5.5. ^1H NMR spectra of (A) PEG-PLA, (B) Boc-NH-PEG-PLA, (C) deprotected H_2N -PEG-PLA, and (D) RITC-PEG-PLA. The ^1H NMR spectrum of PEG-PLA shows two characteristic peaks of PLA at 5.15 and 1.55 ppm (b and c). As for mPEG, the characteristic peak corresponding to the ethylene glycol repeating units (b) was observed at 3.62 ppm. The MWs of PEG-PLA were estimated using the relative integration ratios of peaks b and c, based on the integral value for peak a of mPEG. This was calculated to be 44,900 g/mol for PEG-PLA and 48,800 g/mol for Boc-NH-PEG-PLA. Deprotection of Boc-NH-PEG-PLA was confirmed by the disappearance of peak d (0.85 ppm) corresponding to the Boc group. Conjugation of RITC to H_2N -PEG-PLA was confirmed by the appearance of peak e at 6.45 ppm corresponding to the aromatic protons of RITC, and it was calculated that 0.9 RITC molecules were attached to the polymer based on the relative integration ratio of peaks a and e.

Figure 5.6, both generations of FA-targeted dendrimers show similar penetration efficiency and kinetics starting from 1 h, and reaching a maximum at 24 h. At the same

time, nontargeted conjugates exhibited significantly lower penetration ability and much slower uptake kinetics compared to their targeted counterparts. The significance of these observations to our hypothesis is that FA-targeted G4 dendrimer conjugates have

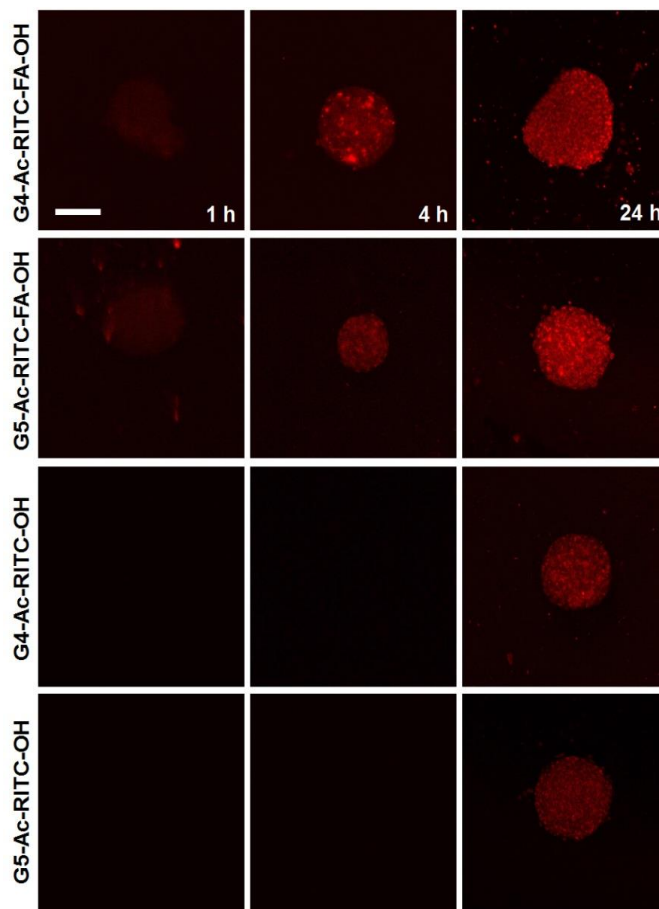


Figure 5.6. CLSM images of KB FR⁺ MCTS upon incubation with G4-RITC-FA-OH (top row), G5-RITC-FA-OH (2nd row), G4-RITC-OH (3rd row), and G5-RITC-OH (4th row) up to 24 h. Red: RITC-labeled dendrimers. Images shown were taken at a depth of 80 μm into each spheroid, scale bar: 100 μm . Only the FA-targeted dendrimers are able to penetrate deep into the spheroids up to 24 h. G4-RITC-FA-OH conjugates display similar penetration ability to G5-RITC-FA-OH, which validates their use as FA-targeted vectors in the nanohybrid system. The nontargeted conjugates, G4-RITC-OH and G5-RITC-OH, exhibit a significantly lower penetration ability compared to FA-targeted conjugates.

demonstrated similar tumor penetration ability to G5 dendrimers. This strongly supports their validity as a choice of targeted vectors incorporated within our nanohybrid system for subsequent *in vivo* biodistribution studies.

5.3.3 Altered biodistribution of dendrimer-encapsulated nanohybrids

Previous biodistribution studies using PAMAM dendrimers have shown that following IV administration, kidneys are the major organs of elimination, which is often associated with short blood residence times (< 10% ID remaining within 24 h) [27, 33, 34]. On the other hand, PEGylated polymeric NPs are mostly eliminated by the RES (liver and spleen) and are longer circulating [35-37]. In order to see whether the nanohybrid system can improve the elimination kinetics of dendrimer conjugates, we first investigated the biodistribution and elimination of nontargeted nanohybrids compared to free dendrimer conjugates and empty NPs in non-tumor bearing mice. As shown in Figure 5.7(A), following a single IV injection, nontargeted dendrimer conjugates (G4-RITC-OH) are quickly cleared from the blood (<10% ID remaining) after 24 h, and appear mostly in the kidneys, with minimal amounts found in the liver or spleen. In contrast, an equivalent dose of dendrimers encapsulated within the nanohybrids displayed a markedly different biodistribution profile (Figure 5.7(B)), which more closely resembled empty NPs (Figure 5.7(C)). For example, the nanohybrids and RITC-NPs persisted longer in the blood, with 18-23% ID found after 24 h, and they were both mostly eliminated by the liver and spleen, with some accumulation in the heart and lung.

These observations support the hypothesis that the nanohybrid system can protect the encapsulated dendrimers from premature systemic elimination. This could

be attributed to the combination of the larger particle size and sustained release of the dendrimer conjugates from the PEG-PLA matrix. The size of the nanohybrids is larger than the renal threshold, switching the elimination pathway to organs of the RES such as the liver and spleen. The outer PEG layer also imparts stealth properties to the

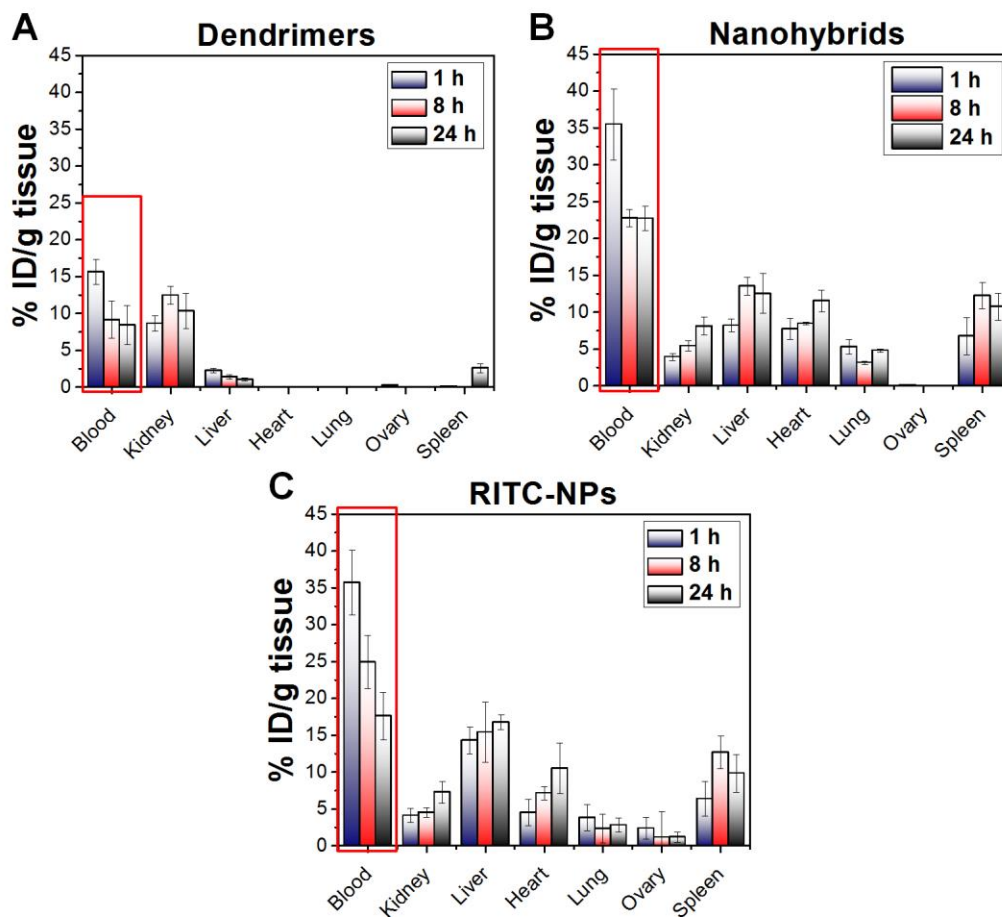


Figure 5.7. Biodistribution profile of (A) nontargeted G4 dendrimers (G4-RITC-OH), (B) nontargeted nanohybrids, and (C) empty RITC-NPs, following a single IV injection. Nontargeted dendrimer conjugates are quickly cleared from the blood (<10% ID remaining) after 24 h, and appear mostly in the kidneys. In contrast, an equivalent dose of dendrimers encapsulated within the nanohybrids display a biodistribution profile closer to RITC-NPs. The nanohybrids and RITC-NPs persisted longer in the blood, with 18-23% ID found after 24 h, and they were both mostly eliminated by the liver and spleen.

system, similar to the PEGylated RITC-NPs and other nanocarriers reported in the literature [11, 35, 36]. These findings support part of the design rationale of the nanohybrid system, where prolonged circulation time of dendrimer conjugates can be successfully achieved through the nanohybrid platform.

5.3.4 Enhanced targeting efficacy and tumor retention of FA-targeted nanohybrids

Next, we tested the biodistribution of FA-targeted nanohybrids in mice carrying, human KB FR⁺ tumors, compared to FA-targeted dendrimers and RITC-NPs. As shown in Figure 5.8(A), free FA-targeted dendrimers (G4-RITC-FA-OH) are cleared even more rapidly than nontargeted conjugates (Figure 5.7(A)), with <5% ID remaining after 24 h. The faster elimination of FA-targeted dendrimers was attributed to the significant liver uptake (~15% ID was found in the liver after 24 h) due to the presence of FA receptors in the liver and other RES organs such as the spleen [27]. At the same time, only ~5% ID could be found in the tumor tissue after 1 h, and ~3% ID after 24 h, highlighting the limitation of using FA-targeted dendrimers for tumor targeting. We had previously observed that dendrimer-encapsulated nanohybrids are shielded from elimination and subsequently achieve longer circulation times compared to free conjugates (Figure 5.7(B)). This led us to hypothesize that in the presence of tumors, FA-targeted nanohybrids will achieve higher concentrations in the tumor tissue through a combination of prolonged circulation time and passive targeting. As shown in Figure 5.8(B), FA-targeted nanohybrids not only persisted longer in the blood (14% ID remaining after 24 h), but also a higher % ID was found in the tumor tissue (12% compared to 3% for the free conjugates). A similar biodistribution pattern was observed

for RITC-NPs, including in tumor tissue (Figure 5.8(C)). Note that the blood

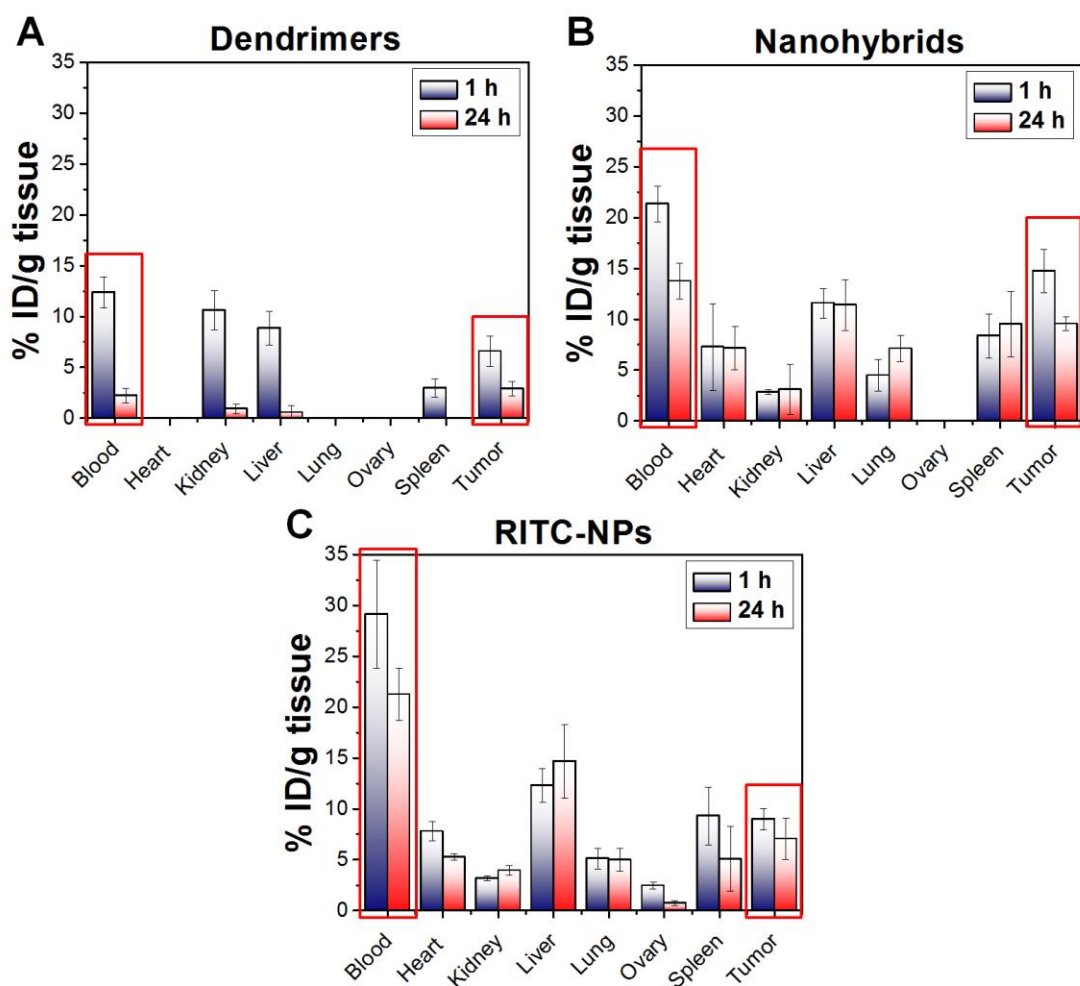


Figure 5.8. Biodistribution profile of (A) FA-targeted G4 dendrimers (G4-RITC-FA-OH), (B) FA-targeted nanohybrids, and (C) empty RITC-NPs, in BALB/c mice carrying human KB FR⁺ xenografts, following a single IV injection. FA-targeted dendrimers (A) are cleared from the blood faster than nontargeted conjugates (Figure 37(A)), with <5% ID remaining after 24 h, due to significant liver uptake (~15% ID). Only ~5% ID could be found in the tumor tissue after 1 h, and ~3% ID after 24 h. FA-targeted nanohybrids (B) not only persisted longer in the blood (14%ID remaining after 24 h), but also a higher % ID was found in the tumor tissue (12%) compared to the free conjugates. A similar biodistribution pattern was observed for RITC-NPs, including in tumor tissue (C).

concentrations of FA-targeted nanohybrids in tumor-bearing mice were slightly lower than RITC-NPs and the levels obtained with the nontargeted systems in healthy animals (Figure 5.7(B)). This was attributed to the faster elimination of FA-targeted conjugates upon their release from the nanohybrids, in addition to their significant accumulation at the tumor site.

The enhanced targeting efficacy of the nanohybrids is attributed to the sequential utilization of passive and active targeting. The protective PEG-PLA matrix shields the targeted conjugates from premature elimination, while providing a stealth layer to prolong the circulation. The larger size of the nanohybrids allows them to accumulate at the tumor site through the EPR effect, where by controlling their release, FA-targeted dendrimer conjugates are able to selectively target individual cancer cells. Similar levels of nontargeted polymeric NPs were also found in the tumor tissue. However, the high flexibility and efficient tissue penetration properties of dendrimers will be able to achieve more efficient tumor penetration and targeting compared to the rigid NPs. This is supported by our previous findings from simulated penetration assays in MCTS, where only the FA-targeted dendrimers were able to penetrate deeper into the spheroids, while the empty NPs remained clustered at the periphery [30]. Additionally, it is expected that nontargeted nanohybrids will be able to achieve similar tumor concentrations to FA-targeted ones. However, as observed in Figure 5.6, without the targeting ligand, nontargeted dendrimer conjugates have significantly lower penetration efficiency compared to targeted conjugates. This further supports our argument that the synergistic combination of active and passive targeting within the nanohybrid system is essential to enhance the targeting efficacy of the nanocarriers.

5.4 CONCLUSION

We report on the *in vivo* targeting efficacy of novel FA-targeted dendrimer-biodegradable polymer hybrid NPs. The multi-scale nanohybrid system was designed to overcome the limitations of existing nanocarriers such as the short circulation time (dendrimers) and poor penetration efficiency (polymeric NPs). By encapsulating FA-targeted dendrimers within long circulating PEG-PLA NPs, the larger size of the nanohybrids and the controlled release of the dendrimer conjugates prevented their premature renal elimination. This allowed for sufficient concentrations to accumulate at the tumor site, through a combination of passive and active targeting. Thus, the nanohybrids resulted in enhanced tumor accumulation and retention compared to the free FA-targeted dendrimers. Compared to polymeric NPs, it is expected that the favorable tissue diffusion and penetration properties of dendrimer conjugates will impart superior targeting efficacy and more efficient tumor distribution of drug molecules, which will be the subject of our future investigations.

5.5 REFERENCES

1. Peer, D., et al., *Nanocarriers as an emerging platform for cancer therapy*. Nat. Nanotechnol., 2007. **2**(12): p. 751-760.
2. Torchilin, V., *Tumor delivery of macromolecular drugs based on the EPR effect*. Adv. Drug Deliver. Rev., 2011. **63**(3): p. 131-135.
3. Torchilin, V.P., *Recent advances with liposomes as pharmaceutical carriers*. Nat. Rev. Drug Discov., 2005. **4**(2): p. 145-160.
4. Torchilin, V.P., *Multifunctional nanocarriers*. Adv. Drug Deliver. Rev., 2006. **58**(14): p. 1532-1555.
5. Kataoka, K., A. Harada, and Y. Nagasaki, *Block copolymer micelles for drug delivery: design, characterization and biological significance*. Adv. Drug Deliver. Rev., 2001. **47**(1): p. 113-131.
6. Maeda, H., *Tumor-selective delivery of macromolecular drugs via the EPR effect: Background and future prospects*. Bioconjugate Chem., 2010. **21**(5): p. 797-802.
7. Gradishar, W.J., et al., *Phase III trial of nanoparticle albumin-bound paclitaxel compared with polyethylated castor oil-based paclitaxel in women with breast cancer*. J. Clin. Oncol., 2005. **23**(31): p. 7794-7803.
8. Gordon, A.N., et al., *Recurrent epithelial ovarian carcinoma: A randomized phase III study of pegylated liposomal doxorubicin versus topotecan*. J. Clin. Oncol., 2001. **19**(14): p. 3312-3322.

9. Green, M.R., et al., *Abraxane((R)), a novel Cremophor((R))-free, albumin-bound particle form of paclitaxel for the treatment of advanced non-small-cell lung cancer*. *Ann. Oncol.*, 2006. **17**(8): p. 1263-1268.
10. Cuong, N.-V., Y.-L. Li, and M.-F. Hsieh, *Targeted delivery of doxorubicin to human breast cancers by folate-decorated star-shaped PEG-PCL micelle*. *J. Mater. Chem.*, 2012. **22**(3): p. 1006-1020.
11. Gabizon, A., et al., *In vivo fate of folate-targeted polyethylene-glycol liposomes in tumor-bearing mice*. *Clin. Cancer Res.*, 2003. **9**(17): p. 6551-6559.
12. Gabizon, A., et al., *Tumor cell targeting of liposome-entrapped drugs with phospholipid-anchored folic acid-PEG conjugates*. *Adv. Drug Deliver. Rev.*, 2004. **56**(8): p. 1177-1192.
13. Lee, R.J. and P.S. Low, *Folate-mediated tumor-cell targeting of liposome-entrapped doxorubicin in-vitro*. *BBA-Biomembranes*, 1995. **1233**(2): p. 134-144.
14. Liu, Y.T., et al., *Folic acid conjugated nanoparticles of mixed lipid monolayer shell and biodegradable polymer core for targeted delivery of Docetaxel*. *Biomaterials*, 2010. **31**(2): p. 330-338.
15. Bae, Y., et al., *Multifunctional polymeric micelles with folate-mediated cancer cell targeting and pH-triggered drug releasing properties for active intracellular drug delivery*. *Mol. Biosyst.*, 2005. **1**(3): p. 242-250.
16. Popovic, Z., et al., *A Nanoparticle size series for in vivo fluorescence imaging*. *Angew. Chem. Int. Ed.*, 2010. **49**(46): p. 8649-8652.

17. Yuan, F., et al., *Microvascular permeability and interstitial penetration of sterically stabilized (stealth) liposomes in a human tumor xenograft*. *Cancer Res.*, 1994. **54**(13): p. 3352-3356.
18. Wong, C., et al., *Multistage nanoparticle delivery system for deep penetration into tumor tissue*. *P. Natl. Acad. Sci. USA*, 2011. **108**(6): p. 2426-2431.
19. Waite, C.L. and C.M. Roth, *PAMAM-RGD conjugates enhance siRNA delivery through a multicellular spheroid model of malignant glioma*. *Bioconjugate Chem.*, 2009. **20**(10): p. 1908-1916.
20. Dhanikula, R.S., et al., *Methotrexate loaded polyether-copolyester dendrimers for the treatment of gliomas: Enhanced efficacy and intratumoral transport capability*. *Mol. Pharm.*, 2008. **5**(1): p. 105-116.
21. Tang, L., et al., *Synthesis and biological response of size-specific, monodisperse drug-silica nanoconjugates*. *ACS Nano*, 2012. **6**(5): p. 3954-3966.
22. Huang, K., et al., *Size-dependent localization and penetration of ultrasmall gold nanoparticles in cancer cells, multicellular spheroids, and tumors in vivo*. *ACS Nano*, 2012. **6**(5): p. 4483-4493.
23. Hong, S., et al., *The binding avidity of a nanoparticle-based multivalent targeted drug delivery platform*. *Chem. Biol.*, **2007**. **14**(1): p. 107-115.
24. Majoros, I.J., et al., *PAMAM dendrimer-based multifunctional conjugate for cancer therapy: Synthesis, characterization, and functionality*. *Biomacromolecules*, 2006. **7**(2): p. 572-579.

25. Myc, A., et al., *Preclinical antitumor efficacy evaluation of dendrimer-based methotrexate conjugates*. *Anti-Cancer Drug.*, 2008. **19**(2): p. 143-149.
26. Quintana, A., et al., *Design and function of a dendrimer-based therapeutic nanodevice targeted to tumor cells through the folate receptor*. *Pharm. Res.*, 2002. **19**(9): p. 1310-1316.
27. Kukowska-Latallo, J.F., et al., *Nanoparticle targeting of anticancer drug improves therapeutic response in animal model of human epithelial cancer*. *Cancer Res.*, 2005. **65**(12): p. 5317-5324.
28. Singh, P., et al., *Folate and folate-PEG-PAMAM dendrimers: Synthesis, characterization, and targeted anticancer drug delivery potential in tumor bearing mice*. *Bioconjugate Chem.*, 2008. **19**(11): p. 2239-2252.
29. Sunoqrot, S., et al., *Temporal control over cellular targeting through hybridization of folate-targeted dendrimers and PEG-PLA nanoparticles*. *Biomacromolecules*, 2012. **13**: p. 1223-1230.
30. Sunoqrot, S., et al., *In vitro evaluation of dendrimer-polymer hybrid nanoparticles on their controlled cellular targeting kinetics*. *Mol. Pharm.*, 2013. **ASAP Article**. DOI: 10.1021/mp300560n.
31. Sunoqrot, S., et al., *Kinetically controlled cellular interactions of polymer-polymer and polymer-liposome nanohybrid systems*. *Bioconjugate Chem.*, 2011. **22**(3): p. 466-474.

32. Majoros, I.J., et al., *Poly(amidoamine) dendrimer-based multifunctional engineered nanodevice for cancer therapy*. J. Med. Chem., 2005. **48**(19): p. 5892-5899.
33. Kobayashi, H., et al., *Macromolecular MRI contrast agents with small dendrimers: Pharmacokinetic differences between sizes and cores*. Bioconjugate Chem., 2003. **14**(2): p. 388-394.
34. Nigavekar, S.S., et al., *H-3 dendrimer nanoparticle organ/tumor distribution*. Pharm. Res., 2004. **21**(3): p. 476-483.
35. Gref, R., et al., *Biodegradable long-circulating polymeric nanospheres*. Science, 1994. **263**(5153): p. 1600-1603.
36. Li, Y.P., et al., *PEGylated PLGA nanoparticles as protein carriers: synthesis, preparation and biodistribution in rats*. J. Control. Release, 2001. **71**(2): p. 203-211.
37. Owens, D.E. and N.A. Peppas, *Opsonization, biodistribution, and pharmacokinetics of polymeric nanoparticles*. Int. J. Pharm., 2006. **307**(1): p. 93-102.

CHAPTER 6

CONCLUSIONS AND OUTLOOK

Presented herein is the first multi-scale dendrimer-polymer based nanohybrid system that can systematically address the limitations of existing nanocarriers such as dendrimers and polymeric NPs. One of the key features of the nanohybrid system is the use of simple methodology to incorporate nanocarriers with different size scales, in an effort to harness their therapeutic potential.

As a proof of concept study, we first designed nanohybrid systems (100-150 nm in diameter) that combined a polycation, PEI, with protective outer layers consisting of biodegradable polymeric NPs or liposomes (Chapter 2). PEI was chosen as a model multifunctional polycation as it is associated with spontaneous, nonspecific cellular interactions that often result in cytotoxicity, creating the need to control its cellular interaction kinetics. After conjugation with RITC, PEI-RITC conjugates were encapsulated into: i) polymeric NPs made of either polylactide-co-glycolide (PLGA) or polyethylene glycol-b-polylactide-co-glycolide (PEG-PLGA); or ii) PEGylated liposomes, resulting in three nanohybrid systems. Through the nano-hybridization, both cellular uptake and cytotoxicity of the nanohybrids were kinetically controlled. The cytotoxicity assay using MCF-7 cells revealed that liposome-based nanohybrids exhibited the least toxicity, followed by PEG-PLGA- and PLGA-based NPs after 24 hr incubation. The different kinetics of cellular uptake was also observed; the liposome-based systems being the fastest and PLGA-based systems being the slowest. The results presented a

potential delivery platform with enhanced control over its biological interaction kinetics and passive targeting capability through size control.

Based on the controlled cytotoxicity and cellular uptake kinetics obtained with the PEI-based nanohybrids, we then hypothesized that the nanohybrid platform can also enable controlled cellular targeting kinetics by using targeted nanovectors in the core (Chapter 3). Polymeric NPs and dendrimers are two major classes of nanomaterials that have demonstrated great potential for targeted drug delivery. However, their targeting efficacy has not yet met clinical needs largely because of a lack of control over their targeting kinetics, which often results in rapid clearance and off-target drug delivery. To address this issue, we decided to modify the nanohybrid design through hybridization of targeted dendrimers with polymeric NPs. FA-targeted G4 PAMAM dendrimers were thus encapsulated into PEG-PLA NPs using a double emulsion method, forming nanohybrids with a uniform size (~100 nm in diameter) at high encapsulation efficiencies (69–85%). Targeted dendrimers encapsulated within the NPs selectively interacted with KB FR⁺ cells upon release in a temporally controlled manner. The targeting kinetics of the nanohybrids were further modulated using three different molecular weights (MW) of the PLA block (23, 30, and 45 kDa). We also observed that the release rates of the dendrimers from the nanohybrids were inversely proportional to the MW of the PLA block, which dictated their binding and internalization kinetics with KB cells. Our results provided evidence that selective cellular interactions can be kinetically controlled by the nanohybrid design, which can potentially enhance the targeting efficacy of nanocarriers.

In order to achieve more in depth understanding of the cellular interactions of the

nanohybrids, we conducted a series of *in vitro* experiments that validate the design rationale of the system, in order to better predict their *in vivo* behavior (Chapter 4). Cellular uptake studies in KB FR⁺ cells revealed that the nanohybrids maintained high FR selectivity resembling the selectivity of free dendrimers, while displaying temporally controlled cellular interactions due to the presence of the polymeric NP shells. The cellular interactions of the nanohybrids were clathrin-dependent (characteristic of polymer NPs) at early incubation time points (4 h), which were partially converted to caveolae-mediated internalization (characteristic of FA-targeted dendrimers) at longer incubation hours (24 h). Simulated penetration assays using MCTS of KB FR⁺ cells also revealed that the targeted dendrimers penetrated deep into the spheroids upon their release from the nanohybrids, whereas the NP shell did not. Additionally, methotrexate-containing systems showed the selective, controlled cytotoxicity kinetics of the nanohybrids. These results all demonstrated that our nanohybrids successfully integrate the unique characteristics of dendrimers (effective targeting and penetration) and polymeric NPs (controlled release and suitable size for long circulation) in a kinetically controlled manner.

Finally, we investigated the *in vivo* fate of the dendrimer-based nanohybrids in a mouse model, in order to validate the design rationale of the nanohybrid system and its potential to enhance the targeting efficacy of FA-targeted dendrimers (Chapter 5). The biodistribution profile of nontargeted nanohybrids was constructed following a single IV injection into non-tumor bearing animals to obtain an idea of the general distribution pattern of the system, compared to free dendrimers and polymeric NPs. While free dendrimer conjugates were eliminated rapidly from the blood by the kidneys within 24 h,

dendrimer-encapsulated nanohybrids were longer circulating and mostly cleared by macrophages in the liver and spleen, similar to the polymeric NPs. Next, biodistribution studies were conducted in nude mice carrying KB FR⁺ tumor xenografts following a single IV injection of FA-targeted dendrimers, nanohybrids, and polymeric NPs. Consistent with previous reports using FA-targeted dendrimers, the conjugates were rapidly cleared from the blood, and mainly found in the kidneys, as well as the liver and spleen, due to the presence of FR in these organs. The short blood residence time caused modest amounts of the free dendrimers to be found in the tumor, which was also attributed to their small size that does not allow tumor accumulation through passive targeting. On the other hand, FA-targeted, dendrimer-encapsulated nanohybrids were longer circulating and able to achieve higher tumor concentrations through a combination of passive and active targeting.

When comparing the nanohybrids with nontargeted polymeric NPs, both systems followed a similar biodistribution pattern. However, the high molecular flexibility and favorable tissue diffusivity of dendrimers make them more efficient in tumor penetration and distribution. Therefore, by combining the superior tumor penetration properties of targeted dendrimers and the larger size and longer circulation times of polymeric NPs, our nanohybrid system can enhance the targeting efficacy of the individual nanocarriers. Further evidence of tumor penetration and homogeneous distribution will be the subject of future investigations, through the use of fluorescence and near IR imaging techniques, as well as the incorporation of a chemotherapeutic drug conjugated to the dendrimers.

One of the advantages of using dendrimers in the core of the nanohybrid system

is that a variety of drug molecules can be conjugated to the terminal amine groups following surface modification (e.g. hydroxylation) using relatively simple coupling chemistries. For example, a drug molecule with a carboxyl group such as doxorubicin or methotrexate can be easily attached to the hydroxylated dendrimers through EDC/NHS chemistry, resulting in an ester bond. This type of bond is readily cleaved by esterases inside the body, allowing the free drug to be released. It is important to note that for scale-up purposes, large scale production of the multifunctional dendrimer conjugates remains a challenge, and can potentially be the rate-limiting step in nanohybrid preparation for clinical translation. For this technology to move forward, conjugation chemistries need to be carefully optimized in order to produce the dendrimer conjugates in sufficient amounts without sacrificing their physicochemical and biological properties.

Nanomedicine offers a plethora of opportunities to improve the quality of life of cancer patients. Dendrimers and other dendritic polymers have attracted a great deal of scientific interest as multifunctional nano-scale devices because of their unique structures and precise controllability over their physical and biological properties. Although further work is still warranted to achieve widespread clinical use, dendrimer-based nanocarriers are undoubtedly making a huge impact on the field of nanomedicine, and will continue to do so for years to come. Hybrid structures of dendrimers and linear copolymers can add to the numerous advantages of plain dendrimers and polymeric NPs, by imparting unique properties that can be functionally tuned to address some of the limitations of the individual nanocarriers. The combination of pre-existing dendrimer-based nanomaterials with other polymers using a multi-

layered design strategy is a promising alternative approach that can be used to enhance the therapeutic efficacy and broaden the applications of dendritic materials. Additionally, the ever growing advancement in dendrimer chemistry will definitely enable the design of more biocompatible dendrimer-based nanodevices. This in turn will help address the challenges on the road to their successful clinical applications, such as prolonging their blood circulation times and enhancing their tumor targeting efficacy.

BIBLIOGRAPHY

- Akinc, A., M. Thomas, et al. (2005). "Exploring polyethylenimine-mediated DNA transfection and the proton sponge hypothesis." *J. Gene Med.* 7(5): 657-663.
- Al-Jamal, K. T., W. T. Al-Jamal, et al. (2010). "Systemic antiangiogenic activity of cationic poly-L-lysine dendrimer delays tumor growth." *P. Natl. Acad. Sci. USA* 107(9): 3966-3971.
- Albertazzi, L., M. Serresi, et al. (2010). "Dendrimer Internalization and Intracellular Trafficking in Living Cells." *Mol. Pharm.* 7(3): 680-688.
- Almutairi, A., R. Rossin, et al. (2009). "Biodegradable dendritic positron-emitting nanoprobes for the noninvasive imaging of angiogenesis." *P. Natl. Acad. Sci. USA* 106(3): 685-690.
- Anderson, J. M. and M. S. Shive (1997). "Biodegradation and biocompatibility of PLA and PLGA microspheres." *Adv. Drug Deliver. Rev.* 28(1): 5-24.
- Ashton, P. R., E. F. Hounsell, et al. (1998). "Synthesis and biological evaluation of alpha-D-mannopyranoside-containing dendrimers." *J. Org. Chem.* 63(10): 3429-3437.
- Atyabi, F., A. Farkhondehfar, et al. (2009). "Preparation of pegylated nano-liposomal formulation containing SN-38: In vitro characterization and in vivo biodistribution in mice." *Acta Pharmaceut.* 59(2): 133-144.
- Avgoustakis, K., A. Beletsi, et al. (2002). "PLGA-mPEG nanoparticles of cisplatin: in vitro nanoparticle degradation, in vitro drug release and in Vivo drug residence in blood properties." *J. Control. Release* 79(1-3): 123-135.

- Azarmi, S., W. H. Roa, et al. (2008). "Targeted delivery of nanoparticles for the treatment of lung diseases." *Adv. Drug Deliver. Rev.* 60(8): 863-875.
- Bae, J. W., R. M. Pearson, et al. (2011). "Dendron-mediated self-assembly of highly PEGylated block copolymers: a modular nanocarrier platform." *Chem. Commun.* 47(37): 10302-10304.
- Bae, Y., W. D. Jang, et al. (2005). "Multifunctional polymeric micelles with folate-mediated cancer cell targeting and pH-triggered drug releasing properties for active intracellular drug delivery." *Mol. Biosyst.* 1(3): 242-250.
- Baird, E. J., D. Holowka, et al. (2003). "Highly effective poly(ethylene glycol) architectures for specific inhibition of immune receptor activation." *Biochemistry-U S* 42(44): 12739-12748.
- Baker, J. R., A. Quintana, et al. (2001). "The Synthesis and testing of anti-cancer therapeutic nanodevices." *Biomed. Microdevices* 3(1): 61-69.
- Barreto, J. A., W. O'Malley, et al. (2011). "Nanomaterials: Applications in cancer imaging and therapy." *Adv. Mater.* 23(12): H18-H40.
- Belbella, A., C. Vauthier, et al. (1996). "In vitro degradation of nanospheres from poly(D,L-lactides) of different molecular weights and polydispersities." *Int. J. Pharm.* 129(1-2): 95-102.
- Beletsi, A., Z. Panagi, et al. (2005). "Biodistribution properties of nanoparticles based on mixtures of PLGA with PLGA-PEG diblock copolymers." *Int. J. Pharm.* 298(1): 233-241.
- Bielinska, A. U., C. Chen, et al. (1999). "DNA complexing with polyamidoamine dendrimers: Implications for transfection." *Bioconjugate Chem.* 10(5): 843-850.

- Bosman, A. W., H. M. Janssen, et al. (1999). "About dendrimers: Structure, physical properties, and applications." *Chem. Rev.* 99(7): 1665-1688.
- Boussif, O., F. Lezoualch, et al. (1995). "A Versatile vector for gene and oligonucleotide transfer into cells in culture and in vivo - Polyethylenimine " *P. Natl. Acad. Sci. USA* 92(16): 7297-7301.
- Catiker, E., M. Gumusderelioglu, et al. (2000). "Degradation of PLA, PLGA homo- and copolymers in the presence of serum albumin: a spectroscopic investigation." *Polym. Int.* 49(7): 728-734.
- Chen, H., S. Kim, et al. (2008). "Release of hydrophobic molecules from polymer micelles into cell membranes revealed by Forster resonance energy transfer imaging." *P. Natl. Acad. Sci. USA* 105(18): 6596-6601.
- Cheng, J., B. A. Teply, et al. (2007). "Formulation of functionalized PLGA-PEG nanoparticles for in vivo targeted drug delivery." *Biomaterials* 28(5): 869-876.
- Cheng, Y., L. Zhao, et al. (2011). "Design of biocompatible dendrimers for cancer diagnosis and therapy: current status and future perspectives." *Chem. Soc. Rev.* 40(5): 2673-2703.
- Cheng, Z., D. L. J. Thorek, et al. (2010). "Gadolinium-conjugated dendrimer nanoclusters as a tumor-targeted T(1) magnetic resonance imaging contrast agent." *Angew. Chem. Int. Ed.* 49(2): 346-350.
- Chisholm, E. J., G. Vassaux, et al. (2009). "Cancer-specific transgene expression mediated by systemic injection of nanoparticles." *Cancer Res.* 69(6): 2655-2662.

- Choe, Y. H., C. D. Conover, et al. (2002). "Anticancer drug delivery systems: multi-loaded N-4-acyl poly(ethylene glycol) prodrugs of ara-C. II. Efficacy in ascites and solid tumors." *J. Control. Release* 79(1-3): 55-70.
- Civiale, C., M. Licciardi, et al. (2009). "Polyhydroxyethylaspartamide-based micelles for ocular drug delivery." *Int. J. Pharm.* 378(1-2): 177-186.
- Cohen, S., T. Yoshioka, et al. (1991). "Controlled delivery systems for proteins based on poly(lactic glycolic acid) microspheres." *Pharm. Res.* 8(6): 713-720.
- Couvreur, P. and C. Vauthier (2006). "Nanotechnology: Intelligent design to treat complex disease." *Pharm. Res.* 23(7): 1417-1450.
- Crotts, G., H. Sah, et al. (1997). "Adsorption determines in-vitro protein release rate from biodegradable microspheres: Quantitative analysis of surface area during degradation." *J. Control. Release* 47(1): 101-111.
- Cuong, N.-V., Y.-L. Li, et al. (2012). "Targeted delivery of doxorubicin to human breast cancers by folate-decorated star-shaped PEG-PCL micelle." *J. Mater. Chem.* 22(3): 1006-1020.
- D'Emanuele, A. and D. Attwood (2005). "Dendrimer-drug interactions." *Adv. Drug Deliver. Rev.* 57(15): 2147-2162.
- Danhier, F., O. Feron, et al. (2010). "To exploit the tumor microenvironment: Passive and active tumor targeting of nanocarriers for anti-cancer drug delivery." *J. Control. Release* 148(2): 135-146.
- Davies, C. D., H. Muller, et al. (1997). "Comparison of extracellular matrix in human osteosarcomas and melanomas growing as xenografts, multicellular spheroids, and monolayer cultures." *Anticancer Res.* 17(6D): 4317-4326.

- Davis, M. E. and M. E. Brewster (2004). "Cyclodextrin-based pharmaceuticals: Past, present and future." *Nat. Rev. Drug Discov.* 3(12): 1023-1035.
- Defoort, J. P., B. Nardelli, et al. (1992). "Macromolecular assemblage in the design of a synthetic AIDS vaccine." *P. Natl. Acad. Sci. USA* 89(9): 3879-3883.
- Dhanikula, R. S., A. Argaw, et al. (2008). "Methotrexate loaded polyether-copolyester dendrimers for the treatment of gliomas: Enhanced efficacy and intratumoral transport capability." *Mol. Pharm.* 5(1): 105-116.
- Dudia, A., A. Kocer, et al. (2008). "Biofunctionalized lipid-polymer hybrid nanocontainers with controlled permeability." *Nano Lett.* 8(4): 1105-1110.
- Duncan, R. (2003). "The dawning era of polymer therapeutics." *Nat. Rev. Drug Discov.* 2(5): 347-360.
- Duncan, R. (2006). "Polymer conjugates as anticancer nanomedicines." *Nat. Rev. Cancer* 6(9): 688-701.
- Duncan, R. and L. Izzo (2005). "Dendrimer biocompatibility and toxicity." *Adv. Drug Deliver. Rev.* 57(15): 2215-2237.
- Eavarone, D. A., X. J. Yu, et al. (2000). "Targeted drug delivery to C6 glioma by transferrin-coupled liposomes." *J. Biomed. Mater. Res.* 51(1): 10-14.
- Esfand, R. and D. A. Tomalia (2001). "Poly(amidoamine) (PAMAM) dendrimers: from biomimicry to drug delivery and biomedical applications." *Drug Discov. Today* 6(8): 427-436.
- Faisant, N., J. Akiki, et al. (2006). "Effects of the type of release medium on drug release from PLGA-based microparticles: Experiment and theory." *Int. J. Pharm.* 314(2): 189-197.

- Fischer, D., Y. X. Li, et al. (2003). "In vitro cytotoxicity testing of polycations: influence of polymer structure on cell viability and hemolysis." *Biomaterials* 24(7): 1121-1131.
- Forrest, M. L., J. T. Koerber, et al. (2003). "A degradable polyethylenimine derivative with low toxicity for highly efficient gene delivery." *Bioconjugate Chem.* 14(5): 934-940.
- Fox, M. E., S. Guillaudeu, et al. (2009). "Synthesis and in vivo antitumor efficacy of PEGylated poly(L-lysine) dendrimer-camptothecin conjugates." *Mol. Pharm.* 6(5): 1562-1572.
- Fox, M. E., F. C. Szoka, et al. (2009). "Soluble polymer carriers for the treatment of cancer: The importance of molecular architecture." *Acc. Chem. Res.* 42(8): 1141-1151.
- Freiberg, S. and X. Zhu (2004). "Polymer microspheres for controlled drug release." *Int. J. Pharm.* 282(1-2): 1-18.
- Friedrich, J., C. Seidel, et al. (2009). "Spheroid-based drug screen: considerations and practical approach." *Nat. Protoc.* 4(3): 309-324.
- Fu, K., D. W. Pack, et al. (2000). "Visual evidence of acidic environment within degrading poly(lactic-co-glycolic acid) (PLGA) microspheres." *Pharm. Res.* 17(1): 100-106.
- Fu, Y. and W. J. Kao (2010). "Drug release kinetics and transport mechanisms of non-degradable and degradable polymeric delivery systems." *Expert Opin. Drug Deliv.* 7(4): 429-444.

- Gabizon, A., R. Catane, et al. (1994). "Prolonged circulation time and enhanced accumulation in malignant exudates of doxorubicin encapsulated in polyethylene-glycol coated liposomes." *Cancer Res.* 54(4): 987-992.
- Gabizon, A., A. T. Horowitz, et al. (2003). "In vivo fate of folate-targeted polyethylene-glycol liposomes in tumor-bearing mice." *Clin. Cancer Res.* 9(17): 6551-6559.
- Gabizon, A., H. Shmeeda, et al. (2004). "Tumor cell targeting of liposome-entrapped drugs with phospholipid-anchored folic acid-PEG conjugates." *Adv. Drug Deliver. Rev.* 56(8): 1177-1192.
- Gabizon, A. A., H. Shmeeda, et al. (2006). "Pros and cons of the liposome platform in cancer drug targeting." *J. Lipos. Res.* 16(3): 175-183.
- Gao, C. and D. Yan (2004). "Hyperbranched polymers: from synthesis to applications." *Prog. Polym. Sci.* 29(3): 183-275.
- Gavini, E., P. Chetoni, et al. (2004). "PLGA microspheres for the ocular delivery of a peptide drug, vancomycin using emulsification/spray-drying as the preparation method: in vitro/in vivo studies." *Eur. J. Pharm. Biopharm.* 57(2): 207-212.
- Gebhart, C. L. and A. V. Kabanov (2001). "Evaluation of polyplexes as gene transfer agents." *J. Control. Release* 73(2-3): 401-416.
- Gestwicki, J. E., C. W. Cairo, et al. (2002). "Influencing receptor-ligand binding mechanisms with multivalent ligand architecture." *J. Am. Chem. Soc.* 124(50): 14922-14933.
- Giannavola, C., C. Bucolo, et al. (2003). "Influence of preparation conditions on acyclovir-loaded poly-d,l-lactic acid nanospheres and effect of PEG coating on ocular drug bioavailability." *Pharm. Res.* 20(4): 584-590.

- Gillies, E. R., E. Dy, et al. (2005). "Biological evaluation of polyester dendrimer: Poly(ethylene oxide) "bow-tie" hybrids with tunable molecular weight and architecture." *Mol. Pharm.* 2(2): 129-138.
- Gillies, E. R. and J. M. Frechet (2002). "Designing macromolecules for therapeutic applications: polyester dendrimer-poly(ethylene oxide) "bow-tie" hybrids with tunable molecular weight and architecture." *J. Am. Chem. Soc.* 124(47): 14137-14146.
- Gillies, E. R. and J. M. J. Frechet (2005). "Dendrimers and dendritic polymers in drug delivery." *Drug Discov. Today* 10(1): 35-43.
- Godbey, W. T., K. K. Wu, et al. (1999). "Size matters: Molecular weight affects the efficiency of poly(ethylenimine) as a gene delivery vehicle." *J. Biomed. Mater. Res.* 45(3): 268-275.
- Gonzalez, L., R. J. Loza, et al. (2013). "Nanotechnology in Corneal Neovascularization Therapy-A Review." *J. Ocul. Pharmacol. Th.* 29(2): 124-134.
- Gordon, A. N., J. T. Fleagle, et al. (2001). "Recurrent epithelial ovarian carcinoma: A randomized phase III study of pegylated liposomal doxorubicin versus topotecan." *J. Clin. Oncol.* 19(14): 3312-3322.
- Gradishar, W. J., S. Tjulandin, et al. (2005). "Phase III trial of nanoparticle albumin-bound paclitaxel compared with polyethylated castor oil-based paclitaxel in women with breast cancer." *J. Clin. Oncol.* 23(31): 7794-7803.
- Green, M. R., G. M. Manikhas, et al. (2006). "Abraxane((R)), a novel Cremophor((R))-free, albumin-bound particle form of paclitaxel for the treatment of advanced non-small-cell lung cancer." *Ann. Oncol.* 17(8): 1263-1268.

- Gref, R., Y. Minamitake, et al. (1994). "Biodegradable long-circulating polymeric nanospheres." *Science* 263(5153): 1600-1603.
- Gu, F. X., R. Karnik, et al. (2007). "Targeted nanoparticles for cancer therapy." *Nano Today* 2(3): 14-21.
- Guillaudeu, S. J., M. E. Fox, et al. (2008). "PEGylated dendrimers with core functionality for biological applications." *Bioconjugate Chem.* 19(2): 461-469.
- Haensler, J. and F. C. Szoka (1993). "Polyamidoamine cascade polymers mediate efficient transfection of cells in culture." *Bioconjugate Chem.* 4(5): 372-379.
- Hawker, C. J. and J. M. J. Frechet (1990). "Preparation of polymers with controlled molecular architecture. A new convergent approach to dendritic macromolecules." *J. Am. Chem. Soc.* 112(21): 7638-7647.
- He, W., H. F. Wang, et al. (2007). "In vivo quantitation of rare circulating tumor cells by multiphoton intravital flow cytometry." *P. Natl. Acad. Sci. USA* 104(28): 11760-11765.
- Heegaard, P. M. H., U. Boas, et al. (2009). "Dendrimers for vaccine and immunostimulatory uses. A Review." *Bioconjugate Chem.* 21(3): 405-418.
- Herborn, C. U., J. Barkhausen, et al. (2003). "Coronary arteries: Contrast-enhanced MR imaging with SH L 643A - Experience in 12 volunteers." *Radiology* 229(1): 217-223.
- Hillaireau, H. and P. Couvreur (2009). "Nanocarriers' entry into the cell: relevance to drug delivery." *Cell. Mol. Life Sci.* 66(17): 2873-2896.

- Hong, S., A. U. Bielinska, et al. (2004). "Interaction of poly(amidoamine) dendrimers with supported lipid bilayers and cells: Hole formation and the relation to transport." *Bioconjugate Chem.* 15(4): 774-782.
- Hong, S., P. R. Leroueil, et al. (2006). "Interaction of polycationic polymers with supported lipid bilayers and cells: Nanoscale hole formation and enhanced membrane permeability." *Bioconjugate Chem.* 17(3): 728-734.
- Hong, S., P. R. Leroueil, et al. (2007). "The binding avidity of a nanoparticle-based multivalent targeted drug delivery platform." *Chem. Biol.* 14(1): 107-115.
- Hong, S., R. Rattan, et al. (2009). "The role of ganglioside GM(1) in cellular internalization mechanisms of poly(amidoamine) dendrimers." *Bioconjugate Chem.* 20(8): 1503-1513.
- Hu, C. M. J., S. Kaushal, et al. (2010). "Half-antibody functionalized lipid-polymer hybrid nanoparticles for targeted drug delivery to carcinoembryonic antigen presenting pancreatic cancer cells." *Mol. Pharm.* 7(3): 914-920.
- Huang, K., H. Ma, et al. (2012). "Size-dependent localization and penetration of ultrasmall gold nanoparticles in cancer cells, multicellular spheroids, and tumors in vivo." *ACS Nano* 6(5): 4483-4493.
- Ihre, H. R., O. L. Padilla De Jesus, et al. (2002). "Polyester dendritic systems for drug delivery applications: design, synthesis, and characterization." *Bioconjugate Chem.* 13(3): 443-452.
- Ishihara, T., T. Kubota, et al. (2009). "Polymeric nanoparticles encapsulating betamethasone phosphate with different release profiles and stealthiness." *Int. J. Pharm.* 375(1-2): 148-154.

- Jain, K., P. Kesharwani, et al. (2010). "Dendrimer toxicity: Let's meet the challenge." *Int. J. Pharm.* 394(1-2): 122-142.
- Jain, R. K. (2001). "Delivery of molecular and cellular medicine to solid tumors." *Adv. Drug Deliver. Rev.* 46(1-3): 149-168.
- Jain, R. K. and T. Stylianopoulos (2010). "Delivering nanomedicine to solid tumors." *Nat. Rev. Clin. Oncol.* 7(11): 653-664.
- Jang, W. D., K. M. K. Selim, et al. (2009). "Bioinspired application of dendrimers: From bio-mimicry to biomedical applications." *Prog. Polym. Sci.* 34(1): 1-23.
- Jevprasesphant, R., J. Penny, et al. (2004). "Transport of dendrimer nanocarriers through epithelial cells via the transcellular route." *J. Control. Release* 97(2): 259-267.
- Jevprasesphant, R., J. Penny, et al. (2003). "The influence of surface modification on the cytotoxicity of PAMAM dendrimers." *Int. J. Pharm.* 252(1-2): 263-266.
- Jiang, H. L., Y. K. Kim, et al. (2007). "Chitosan-graft-polyethylenimine as a gene carrier." *J. Control. Release* 117(2): 273-280.
- Jin, S.-E., J. W. Bae, et al. (2010). "Multiscale observation of biological interactions of nanocarriers: From nano to macro." *Microsc. Res. Techniq.* 73(9): 813-823.
- Kane, R. S. (2010). "Thermodynamics of multivalent interactions: Influence of the linker." *Langmuir* 26(11): 8636-8640.
- Karakoti, A. S., S. Das, et al. (2011). "PEGylated inorganic nanoparticles." *Angew. Chem. Int. Ed.* 50(9): 1980-1994.

- Kataoka, K., A. Harada, et al. (2001). "Block copolymer micelles for drug delivery: design, characterization and biological significance." *Adv. Drug Deliver. Rev.* 47(1): 113-131.
- Kiessling, L. L., J. E. Gestwicki, et al. (2006). "Synthetic multivalent ligands as probes of signal transduction." *Angew. Chem. Int. Ed. Engl.* 45(15): 2348-2368.
- Kim, H. S. and H. S. Yoo (2010). "MMPs-responsive release of DNA from electrospun nanofibrous matrix for local gene therapy: In vitro and in vivo evaluation." *J. Control. Release* 145(3): 264-271.
- Kim, I. S., S. K. Lee, et al. (2005). "Physicochemical characterization of poly(L-lactic acid) and poly(D,L-lactide-co-glycolide) nanoparticles with polyethylenimine as gene delivery carrier." *Int. J. Pharm.* 298(1): 255-262.
- Kim, J., Y. Piao, et al. (2009). "Multifunctional nanostructured materials for multimodal imaging, and simultaneous imaging and therapy." *Chem. Soc. Rev.* 38(2): 372-390.
- Kim, Y. H., J. H. Park, et al. (2005). "Polyethylenimine with acid-labile linkages as a biodegradable gene carrier." *J. Control. Release* 103(1): 209-219.
- Kitchens, K. M., I. B. Kolhatkar, et al. (2008). "Endocytosis inhibitors prevent poly(amidoamine) dendrimer internalization and permeability across Caco-2 cells." *Mol. Pharm.* 5(2): 364-369.
- Ko, Y. T., R. Bhattacharya, et al. (2009). "Liposome encapsulated polyethylenimine/ODN polyplexes for brain targeting." *J. Control. Release* 133(3): 230-237.

- Kobayashi, H., S. Kawamoto, et al. (2003). "Macromolecular MRI contrast agents with small dendrimers: Pharmacokinetic differences between sizes and cores." *Bioconjugate Chem.* 14(2): 388-394.
- Kojima, C. (2010). "Design of stimuli-responsive dendrimers." *Expert Opin. Drug Deliv.* 7(3): 307-319.
- Kojima, C., K. Kono, et al. (2000). "Synthesis of polyamidoamine dendrimers having poly(ethylene glycol) grafts and their ability to encapsulate anticancer drugs." *Bioconjugate Chem.* 11(6): 910-917.
- Kojima, C., C. Regino, et al. (2010). "Influence of dendrimer generation and polyethylene glycol length on the biodistribution of PEGylated dendrimers." *Int. J. Pharm.* 383(1-2): 293-296.
- Konda, S. D., S. Wang, et al. (2002). "Biodistribution of a Gd-153-folate dendrimer, generation=4, in mice with folate-receptor positive and negative ovarian tumor xenografts." *Invest. Radiol.* 37(4): 199-204.
- Kopatz, I., J. S. Remy, et al. (2004). "A model for non-viral gene delivery: through syndecan adhesion molecules and powered by actin." *J. Gene Med.* 6(7): 769-776.
- Kostiainen, M. A., O. Kasyutich, et al. (2010). "Self-assembly and optically triggered disassembly of hierarchical dendron-virus complexes." *Nature Chemistry* 2(5): 394-399.

- Kranz, D. M., T. A. Patrick, et al. (1995). "Conjugates of folate and anti-T-cell-receptor antibodies specifically target folate-receptor-positive tumor cells for lysis." *P. Natl. Acad. Sci. USA* 92(20): 9057-9061.
- Kukowska-Latallo, J. F., K. A. Candido, et al. (2005). "Nanoparticle targeting of anticancer drug improves therapeutic response in animal model of human epithelial cancer." *Cancer Res.* 65(12): 5317-5324.
- Kunath, K., A. von Harpe, et al. (2003). "Low-molecular-weight polyethylenimine as a non-viral vector for DNA delivery: comparison of physicochemical properties, transfection efficiency and in vivo distribution with high-molecular-weight polyethylenimine." *J. Control. Release* 89(1): 113-125.
- Lawrence, M. J. and G. D. Rees (2000). "Microemulsion-based media as novel drug delivery systems." *Adv. Drug Deliver. Rev.* 45(1): 89-121.
- Lee, C. C., E. R. Gillies, et al. (2006). "A single dose of doxorubicin-functionalized bow-tie dendrimer cures mice bearing C-26 colon carcinomas." *P. Natl. Acad. Sci. USA* 103(45): 16649-16654.
- Lee, C. C., J. A. MacKay, et al. (2005). "Designing dendrimers for biological applications." *Nat. Biotechnol.* 23(12): 1517-1526.
- Lee, C. H., Y. H. Ni, et al. (2003). "Synergistic effect of polyethylenimine and cationic liposomes in nucleic acid delivery to human cancer cells." *BBA-Biomembranes* 1611(1-2): 55-62.
- Lee, H., H. Fonge, et al. (2010). "The Effects of particle size and molecular targeting on the intratumoral and subcellular distribution of polymeric nanoparticles." *Mol. Pharm.* 7(4): 1195-1208.

- Lee, R. J. and P. S. Low (1995). "Folate-mediated tumor-cell targeting of liposome-entrapped doxorubicin in-vitro." *BBA-Biomembranes* 1233(2): 134-144.
- Leroueil, P. R., S. Hong, et al. (2007). "Nanoparticle interaction with biological membranes: Does nanotechnology present a janus face?" *Acc. Chem. Res.* 40(5): 335-342.
- Li, J., G. Q. Jiang, et al. (2008). "The effect of pH on the polymer degradation and drug release from PLGA-mPEG microparticles." *J. Appl. Polym. Sci.* 109(1): 475-482.
- Li, Y., X. R. Qi, et al. (2009). "PEG-PLA diblock copolymer micelle-like nanoparticles as all-trans-retinoic acid carrier: in vitro and in vivo characterizations." *Nanotechnology* 20(5): 055106.
- Li, Y. P., Y. Y. Pei, et al. (2001). "PEGylated PLGA nanoparticles as protein carriers: synthesis, preparation and biodistribution in rats." *J. Control. Release* 71(2): 203-211.
- Li, Y. Q., N. Taulier, et al. (2006). "Screening of lipid carriers and characterization of drug-polymer-lipid interactions for the rational design of polymer-lipid hybrid nanoparticles (PLN)." *Pharm. Res.* 23(8): 1877-1887.
- Lim, Y. B., E. Lee, et al. (2007). "Controlled bioactive nanostructures from self-assembly of peptide building blocks." *Angew. Chem. Int. Ed. Engl.* 46(47): 9011-9014.
- Liu, S. Y., L. Jones, et al. (2012). "Nanomaterials for ocular drug delivery." *Macromol. Biosci.* 12(5): 608-620.
- Liu, Y. T., K. Li, et al. (2010). "Folic acid conjugated nanoparticles of mixed lipid monolayer shell and biodegradable polymer core for targeted delivery of Docetaxel." *Biomaterials* 31(2): 330-338.

- Liu, Y. T., J. Pan, et al. (2010). "Nanoparticles of lipid monolayer shell and biodegradable polymer core for controlled release of paclitaxel: Effects of surfactants on particles size, characteristics and in vitro performance." *Int. J. Pharm.* 395(1-2): 243-250.
- Lockridge, O., W. H. Xue, et al. (2008). "Pseudo-esterase activity of human albumin - Slow turnover on tyrosine 411 and stable acetylation of 82 residues including 59 lysines." *J. Biol. Chem.* 283(33): 22582-22590.
- Maeda, H. (2010). "Tumor-selective delivery of macromolecular drugs via the EPR effect: Background and future prospects." *Bioconjugate Chem.* 21(5): 797-802.
- Majoros, I. J., A. Myc, et al. (2006). "PAMAM dendrimer-based multifunctional conjugate for cancer therapy: Synthesis, characterization, and functionality." *Biomacromolecules* 7(2): 572-579.
- Majoros, I. J., T. P. Thomas, et al. (2005). "Poly(amidoamine) dendrimer-based multifunctional engineered nanodevice for cancer therapy." *J. Med. Chem.* 48(19): 5892-5899.
- Malik, N., E. G. Evagorou, et al. (1999). "Dendrimer-platinate: a novel approach to cancer chemotherapy." *Anti-Cancer Drugs* 10(8): 767-776.
- Malik, N., R. Wiwattanapatapee, et al. (2000). "Dendrimers: relationship between structure and biocompatibility in vitro, and preliminary studies on the biodistribution of 125I-labelled polyamidoamine dendrimers in vivo." *J. Control. Release* 65(1-2): 133-148.

- Mammen, M., S. K. Choi, et al. (1998). "Polyvalent interactions in biological systems: Implications for design and use of multivalent ligands and inhibitors." *Angew. Chem. Int. Ed.* 37(20): 2755-2794.
- Manunta, M., B. J. Nichols, et al. (2006). "Gene delivery by dendrimers operates via different pathways in different cells, but is enhanced by the presence of caveolin." *J. Immunol. Methods* 314(1-2): 134-146.
- Martin, A. L., B. Li, et al. (2008). "Surface functionalization of nanomaterials with dendritic groups: toward enhanced binding to biological targets." *J. Am. Chem. Soc.* 131(2): 734-741.
- Matsumura, Y. and H. Maeda (1986). "A New concept for macromolecular therapeutics in cancer chemotherapy - Mechanism of tumorotropic accumulation of proteins and the antitumor agent SMANCS." *Cancer Res.* 46(12): 6387-6392.
- McNeeley, K. M., A. Annapragada, et al. (2007). "Decreased circulation time offsets increased efficacy of PEGylated nanocarriers targeting folate receptors of glioma." *Nanotechnology* 18(38).
- McNeeley, K. M., E. Karathanasis, et al. (2009). "Masking and triggered unmasking of targeting ligands on nanocarriers to improve drug delivery to brain tumors." *Biomaterials* 30(23-24): 3986-3995.
- McNerny, D. Q., J. F. Kukowska-Latallo, et al. (2009). "RGD dendron bodies; Synthetic avidity agents with defined and potentially interchangeable effector sites that can substitute for antibodies." *Bioconjugate Chem.* 20(10): 1853-1859.
- Mecke, A., I. Lee, et al. (2004). "Deformability of poly(amidoamine) dendrimers." *Eur. Phys. J. E* 14(1): 7-16.

- Menjoge, A. R., R. M. Kannan, et al. (2010). "Dendrimer-based drug and imaging conjugates: design considerations for nanomedical applications." *Drug Discov. Today* 15(5-6): 171-185.
- Merdan, T., K. Kunath, et al. (2005). "PEGylation of poly(ethylene imine) affects stability of complexes with plasmid DNA under in vivo conditions in a dose-dependent manner after intravenous injection into mice." *Bioconjugate Chem.* 16(4): 785-792.
- Minchinton, A. I. and I. F. Tannock (2006). "Drug penetration in solid tumours." *Nat. Rev. Cancer* 6(8): 583-592.
- Modi, S., J. P. Jain, et al. (2006). "Exploiting EPR in polymer drug conjugate delivery for tumor targeting." *Curr. Pharm. Design* 12(36): 4785-4796.
- Mukherjee, B., K. Santra, et al. (2008). "Preparation, characterization and in-vitro evaluation of sustained release protein-loaded nanoparticles based on biodegradable polymers." *Int. J. Nanomed.* 3(4): 487-496.
- Mullen, D. G., E. L. Borgmeier, et al. (2010). "Isolation and characterization of dendrimers with precise numbers of functional groups." *Chem.-Eur. J.* 16(35): 10675-10678.
- Mullen, D. G., A. M. Desai, et al. (2008). "The implications of stochastic synthesis for the conjugation of functional groups to nanoparticles." *Bioconjugate Chem.* 19(9): 1748-1752.
- Mullen, D. G., M. Fang, et al. (2010). "A Quantitative assessment of nanoparticle-ligand distributions: Implications for targeted drug and imaging delivery in dendrimer conjugates." *ACS Nano* 4(2): 657-670.

- Muller-Goymann, C. C. (2004). "Physicochemical characterization of colloidal drug delivery systems such as reverse micelles, vesicles, liquid crystals and nanoparticles for topical administration." *Eur. J. Pharm. Biopharm.* 58(2): 343-356.
- Myc, A., T. B. Douce, et al. (2008). "Preclinical antitumor efficacy evaluation of dendrimer-based methotrexate conjugates." *Anti-Cancer Drugs* 19(2): 143-149.
- Myc, A., J. Kukowska-Latallo, et al. (2010). "Targeting the efficacy of a dendrimer-based nanotherapeutic in heterogeneous xenograft tumors in vivo." *Anti-Cancer Drugs* 21(2): 186-192.
- Myung, J., K. A. Gajjar, et al. (2011). "Dendrimer-mediated multivalent binding for the enhanced capture of tumor cells." *Angew. Chem. Int. Ed.* 50(49): 11769-11772.
- Nagrath, S., L. V. Sequist, et al. (2007). "Isolation of rare circulating tumour cells in cancer patients by microchip technology." *Nature* 450(7173): 1235-U1210.
- Nasongkla, N., E. Bey, et al. (2006). "Multifunctional polymeric micelles as cancer-targeted, MRI-ultrasensitive drug delivery systems." *Nano Lett.* 6(11): 2427-2430.
- Neu, M., D. Fischer, et al. (2005). "Recent advances in rational gene transfer vector design based on poly(ethylene imine) and its derivatives." *J. Gene Med.* 7(8): 992-1009.
- Nguyen-Van, C., Y.-L. Li, et al. (2012). "Targeted delivery of doxorubicin to human breast cancers by folate-decorated star-shaped PEG-PCL micelle." *J. Mater. Chem.* 22(3): 1006-1020.
- Nigavekar, S. S., L. Y. Sung, et al. (2004). "H-3 dendrimer nanoparticle organ/tumor distribution." *Pharm. Res.* 21(3): 476-483.

- Nishiyama, N., Y. Nakagishi, et al. (2009). "Enhanced photodynamic cancer treatment by supramolecular nanocarriers charged with dendrimer phthalocyanine." *J. Control. Release* 133(3): 245-251.
- Nori, A. and J. Kopecek (2005). "Intracellular targeting of polymer-bound drugs for cancer chemotherapy." *Adv. Drug Deliver. Rev.* 57(4): 609-636.
- Okuda, T., S. Kawakami, et al. (2006). "Biodistribution characteristics of amino acid dendrimers and their PEGylated derivatives after intravenous administration." *J. Control. Release* 114(1): 69-77.
- Olson, E. S., T. Jiang, et al. (2010). "Activatable cell penetrating peptides linked to nanoparticles as dual probes for in vivo fluorescence and MR imaging of proteases." *P. Natl. Acad. Sci. USA* 107(9): 4311-4316.
- Oupicky, D., M. Ogris, et al. (2002). "Development of long-circulating polyelectrolyte complexes for systemic delivery of genes." *J. Drug Target.* 10(2): 93-98.
- Owens, D. E. and N. A. Peppas (2006). "Opsonization, biodistribution, and pharmacokinetics of polymeric nanoparticles." *Int. J. Pharm.* 307(1): 93-102.
- Padilla De Jesus, O. L., H. R. Ihre, et al. (2002). "Polyester dendritic systems for drug delivery applications: in vitro and in vivo evaluation." *Bioconjugate Chem.* 13(3): 453-461.
- Panyam, J., M. M. Dali, et al. (2003). "Polymer degradation and in vitro release of a model protein from poly(,-lactide-co-glycolide) nano- and microparticles." *J. Control. Release* 92(1-2): 173-187.

- Panyam, J., S. K. Sahoo, et al. (2003). "Fluorescence and electron microscopy probes for cellular and tissue uptake of poly(-lactide-co-glycolide) nanoparticles." *Int. J. Pharm.* 262(1-2): 1-11.
- Panyam, J., W.-Z. Zhou, et al. (2002). "Rapid endo-lysosomal escape of poly(DL-lactide-co-glycolide) nanoparticles: implications for drug and gene delivery." *FASEB J.* 16(10): 1217-1226.
- Park, J., P. M. Fong, et al. (2009). "PEGylated PLGA nanoparticles for the improved delivery of doxorubicin." *Nanomed.-Nanotechnol.* 5(4): 410-418.
- Parker, N., M. J. Turk, et al. (2005). "Folate receptor expression in carcinomas and normal tissues determined by a quantitative radioligand binding assay." *Anal. Biochem.* 338(2): 284-293.
- Patri, A. K., J. F. Kukowska-Latallo, et al. (2005). "Targeted drug delivery with dendrimers: Comparison of the release kinetics of covalently conjugated drug and non-covalent drug inclusion complex." *Adv. Drug Deliver. Rev.* 57(15): 2203-2214.
- Patri, A. K., I. J. Majoros, et al. (2002). "Dendritic polymer macromolecular carriers for drug delivery." *Curr. Opin. Chem. Biol.* 6(4): 466-471.
- Paulus, W., C. Huettner, et al. (1994). "Collagens, integrins and the mesenchymal drift in glioblastomas: a comparison of biopsy specimens, spheroid and early monolayer cultures." *Int. J. Cancer* 58(6): 841-846.
- Pearson, R. M., S. Sunoqrot, et al. (2012). "Dendritic nanoparticles: the next generation of nanocarriers?" *Therapeutic delivery* 3(8): 941-959.

- Peer, D., J. M. Karp, et al. (2007). "Nanocarriers as an emerging platform for cancer therapy." *Nat. Nanotechnol.* 2(12): 751-760.
- Penco, M., S. Marcioni, et al. (1996). "Degradation behaviour of block copolymers containing poly(lactic-glycolic acid) and poly(ethylene glycol) segments." *Biomaterials* 17(16): 1583-1590.
- Percec, V., D. A. Wilson, et al. (2010). "Self-assembly of Janus dendrimers into uniform dendrimersomes and other complex architectures." *Science* 328(5981): 1009-1014.
- Perez, C., A. Sanchez, et al. (2001). "Poly(lactic acid)-poly(ethylene glycol) nanoparticles as new carriers for the delivery of plasmid DNA." *J. Control. Release* 75(1-2): 211-224.
- Perl, A., A. Gomez-Casado, et al. (2011). "Gradient-driven motion of multivalent ligand molecules along a surface functionalized with multiple receptors." *Nature Chemistry* 3(4): 317-322.
- Perumal, O. P., R. Inapagolla, et al. (2008). "The effect of surface functionality on cellular trafficking of dendrimers." *Biomaterials* 29(24-25): 3469-3476.
- Polakovic, M., T. Gorner, et al. (1999). "Lidocaine loaded biodegradable nanospheres II. Modelling of drug release." *J. Control. Release* 60(2-3): 169-177.
- Poon, Z., S. Chen, et al. (2010). "Ligand-clustered "patchy" nanoparticles for modulated cellular uptake and in vivo tumor targeting." *Angew. Chem. Int. Ed. Engl.* 49(40): 7266-7270.
- Poon, Z., J. A. Lee, et al. (2010). "Highly stable, ligand-clustered "patchy" micelle nanocarriers for systemic tumor targeting." *Nanomedicine*.

- Popovic, Z., W. H. Liu, et al. (2010). "A Nanoparticle size series for in vivo fluorescence imaging." *Angew. Chem. Int. Ed.* 49(46): 8649-8652.
- Qiu, L. Y. and Y. H. Bae (2007). "Self-assembled polyethylenimine-graft-poly(epsilon-caprolactone) micelles as potential dual carriers of genes and anticancer drugs." *Biomaterials* 28(28): 4132-4142.
- Quintana, A., E. Raczka, et al. (2002). "Design and function of a dendrimer-based therapeutic nanodevice targeted to tumor cells through the folate receptor." *Pharm. Res.* 19(9): 1310-1316.
- Rajendran, L., H. J. Knolker, et al. (2010). "Subcellular targeting strategies for drug design and delivery." *Nat. Rev. Drug Discov.* 9(1): 29-42.
- Riehemann, K., S. W. Schneider, et al. (2009). "Nanomedicine-Challenge and perspectives." *Angew. Chem. Int. Ed.* 48(5): 872-897.
- Rizkalla, N., C. Range, et al. (2006). "Effect of various formulation parameters on the properties of polymeric nanoparticles prepared by multiple emulsion method." *J. Microencapsul.* 23(1): 39-57.
- Rodal, S. K., G. Skretting, et al. (1999). "Extraction of cholesterol with methyl-beta-cyclodextrin perturbs formation of clathrin-coated endocytic vesicles." *Mol. Biol. Cell* 10(4): 961-974.
- Ross, J. F., P. K. Chaudhuri, et al. (1994). "Differential regulation of folate receptor isoforms in normal and malignant tissues in vivo and in established cell lines - Physiological and clinical implications " *Cancer* 73(9): 2432-2443.

- Rothberg, K. G., Y. S. Ying, et al. (1990). "The glycopospholipid-linked folate receptor internalizes folate without entering the clathrin-coated pit endocytic pathway." *J. Cell Biol.* 110(3): 637-649.
- Ruenraroengsak, P., J. M. Cook, et al. (2010). "Nanosystem drug targeting: Facing up to complex realities." *J. Control. Release* 141(3): 265-276.
- Ruoslahti, E., S. N. Bhatia, et al. (2010). "Targeting of drugs and nanoparticles to tumors." *J. Cell Biol.* 188(6): 759-768.
- Sahoo, S. K., F. Diinawaz, et al. (2008). "Nanotechnology in ocular drug delivery." *Drug Discov. Today* 13(3-4): 144-151.
- Sahoo, S. K., J. Panyam, et al. (2002). "Residual polyvinyl alcohol associated with poly (-lactide-co-glycolide) nanoparticles affects their physical properties and cellular uptake." *J. Control. Release* 82(1): 105-114.
- Saul, J. M., A. Annapragada, et al. (2003). "Controlled targeting of liposomal doxorubicin via the folate receptor in vitro." *J. Control. Release* 92(1-2): 49-67.
- Savic, R., L. B. Luo, et al. (2003). "Micellar nanocontainers distribute to defined cytoplasmic organelles." *Science* 300(5619): 615-618.
- Schnitzer, J. E., P. Oh, et al. (1994). "Filipin-sensitive caveolae-mediated transport in endothelium - Reduced transcytosis, scavenger endocytosis, and capillary permeability of select macromolecules." *J. Cell Biol.* 127(5): 1217-1232.
- Seib, F. P., A. T. Jones, et al. (2007). "Comparison of the endocytic properties of linear and branched PEIs, and cationic PAMAM dendrimers in B16f10 melanoma cells." *J. Control. Release* 117(3): 291-300.

- Singh, P., U. Gupta, et al. (2008). "Folate and folate-PEG-PAMAM dendrimers: Synthesis, characterization, and targeted anticancer drug delivery potential in tumor bearing mice." *Bioconjugate Chem.* 19(11): 2239-2252.
- Sinha, V. R. and A. Trehan (2003). "Biodegradable microspheres for protein delivery." *J. Control. Release* 90(3): 261-280.
- Son, S. and W. J. Kim (2010). "Biodegradable nanoparticles modified by branched polyethylenimine for plasmid DNA delivery." *Biomaterials* 31(1): 134-143.
- Son, S., W. R. Lee, et al. (2009). "Optimized stability retention of a monoclonal antibody in the PLGA nanoparticles." *Int. J. Pharm.* 368(1-2): 178-185.
- Soppimath, K. S., T. M. Aminabhavi, et al. (2001). "Biodegradable polymeric nanoparticles as drug delivery devices." *J. Control. Release* 70(1-2): 1-20.
- Stella, B., S. Arpicco, et al. (2000). "Design of folic acid-conjugated nanoparticles for drug targeting." *J. Pharm. Sci.* 89(11): 1452-1464.
- Stott, S. L., C. H. Hsu, et al. (2010). "Isolation of circulating tumor cells using a microvortex-generating herringbone-chip." *P. Natl. Acad. Sci. USA* 107(43): 18392-18397.
- Sunogrot, S., J. W. Bae, et al. (2011). "Kinetically controlled cellular interactions of polymer-polymer and polymer-liposome nanohybrid systems." *Bioconjugate Chem.* 22(3): 466-474.
- Sunogrot, S., J. W. Bae, et al. (2012). "Temporal control over cellular targeting through hybridization of folate-targeted dendrimers and PEG-PLA nanoparticles." *Biomacromolecules* 13: 1223-1230.

- Sunogrot, S., Y. Liu, et al. (2013). "In vitro evaluation of dendrimer–polymer hybrid nanoparticles on their controlled cellular targeting kinetics." *Mol. Pharm.* ASAP Article. DOI: 10.1021/mp300560n.
- Tang, L., T. M. Fan, et al. (2012). "Synthesis and biological response of size-specific, monodisperse drug-silica nanoconjugates." *ACS Nano* 6(5): 3954-3966.
- Taratula, O., O. B. Garbuzenko, et al. (2009). "Surface-engineered targeted PPI dendrimer for efficient intracellular and intratumoral siRNA delivery." *J. Control. Release* 140(3): 284-293.
- Thomas, C. E., A. Ehrhardt, et al. (2003). "Progress and problems with the use of viral vectors for gene therapy." *Nat. Rev. Genet.* 4(5): 346-358.
- Thomas, T. P., S. N. Goonewardena, et al. (2011). "Folate-targeted nanoparticles show efficacy in the treatment of inflammatory arthritis." *Arthritis Rheum.* 63(9): 2671-2680.
- Tomalia, D. A., H. Baker, et al. (1985). "A New Class of Polymers - Starburst-Dendritic Macromolecules." *Polym. J.* 17(1): 117-132.
- Torchilin, V. (2011). "Tumor delivery of macromolecular drugs based on the EPR effect." *Adv. Drug Deliver. Rev.* 63(3): 131-135.
- Torchilin, V. P. (2005). "Recent advances with liposomes as pharmaceutical carriers." *Nat. Rev. Drug Discov.* 4(2): 145-160.
- Torchilin, V. P. (2006). "Multifunctional nanocarriers." *Adv. Drug Deliver. Rev.* 58(14): 1532-1555.
- Uchegbu, I. F. and S. P. Vyas (1998). "Non-ionic surfactant based vesicles (niosomes) in drug delivery." *Int. J. Pharm.* 172(1-2): 33-70.

- Urban-Klein, B., S. Werth, et al. (2005). "RNAi-mediated gene-targeting through systemic application of polyethylenimine (PEI)-complexed siRNA in vivo." *Gene Ther.* 12(5): 461-466.
- Valente, I., B. Stella, et al. (2012). "Production of PEGylated Nanocapsules through Solvent Displacement in Confined Impinging Jet Mixers." *J. Pharm. Sci.* 101(7): 2490-2501.
- van der Poll, D. G., H. M. Kieler-Ferguson, et al. (2010). "Design, synthesis, and biological evaluation of a robust, biodegradable dendrimer." *Bioconjugate Chem.* 21(4): 764-773.
- Vance, D., J. Martin, et al. (2009). "The design of polyvalent scaffolds for targeted delivery." *Adv. Drug Deliver. Rev.* 61(11): 931-939.
- Vannucci, L., A. Fiserova, et al. (2003). "Effects of N-acetyl-glucosamine-coated glycodendrimers as biological modulators in the B16F10 melanoma model in vivo." *Int. J. Oncol.* 23(2): 285-296.
- Vasir, J. K. and V. Labhasetwar (2007). "Biodegradable nanoparticles for cytosolic delivery of therapeutics." *Adv. Drug Deliver. Rev.* 59(8): 718-728.
- Vauthier, C. and K. Bouchemal (2009). "Methods for the preparation and manufacture of polymeric nanoparticles." *Pharm. Res.* 26(5): 1025-1058.
- Vega, E., M. A. Egea, et al. (2006). "Flurbiprofen loaded biodegradable nanoparticles for opthalmic administration." *J. Pharm. Sci.* 95(11): 2393-2405.
- Verma, I. M. and N. Somia (1997). "Gene therapy - promises, problems and prospects." *Nature* 389(6648): 239-242.

- Vila, A., H. Gill, et al. (2004). "Transport of PLA-PEG particles across the nasal mucosa: effect of particle size and PEG coating density." *J. Control. Release* 98(2): 231-244.
- Vincent, L., J. Varet, et al. (2003). "Efficacy of dendrimer-mediated angiostatin and TIMP-2 gene delivery on inhibition of tumor growth and angiogenesis: In vitro and in vivo studies." *Int. J. Cancer* 105(3): 419-429.
- Waite, C. L. and C. M. Roth (2009). "PAMAM-RGD conjugates enhance siRNA delivery through a multicellular spheroid model of malignant glioma." *Bioconjugate Chem.* 20(10): 1908-1916.
- Weitman, S. D., R. H. Lark, et al. (1992). "Distribution of the folate receptor GP38 in normal and malignant cell lines and tissues " *Cancer Res.* 52(12): 3396-3401.
- Wiener, E. C., M. W. Brechbiel, et al. (1994). "Dendrimer-based metal-chelates - A new class of magnetic-resonance-imaging contrast agents " *Magn. Reson. Med.* 31(1): 1-8.
- Wijagkanalan, W., S. Kawakami, et al. (2011). "Designing dendrimers for drug delivery and imaging: Pharmacokinetic considerations." *Pharm. Res.* 28(7): 1500-1519.
- Winnicka, K., K. Bielawski, et al. (2009). "The Effect of Generation 2 and 3 Poly(amidoamine) Dendrimers on Viability of Human Breast Cancer Cells." *J. Health Sci.* 55(2): 169-177.
- Wolinsky, J. B. and M. W. Grinstaff (2008). "Therapeutic and diagnostic applications of dendrimers for cancer treatment." *Adv. Drug Deliver. Rev.* 60(9): 1037-1055.
- Wong, C., T. Stylianopoulos, et al. (2011). "Multistage nanoparticle delivery system for deep penetration into tumor tissue." *P. Natl. Acad. Sci. USA* 108(6): 2426-2431.

- Wu, X. S. and N. Wang (2001). "Synthesis, characterization, biodegradation, and drug delivery application of biodegradable lactic/glycolic acid polymers. Part II: Biodegradation." *J. Biomat. Sci.-Polym. E.* 12(1): 21-34.
- Xiao, R. Z., Z. W. Zeng, et al. (2010). "Recent advances in PEG-PLA block copolymer nanoparticles." *Int. J. Nanomed.* 5: 1057-1065.
- Xu, J., Y. Wang, et al. (2007). "Inhibitory efficacy of intravitreal dexamethasone acetate-loaded PLGA nanoparticles on choroidal neovascularization in a laser-induced rat model." *J. Ocul. Pharmacol. Th.* 23(6): 527-539.
- Xu, P. S., E. Gullotti, et al. (2009). "Intracellular Drug Delivery by Poly(lactic-co-glycolic acid) Nanoparticles, Revisited." *Mol. Pharm.* 6(1): 190-201.
- Yang, Y., S. Sunoqrot, et al. (2012). "Effect of size, surface charge, and hydrophobicity of poly(amidoamine) dendrimers on their skin penetration." *Biomacromolecules* 13(7): 2154-2162.
- Yoo, H. S. and T. G. Park (2001). "Biodegradable polymeric micelles composed of doxorubicin conjugated PLGA-PEG block copolymer." *J. Control. Release* 70(1-2): 63-70.
- Yoo, H. S. and T. G. Park (2004). "Folate-receptor-targeted delivery of doxorubicin nano-aggregates stabilized by doxorubicin-PEG-folate conjugate." *J. Control. Release* 100(2): 247-256.
- Yu, H., M. Kortylewski, et al. (2007). "Crosstalk between cancer and immune cells: role of STAT3 in the tumour microenvironment." *Nat. Rev. Immunol.* 7(1): 41-51.
- Yuan, F., M. Dellian, et al. (1995). "Vascular permeability in a human tumor xenograft - molecular size dependence and cutoff size " *Cancer Res.* 55(17): 3752-3756.

- Yuan, F., M. Leunig, et al. (1994). "Microvascular permeability and interstitial penetration of sterically stabilized (stealth) liposomes in a human tumor xenograft." *Cancer Res.* 54(13): 3352-3356.
- Zhang, L. F., J. M. Chan, et al. (2008). "Self-assembled lipid-polymer hybrid nanoparticles: A robust drug delivery platform." *ACS Nano* 2(8): 1696-1702.
- Zhang, Y., T. P. Thomas, et al. (2010). "Targeted dendrimeric anticancer prodrug: A methotrexate-folic acid-poly(amidoamine) conjugate and a novel, rapid, "one pot" synthetic approach." *Bioconjugate Chem.* 21(3): 489-495.
- Zhang, Z. P., S. H. Lee, et al. (2007). "Folate-decorated poly(lactide-co-glycolide)-vitamin E TPGS nanoparticles for targeted drug delivery." *Biomaterials* 28(10): 1889-1899.
- Zhao, Q. Q., J. L. Chen, et al. (2009). "N/P ratio significantly influences the transfection efficiency and cytotoxicity of a polyethylenimine/chitosan/DNA complex." *Biol. Pharm. Bull.* 32(4): 706-710.
- Zhong, Z. Y., J. Feijen, et al. (2005). "Low molecular weight linear polyethylenimine-b-poly(ethylene glycol)-b-polyethylenimine triblock copolymers: Synthesis, characterization, and in vitro gene transfer properties." *Biomacromolecules* 6(6): 3440-3448.
- Zong, H., T. P. Thomas, et al. (2012). "Bifunctional PAMAM dendrimer conjugates of folic acid and methotrexate with defined ratio." *Biomacromolecules* Just Accepted Manuscript, DOI: 10.1021/bm201639c.

APPENDIX I – Copyright permissions

4/14/13

Rightslink® by Copyright Clearance Center



RightsLink®

[Home](#)[Create Account](#)[Help](#)

ACS Publications Title:

High quality. High impact.

Kinetically Controlled Cellular Interactions of Polymer –Polymer and Polymer –Liposome Nanohybrid Systems

Author: Suhair Sunoqrot, Jin Woo Bae, Su-Eon Jin, Ryan M. Pearson, Ying Liu, and Seungpyo Hong

Publication: Bioconjugate Chemistry

Publisher: American Chemical Society

Date: Mar 1, 2011

Copyright © 2011, American Chemical Society

User ID
Password
<input type="checkbox"/> Enable Auto Login
<input type="button" value="LOGIN"/>
Forgot Password/User ID?
If you're a copyright.com user, you can login to RightsLink using your copyright.com credentials. Already a RightsLink user or want to learn more?

Quick Price Estimate

Permission for this particular request is granted for print and electronic formats, and translations, at no charge. Figures and tables may be modified. Appropriate credit should be given. Please print this page for your records and provide a copy to your publisher. Requests for up to 4 figures require only this record. Five or more figures will generate a printout of additional terms and conditions. Appropriate credit should read: "Reprinted with permission from {COMPLETE REFERENCE CITATION}. Copyright {YEAR} American Chemical Society." Insert appropriate information in place of the capitalized words.

I would like to... ?

reuse in a Thesis/Dissertation

This service provides permission for reuse only. If you do not have a copy of the article you are using, you may copy and paste the content and reuse according to the terms of your agreement. Please be advised that obtaining the content you license is a separate transaction not involving Rightslink.

Requestor Type ?

Author (original work)

Portion ?

Full article

Format ?

Print and Electronic

Will you be translating? ?

No

Select your currency

USD - \$

Quick Price

Click Quick Price

To request permission for a type of use not listed, please contact [the publisher](#) directly.

Copyright © 2013 [Copyright Clearance Center, Inc.](#) All Rights Reserved. [Privacy statement.](#)
Comments? We would like to hear from you. E-mail us at customer-care@copyright.com



RightsLink®

[Home](#)
[Create Account](#)
[Help](#)

ACS Publications

High quality. High impact.

Title: Temporal Control over Cellular Targeting through Hybridization of Folate-targeted Dendrimers and PEG-PLA Nanoparticles

Author: Suhair Sunoqrot, Jin Woo Bae, Ryan M. Pearson, Kevin Shyu, Ying Liu, Dong-Hwan Kim, and Seungpyo Hong

Publication: Biomacromolecules

Publisher: American Chemical Society

Date: Apr 1, 2012

Copyright © 2012, American Chemical Society

User ID
Password
<input type="checkbox"/> Enable Auto Login
LOGIN
Forgot Password/User ID?
If you're a copyright.com user, you can login to RightsLink using your copyright.com credentials. Already a RightsLink user or want to learn more?

Quick Price Estimate

Permission for this particular request is granted for print and electronic formats, and translations, at no charge. Figures and tables may be modified. Appropriate credit should be given. Please print this page for your records and provide a copy to your publisher. Requests for up to 4 figures require only this record. Five or more figures will generate a printout of additional terms and conditions. Appropriate credit should read: "Reprinted with permission from {COMPLETE REFERENCE CITATION}. Copyright {YEAR} American Chemical Society." Insert appropriate information in place of the capitalized words.

I would like to...

reuse in a Thesis/Dissertation

This service provides permission for reuse only. If you do not have a copy of the article you are using, you may copy and paste the content and reuse according to the terms of your agreement. Please be advised that obtaining the content you license is a separate transaction not involving Rightslink.

Requestor Type

Author (original work)

Portion

Full article

Format

Print

Will you be translating?

make a selection

Select your currency

USD - \$

Quick Price

Click Quick Price

QUICK PRICE
CONTINUE

To request permission for a type of use not listed, please contact [the publisher](#) directly.

Copyright © 2013 [Copyright Clearance Center, Inc.](#) All Rights Reserved. [Privacy statement.](#) Comments? We would like to hear from you. E-mail us at customer-care@copyright.com



RightsLink®

[Home](#)
[Create Account](#)
[Help](#)

ACS Publications

High quality. High impact.

Title: In Vitro Evaluation of Dendrimer-Polymer Hybrid Nanoparticles on Their Controlled Cellular Targeting Kinetics

Author: Suhair Sunoqrot, Ying Liu, Dong-Hwan Kim, and Seungpyo Hong

Publication: Molecular Pharmaceutics

Publisher: American Chemical Society

Date: Dec 1, 2012

Copyright © 2012, American Chemical Society

User ID
<input type="text"/>
Password
<input type="text"/>
<input type="checkbox"/> Enable Auto Login
<input type="button" value="LOGIN"/>
Forgot Password/User ID?
If you're a copyright.com user, you can login to RightsLink using your copyright.com credentials. Already a RightsLink user or want to learn more?

Quick Price Estimate

Permission for this particular request is granted for print and electronic formats, and translations, at no charge. Figures and tables may be modified. Appropriate credit should be given. Please print this page for your records and provide a copy to your publisher. Requests for up to 4 figures require only this record. Five or more figures will generate a printout of additional terms and conditions. Appropriate credit should read: "Reprinted with permission from {COMPLETE REFERENCE CITATION}. Copyright {YEAR} American Chemical Society." Insert appropriate information in place of the capitalized words.

I would like to...

This service provides permission for reuse only. If you do not have a copy of the article you are using, you may copy and paste the content and reuse according to the terms of your agreement. Please be advised that obtaining the content you license is a separate transaction not involving Rightslink.

Requestor Type

Portion

Format

Will you be translating?

Select your currency

Quick Price

Click Quick Price

To request permission for a type of use not listed, please contact [the publisher](#) directly.

Copyright © 2013 [Copyright Clearance Center, Inc.](#) All Rights Reserved. [Privacy statement.](#) Comments? We would like to hear from you. E-mail us at customer-care@copyright.com

APPENDIX II – Animal Care Committee approval letters



February 22, 2012

Seungpyo Hong
Biopharmaceutical Sciences
M/C 865

Office of Animal Care and
Institutional Biosafety Committees (MC 672)
Office of the Vice Chancellor for Research
206 Administrative Office Building
1737 West Polk Street
Chicago, Illinois 60612-7227

Dear Dr. Hong:

The protocol indicated below was reviewed at a convened ACC meeting in accordance with the Animal Care Policies of the University of Illinois at Chicago on **12/20/2011**. *The protocol was not initiated until final clarifications were reviewed and approved on 2/22/2012. The protocol is approved for a period of 3 years with annual continuation.*

Title of Application: In Vivo Fate of Dendrimer- and Dendron-Based Nanoparticles

ACC Number: 11-205

Initial Approval Period: 2/22/2012 to 12/20/2012

Current Funding: *Portions of this protocol are supported by the funding sources indicated in the table below.*

Number of funding sources: 1

Funding Agency	Funding Title	Portion of Proposal Matched		
NSF- National Science Foundation	Hybrid Nanoparticles for Kinetically Controlled Cancer Targeting Using Biomimetic Cell Rolling and Multivalent Binding	<i>Matched</i>		
Funding Number	Current Status	UIC PAF NO.	Performance Site	Funding PI
	<i>Pending</i>	<i>2012-00274</i>	<i>UIC</i>	<i>Seungpyo Hong</i>

This institution has Animal Welfare Assurance Number A3460.01 on file with the Office of Laboratory Animal Welfare (OLAW), NIH. **This letter may only be provided as proof of IACUC approval for those specific funding sources listed above in which all portions of the funding proposal are matched to this ACC protocol.**

In addition, all investigators are responsible for ensuring compliance with all federal and institutional policies and regulations related to use of animals under this protocol and the funding sources listed on this protocol. Please use OLAW's "*What Investigators Need to Know about the Use of Animals*" (<http://grants.nih.gov/grants/olaw/InvestigatorsNeed2Know.pdf>) as a reference guide. Thank you for complying with the Animal Care Policies and Procedures of UIC.

Sincerely yours,

Bradley Merrill, PhD
Chair, Animal Care Committee
BM/ss

cc: BRL, ACC File, Yang Yang, Suhair Sunoqrot, Ryan Pearson, **PAF #2012-00274**

12/20/2012

Seungpyo Hong
Biopharmaceutical Sciences
M/C 865

Office of Animal Care and Institutional
Biosafety Committee (OACIB) (M/C 672)
Office of the Vice Chancellor for Research
206 Administrative Office Building
1737 West Polk Street
Chicago, Illinois 60612

Dear Dr. Hong:

The protocol indicated below was reviewed in accordance with the Animal Care Policies and Procedures of the University of Illinois at Chicago and **renewed on 12/20/2012**.

Title of Application: In Vivo Fate of Dendrimer- and Dendron-Based Nanoparticles
ACC NO: 11-205
Original Protocol Approval: 2/22/2012 (3 year approval with annual continuation required).
Current Approval Period: 12/20/2012 to 12/20/2013

Funding: Portions of this protocol are supported by the funding sources indicated in the table below.
Number of funding sources: 2

Funding Agency	Funding Title			Portion of Funding Matched
NSF- National Science Foundation	Hybrid Nanoparticles for Kinetically Controlled Cancer Targeting Using Biomimetic Cell Rolling and Multivalent Binding			All matched
Funding Number	Current Status	UIC PAF NO.	Performance Site	Funding PI
	Pending	2012-00274	UIC	Seungpyo Hong
Funding Agency	Funding Title			Portion of Funding Matched
UIC Chancellor Discovery Fund	Prevention and Therapy of Ovarian Cancer Using Nanocarriers			All matched
Funding Number	Current Status	UIC PAF NO.	Performance Site	Funding PI
	Funded		UIC	Seungpyo Hong

This institution has Animal Welfare Assurance Number A3460.01 on file with the Office of Laboratory Animal Welfare, NIH. **This letter may only be provided as proof of IACUC approval for those specific funding sources listed above in which all portions of the grant are matched to this ACC protocol.**

Thank you for complying with the Animal Care Policies and Procedures of the UIC.

Sincerely,



Bradley Merrill, PhD
Chair, Animal Care Committee

BM/kg

cc: BRL, ACC File, Yang Yang, Suhair Sunoqrot, Ryan Pearson

VITA

Education

- 2013 **Doctor of Philosophy**, Biopharmaceutical Sciences (Advisor: Prof. Seungpyo Hong)
University of Illinois at Chicago (UIC), College of Pharmacy, Chicago, IL, USA
- 2007 **Bachelor of Science**, Pharmacy
University of Jordan, Faculty of Pharmacy, Amman, Jordan

Professional Experience

- 2010 - **Research Assistant**, Department of Biopharmaceutical Sciences, UIC, Chicago, IL
- 2008 - 2010 **Teaching Assistant**, Department of Biopharmaceutical Sciences, UIC, Chicago, IL
- 2007 - 2008 **Dispensing Pharmacist**, Aboud Pharmacy, Amman, Jordan

Publications

1. Turturro, S.* , **Sunoqrot, S.***, Ying, H.* , Hong, S., and Yue, B. Sustained Release of Matrix Metalloproteinase-3 to Trabecular Meshwork Cells using Biodegradable PLGA Microparticles. *Mol. Pharm.* **Under revision 2013**. *Denotes co-first authors.
2. **Sunoqrot, S.**, Liu, Y., Kim, D.H., and Hong, S. In Vitro Evaluation of Dendrimer-Polymer Hybrid Nanoparticles on their Controlled Cellular Targeting Kinetics. *Mol. Pharm.* **ASAP Article 2013**. DOI: 10.1021/mp300560n.
3. Gonzalez, L.* , Loza, R.J.* , Han, K.-Y., **Sunoqrot, S.**, Cunningham, C., Purta, P., Drake, J., Jain, S., Hong, S., and Chang, J.-H. Nanotechnology in Corneal Neovascularization Therapy - A Review. *J. Ocul. Pharmacol. Th.* **2013**, 29(2), 124-134. *Denotes co-first authors
4. Pearson, R.M., **Sunoqrot, S.**, Hsu, H.-J., Bae, J.W., and Hong, S. Dendritic Nanoparticles: The Next Generation of Nanocarriers? *Therapeutic Delivery.* **2012**, 3(8), 941-959.
5. Yang, Y., **Sunoqrot, S.**, Stowell, C., Ji, J., Lee, C.-W., Kim, J.W., Khan, S.A., and Hong, S. The Effect of Size, Surface Charge and Hydrophobicity of Poly(amidoamine) Dendrimers on their Skin Penetration. *Biomacromolecules.* **2012**, 13(7), 2154-2162.
6. **Sunoqrot, S.**, Bae, J.W., Pearson, R.M., Shyu, K., Liu, Y., Kim, D.H., and Hong, S. Temporal Control over Cellular Targeting through Hybridization of Folate-targeted Dendrimers and PEG-

- PLA Nanoparticles. *Biomacromolecules*. **2012**, 13(4), 1223-1230.
7. Bae, J.W.*, Pearson, R.M.*, Patra, N., **Sunoqrot, S.**, Vukovic, L., Král, P. and Hong, S. Dendron-mediated Self-assembly of Highly PEGylated Block Copolymers: A Modular Nanocarrier Platform. *Chem. Commun.* **2011**, 47(37), 10302-10304.
*Denotes co-first authors
 8. **Sunoqrot, S.**, Bae, J.W., Jin, S.-E., Pearson, R.M., Liu, Y. and Hong, S. Kinetically Controlled Cellular Interactions of Novel Polymer-Polymer and Polymer-Liposome Nanohybrid Systems. *Bioconjugate Chem.* **2011**, 22(3), 466-474.

Conference Proceedings

1. **Sunoqrot, S.**, Bae, J.W., Liu, Y., Kim, D.-H., and Hong, S. The Janus-faced Biological Properties of Dendrimer-Polymer Hybrid Nanoparticles. College of Pharmacy Research Day **2013**, Chicago, IL.
2. **Sunoqrot, S.**, Bae, J.W., Liu, Y., Kim, D.-H., and Hong, S. The Janus-faced Biological Properties of Dendrimer-Polymer Hybrid Nanoparticles. American Association of Pharmaceutical Scientists (AAPS) Annual Meeting **2012**, Chicago, IL.
3. **Sunoqrot, S.**, Bae, J.W., Pearson, R.M., Shyu, K., and Hong, S. Hybrid Nanoparticles of Folate-targeted Dendrimers and PEG-PLA for Controlled Cellular Targeting. Midwest Pharmaceutical Graduate Student Research Meeting (PGSRM) **2012**, Omaha, NE.
4. Pearson, R.M., Bae, J.W., **Sunoqrot, S.**, Uddin, S. and Hong, S. Dendron Copolymers for Drug Delivery: From Synthesis and Characterization to Cellular Interactions. Midwest Pharmaceutical Graduate Student Research Meeting (PGSRM) **2012**, Omaha, NE.
5. Hsu, H.-J., Pearson, R.M., Patra, N., **Sunoqrot, S.**, Uddin, S. Kral, P., and Hong, S. Synthesis and Characterization of Surface Modified Dendron Micelles and their Cellular Interactions. Midwest Pharmaceutical Graduate Student Research Meeting (PGSRM) **2012**, Omaha, NE.
6. Pearson, R.M., Patra, N., Hsu, H.-J., **Sunoqrot, S.**, Uddin, S. Kral, P., and Hong, S. End Group Modification of Dendron Micelles and their Interactions with Cells. American Association for Cancer Research (AACR) Annual Meeting **2012**, Chicago, IL.
7. **Sunoqrot, S.**, Bae, J.W., Pearson, R.M., Shyu, K., Liu, Y., and Hong, S. Novel Hybrid Nanoparticles Folate-targeted Dendrimers and PEG-PLA Nanoparticles for Temporal Control

- over Targeting. Cancer Center Research Forum **2012**, Chicago, IL.
8. Yang, Y., **Sunoqrot, S.**, Stowell, C., Ji, J., Lee, C.W., Lee, J.W., and Hong, S. Transdermal Delivery Pathways and Skin Retention of Surface Modified Poly(amidoamine) (PAMAM) Dendrimers. Cancer Center Research Forum **2012**, Chicago, IL.
 9. Pearson, R.M., Patra, N., Hsu, H.-J., **Sunoqrot, S.**, Uddin, S. Kral, P., and Hong, S. End group modification of dendron micelles and their interactions with cells. Cancer Center Research Forum **2012**, Chicago, IL.
 10. **Sunoqrot, S.**, Bae, J.W., Pearson, R.M., Shyu, K., Liu, Y., and Hong, S. Novel Hybrid Nanoparticles Folate-targeted Dendrimers and PEG-PLA Nanoparticles for Temporal Control over Targeting. College of Pharmacy Research Day **2012**, Chicago, IL.
 11. Yang, Y., **Sunoqrot, S.**, Stowell, C., Ji, J., Lee, C.W., Lee, J.W., and Hong, S. Transdermal Delivery Pathways and Skin Retention of Surface Modified Poly(amidoamine) (PAMAM) Dendrimers. College of Pharmacy Research Day **2012**, Chicago, IL.
 12. Pearson, R.M., Patra, N., Hsu, H.-J., **Sunoqrot, S.**, Uddin, S. Kral, P., and Hong, S. End group modification of dendron micelles and their interactions with cells. College of Pharmacy Research Day **2012**, Chicago, IL.
 13. **Sunoqrot, S.**, Bae, J.W., Pearson, R.M., Shyu, K., Liu, Y., and Hong, S. Novel Hybrid Nanoparticles Folate-targeted Dendrimers and PEG-PLA Nanoparticles for Temporal Control over Targeting. American Association of Pharmaceutical Scientists (AAPS) Annual Meeting **2011**, Washington, DC.
 14. Pearson, R.M., Bae, J.W., **Sunoqrot, S.**, Uddin, S. and Hong, S. Highly PEGylated Dendron-based Micelles as a Potential Nanocarrier Platform. American Association of Pharmaceutical Scientists Annual Meeting (AAPS) **2011**, Washington, DC.
 15. **Sunoqrot, S.**, Bae, J.W., Jin, S.-E., Pearson, R.M., Liu, Y., and Hong, S. Kinetically Controlled Cellular Interactions of Novel Polymer-Polymer and Polymer-Liposome Nanohybrid Systems. Chicago Biomedical Consortium (CBC) Annual Symposium **2011**, Chicago, IL.
 16. Pearson, R.M., Bae, J.W., **Sunoqrot, S.**, Uddin, S. and Hong, S. Facilitated Self-Assembly of Novel Dendron-based copolymers. Annual International Conference of the IEEE Engineering in Medicine and Biology Society (EMBC) **2011**, Boston, MA.
 17. Yang, Y., **Sunoqrot, S.**, Stowell, C., Ji, J., Lee, C.W., Lee, J.W., and Hong, S. Transdermal Delivery Pathways and Skin Retention of Surface Modified Poly(amidoamine) (PAMAM)

- Dendrimers. Controlled Release Society (CRS) Annual Meeting **2011**, Baltimore, MD.
18. **Sunoqrot, S.**, Bae, J.W., Jin, S.-E., Pearson, R.M., Liu, Y. and Hong, S. Kinetically Controlled Cellular Interactions of Novel Polymer-Polymer and Polymer-Liposome Nanohybrid Systems. Midwest Pharmaceutical Graduate Student Research Meeting (PGSRM) **2011**, Madison, WI.
 19. Pearson, R.M., Bae, J.W., **Sunoqrot, S.**, Uddin, S. and Hong, S. Synthesis and Self-Assembly of Highly PEGylated Dendron-based Triblock Copolymers. Midwest Pharmaceutical Graduate Student Research Meeting (PGSRM) **2011**, Madison, WI.
 20. Bae, J.W.*, Pearson, R.M.*, **Sunoqrot, S.**, Uddin, S., Xu, L. and Hong, S. Facilitated Self-Assembly of Novel Dendron-Based Copolymers. American Chemical Society (ACS) National Meeting **2011**, Anaheim, CA.
- *Denotes co-first authors
21. **Sunoqrot, S.**, Bae, J.W., Jin, S.-E., Pearson, R.M., Liu, Y. and Hong, S. Kinetically Controlled Cellular Interactions of Novel Polymer-Polymer and Polymer-Liposome Nanohybrid Systems. College of Pharmacy Research Day **2011**, Chicago, IL.
 22. Pearson, R.M., Bae, J.W., **Sunoqrot, S.**, Uddin, S. and Hong, S. Facilitated Self-Assembly of Novel Dendron-Based Copolymers. College of Pharmacy Research Day **2011**, Chicago, IL.
 23. **Sunoqrot, S.**, Bae, J.W., Jin, S.-E., Pearson, R.M., Liu, Y. and Hong, S. Polymer-polymer and polymer-liposome nanohybrid systems with kinetically controlled cellular interactions. Materials Research Society (MRS) Fall Meeting **2010**, Boston, MA.
 24. **Sunoqrot, S.**, Jin, S.-E., Bae, J.W., Liu, Y. and Hong, S. Novel polymer-polymer and polymer-liposome nanohybrid systems as potential targeted delivery vehicles. Midwest Pharmaceutics Graduate Students Research Meeting (PGSRM) **2010**, Columbus, OH.
 25. **Sunoqrot, S.**, Jin, S.-E., Bae, J.W., Liu, Y. and Hong, S. Novel polymer-polymer and polymer-liposome nanohybrid systems as potential targeted delivery vehicles. UIC Graduate Student Research Forum **2010**, Chicago, IL.
 26. **Sunoqrot, S.**, Jin, S.-E., Bae, J.W., Liu, Y. and Hong, S. Novel polymer-polymer and polymer-liposome nanohybrid systems as potential targeted delivery vehicles. College of Pharmacy Research Day **2010**, Chicago, IL.

Honors and Awards

2013

Charles Wesley Petranek Scholarship

	Department of Biopharmaceutical Sciences, College of Pharmacy, UIC, Chicago, IL
2012	Chancellor's Student Service and Leadership Award Office of the Vice Chancellor for Student Affairs, UIC, Chicago, IL
2012	W.E. van Doren Scholarship Department of Biopharmaceutical Sciences, College of Pharmacy, UIC, Chicago, IL
2011	Provost and Deiss Award for Research Graduate College, UIC, Chicago, IL
2009 - 2011	Chancellor's Supplemental Graduate Research Fellowship Graduate College, UIC, Chicago, IL
2010	Rho Chi Pharmacy Honor Society
2010	Phi Kappa Phi Honor Society
2007 - 2008	Graduate tuition waiver Faculty of Pharmacy, University of Jordan, Amman, Jordan
2007	Hikma Pharmaceuticals Award for Academic Excellence Hikma Pharmaceuticals, Amman, Jordan
2003 - 2007	Undergraduate tuition waiver Ministry of Higher Education, Amman, Jordan

Professional and Extracurricular Activities

2012 -	Member , International Society of Pharmaceutical Engineers (ISPE)
2010 - 2011	President , Controlled Release Society (CRS)-IL Student Chapter, UIC, Chicago, IL
2011	Planning Committee Member , The 3 rd CRS-IL Student Chapter Symposium, UIC, Chicago, IL Titled: "Recent Advances in Nanotechnology for Cancer Therapy", featuring keynote speaker Dr. Jindrich (Henry) Kopecek of University of Utah
2011	Planning Committee Member , CRS-IL Student Chapter Annual Seminar Series, UIC, Chicago, IL Titled: "Multifunctional Polymer-Based Nanoparticles for the Targeted Delivery of Antitumor Agents" by Dr. SonBinh T. Nguyen of Northwestern University
2011 -	Member , American Association of Pharmaceutical Scientists (AAPS)
2010 -	Member , Materials Research Society (MRS)
2009 - 2010	Vice President , CRS-IL Student Chapter, UIC, Chicago, IL
2010	Planning Committee Member , The 2 nd CRS-IL Student Chapter Symposium, UIC, Chicago, IL Titled: "Diabetes from Bench to Bedside: Controlled Drug Delivery Progression from the Lab to the Clinic", featuring keynote speaker Dr. W. Mark Saltzman of Yale University
2010	Planning Committee Member , CRS-IL Student Chapter Annual Seminar Series, UIC, Chicago, IL

- Titled: “Synergistic Effect of Therapeutic Ultrasound Particles Delivery into Solid Tumors” by Dr. Mohamed El-Sayed of University of Michigan
- 2008 - 2009 **Events Coordinator**, CRS-IL Student Chapter, UIC, Chicago, IL
- 2009 **Planning Committee Member**, The 1st CRS-IL Student Chapter Symposium, UIC, Chicago, IL
- Titled: “Recent Advances in Parenteral Drug Delivery”, featuring keynote speaker Dr. Theodore Roseman, former Vice President of Baxter Healthcare
- 2009 - **Member**, Controlled Release Society (CRS)
- 2008 - **Member**, CRS-IL Student Chapter, UIC, Chicago, IL
- 2008 - **Member**, AAPS-UIC Student Chapter, UIC, Chicago, IL
- 2007 - **Member**, Jordanian Pharmacists Association (JPA), Amman, Jordan
- 2007 - **Member**, Jordanian Pharmacy Students Federation (JPSF), Amman, Jordan
- 2007 - **Member**, International Pharmacy Students Federation (IPSF)

Students Supervised

Undergraduates

- 2011 **Jacquelyn Handley**, Undergraduate Student, Department of Materials Science and Engineering, University of Illinois at Urbana-Champaign (UIUC), Urbana, IL

High School Teachers

- 2012 **Frehiwot Gebrehiwot**, Academy of Scholastic Achievement, Chicago, IL
- 2010 **Jeromy Bentley**, Naperville Central H.S., Naperville, IL

High School Students

- 2011 - 2012 **Tahir Mohideen**, Illinois Mathematics and Science Academy (IMSA), Aurora, IL